Aust. J. Phys., 1986, **39**, 117–87

Experimental Aspects of the Electroweak Gauge Theory*

Allan G. Clark[A] *and Stuart N. Tovey*[B]

[A] CERN, 1211 Geneva 23, Switzerland.
[B] School of Physics, University of Melbourne, Parkville, Vic. 3052.

Abstract

A review is given of experimental tests that have been made on the validity of electroweak gauge theory and in particular on the validity of the Glashow–Salam–Weinberg model of the weak and electromagnetic interactions. In addition to data from the CERN $\bar{p}p$ Collider, we briefly discuss tests of the model in neutrino–electron, neutrino–hadron and charged-lepton–hadron interactions.

Table of Contents

* Based on a series of lectures presented by one of us (A.G.C.) at the Seventh NUPP Summer School, Australian National University, Canberra, 4–8 February 1985.

0004-9506/86/020117$02.00

1. Introduction

This review examines the experimental support for the SU(2)×U(1) electroweak theory of Glashow, Salam and Weinberg, the so-called 'standard' or GSW model, with particular emphasis on recent results from the CERN $\bar{p}p$ Collider. The past two decades have seen great advances, both experimental and theoretical, in our knowledge of particle physics. There is a growing conviction that gauge field theories provide a correct description of the forces acting between elementary particles. It is therefore important to subject these theories to stringent tests. The predictions of the GSW model for the weak and electromagnetic interactions of fermions are in most cases precise and unambiguous.

In addition to the recent results from the $\bar{p}p$ Collider, many experiments performed over the past decade have given increasing confidence in the GSW model. It is our intension to discuss how well each class of experiment has tested the specific predictions of the model, and its underlying assumptions. However, because of its topicality, special attention has been given to the Collider program. At the time the lectures were presented (February 1985), only published data from the UA1 and UA2 experiments based on the 1983 run at the Collider were available. In this written version, results from the 1984 run are included, as available at the time of writing.

The basic ideas behind the GSW model are given in Section 2, where the place of the model in the scenario of particle physics as a whole is made clear. Section 3 describes the CERN $\bar{p}p$ Collider, the design of the UA1 and UA2 detectors, and the discovery and properties of the W and Z bosons. Section 4 briefly examines tests of the GSW model, in a series of experiments ranging from atomic physics to neutrino interactions and electron–positron annihilation. In Section 5, we combine these results in a short summary of the existing data. In preparing these lectures, we referred frequently to recent reviews or Summer School lectures by Jarlskog (1982), Pullia (1984) and Dowell (1984). These references generally provide a more detailed discussion of specific aspects of the present review.

2. The GSW Model

This section is dedicated to a description of the 'standard' or GSW model of electroweak interactions, originally written down by Glashow (1961) and put in its present form by Salam (1968) and Weinberg (1967). Section 2*c* traces the basic steps in the derivation of the model and Section 2*d* discusses some consequences of the model that should be tested.

The beauty and importance of the model can only be appreciated in the framework of our understanding of the fundamental particles and their interactions. Section 2*a* attempts, very briefly, to provide such a framework. Section 2*b* describes the gauge principle, as applied to the well-known theory of QED.

(2a) Particles and Fields

It is widely believed that matter is built from sets of elementary (i.e. apparently point-like) spin-$\frac{1}{2}$ fermions, called leptons and quarks. These fermions interact through the mediation of four types of force field which, in the language of quantum field theory, propagate through the emission and absorption of integer-spin bosons.

Table 1. Elementary fermions

Each fermion is partnered by an antifermion with quantum numbers equal to the negative of the values given

Charge	Electric q	Lepton number L_e	L_μ	L_τ	Baryon number B
Leptons					
ν_e (e neutrino)	0	1	0	0	0
e (electron)	-1	1	0	0	0
ν_μ (μ neutrino)	0	0	1	0	0
μ (muon)	-1	0	1	0	0
ν_τ (τ neutrino)	0	0	0	1	0
τ (tau)	-1	0	0	1	0
Quarks					
u (up)	$+\frac{2}{3}$	0	0	0	$\frac{1}{3}$
d (down)	$-\frac{1}{3}$	0	0	0	$\frac{1}{3}$
c (charm)	$+\frac{2}{3}$	0	0	0	$\frac{1}{3}$
s (stange)	$-\frac{1}{3}$	0	0	0	$\frac{1}{3}$
t (top)	$+\frac{2}{3}$	0	0	0	$\frac{1}{3}$
b (bottom)	$-\frac{1}{3}$	0	0	0	$\frac{1}{3}$

Present experimental evidence and theoretical ideas suggest that quarks interact via all the force fields, while the leptons are neutral to the strong force. The quantum numbers of these fermions are given in Table 1.

Three families of leptons are known: the electron, the muon and the tau, each with its own, possibly massless, neutrino.

Extensive probing of protons and neutrons with beams of high energy leptons has revealed the existence of point-like scattering centres within nucleons, and equally extensive studies of hadron spectroscopy suggest that those scattering centres are associated with quarks. The known hadron spectrum requires there to be five quarks, of fractional charge and baryon number. Two of these quarks (u, d) form an isospin doublet (the strong isospin of nuclear physics), and are the components of the familiar nucleons. The other three (s, c, b) are strong isospin singlets. It is theoretically desirable that a sixth quark (t) should exist to restore the quark–lepton symmetry; preliminary evidence for its existence has been claimed at the $\bar{p}p$ Collider (Arnison *et al.* 1984*d*) and will be discussed in Section 3*d*.

The electromagnetic interactions of the fermions are well understood. They couple, through their electric charge q, to a massless vector field, with an associated particle, the photon γ. The next subsection will show how this theory, QED, can be derived from the assumption of a local symmetry with respect to phase transformations.

The strong force binding quarks into hadrons has, as a candidate, an equally elegant but less well-tested theory, quantum chromo-dynamics (QCD). Quarks are postulated to carry a new sort of charge, the colour charge, through which they couple to a set of eight massless vector fields, the associated particles being termed gluons. Again, the theory is based on an invariance under local gauge transformations. The existence of a three-fold degree of freedom, such as colour, also provides an explanation for problems related to the Pauli Principle in hadron spectroscopy, and to the rate of e^+e^- annihilation into hadrons.

The best known but least understood force is gravity, and we will not discuss it in this review. It is worth while to note, however, that gravity can also be formulated as a gauge theory.

There now exists a substantial, and continually increasing, body of data which suggests that the GSW model, which unites the weak and electromagnetic interactions, is correct. However, as this model and its tests are the subject of this review, it is instructive to review our knowledge of the weak interactions before the GSW model.

Weak interactions are conveniently divided into two classes, the 'charged currents' in which the participating fermions exchange electric charge, and the 'neutral currents' in which this does not occur. Charged-current interactions were first recognized in β-decay, and have been extensively studied both there, and via neutrino interactions at accelerators. Their properties can be concisely stated in the form of a phenomenological Lagrangian, originally due to Fermi (1933), with important modifications by Feynman and Gell-Mann (1958), Cabbibo (1963) and Glashow *et al.* (1971):

$$L^{\mathrm{CC}} = (G_{\mathrm{F}}/\sqrt{2}) J_{\mu} J_{\mu}^{\dagger}, \tag{1}$$

where G_{F} is the 'universal' Fermi constant, measured to be small, and hence the name 'weak' interactions; J_{μ} represents a fermion current, described below, in which the fermion electric charge increases by one unit, $\Delta Q = +1$; and $J_{\mu}^{\dagger}$, the conjugate current, has $\Delta Q = -1$. The form of J_{μ} is

$$J_{\mu} = 2 \sum \bar{f}_{\mathrm{L}} \gamma_{\mu} f'_{\mathrm{L}}, \tag{2}$$

the subscript L signifying that only left-handed fermions (or right-handed antifermions) 'feel' the weak force. The summation in (2) extends over pairs of fermions:

$$(f, f') \equiv (\nu_l, l^-) \quad \text{or} \quad (q, q'). \tag{3}$$

All three pairs of leptons appear with the same 'universal' coupling G_{F}, but the situation for the quarks is slightly more complicated. The charged-current weak interactions do not conserve strangeness, or other quark flavours, and transitions of the type $\mathrm{s} \rightarrow \mathrm{u}e^-\bar{\nu}$ occur (for example in $\Lambda^0 \rightarrow \mathrm{p}e^-\bar{\nu}$) as well as transitions of the type $\mathrm{d} \rightarrow \mathrm{u}e^-\bar{\nu}$ (in $\mathrm{n} \rightarrow \mathrm{p}e^-\bar{\nu}$). Cabbibo (1963) demonstrated that quark–lepton universality could be partially restored if the quark q' in equation (3) is taken to be a linear combination of the quark mass eigenstates of hadron spectroscopy:

$$(q, q') \equiv (\mathrm{u}, \mathrm{d}'), \qquad \mathrm{d}' = \mathrm{d} \cos\theta_{\mathrm{C}} + \mathrm{s} \sin\theta_{\mathrm{C}}, \tag{4}$$

where θ_{C} is the Cabbibo angle. Glashow, Iliopoulis and Maiani (1971) completed the picture in the so-called GIM ansatz, proposing a fourth quark which coupled via the weak interactions to a state s′ orthogonal to d′:

$$(q, q') \equiv (\mathrm{c}, \mathrm{s}'), \qquad \mathrm{s}' = -\mathrm{d} \sin\theta_{\mathrm{C}} + \mathrm{s} \cos\theta_{\mathrm{C}}. \tag{4'}$$

Thereby lepton–quark universality is restored in an elegant fashion. The GIM

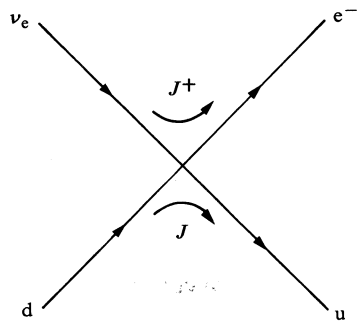

Fig. 1. Charged-current reaction $\nu_e d \to e^- u$ expressed in the Fermi model as a four-point coupling.

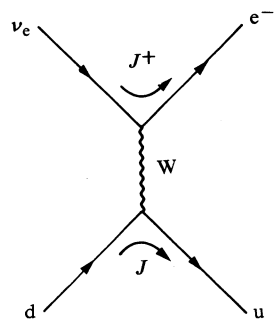

Fig. 2. Charged-current reaction $\nu_e d \to e^- u$ mediated by an intermediate vector boson W.

ansatz was originally invoked by Glashow *et al.* to explain the non-observation of strangeness-changing neutral-current decays such as $K^+ \to \pi^+ \nu\bar{\nu}$ and $K_L \to \mu^+\mu^-$.

The theory was extended to include six quarks by Kobayashi and Maskawa (1973), as will be noted in Section 2*c*. Fig. 1 shows a typical interaction due to equation (1). An electron-neutrino interacts with a d quark (contained within a nucleon), yielding an electron and u quark. The interaction occurs at a point.

The Lagrangian (1) is unsatisfactory, leading to violation of unitarity and to divergences. A partial remedy is to postulate a massive charged field W, as sketched in Fig. 2, coupled to the current with a strength g. Such models require that

$$g^2/m_W^2 = 8G_F/\sqrt{2}, \tag{5}$$

but are unable to predict either g or M_W, and in any case do not allow a fully renormalizable theory.

The weak neutral currents may be ascribed to a Lagrangian

$$L^{NC} \sim (G_F/\sqrt{2})\rho J_\mu^{NC}(J^{NC})_\mu^\dagger, \tag{6}$$

where the parameter ρ is included to allow for a possible difference in strength between

neutral and charged currents (Ross and Veltman 1975; Hung and Sakurai 1978). A typical neutral-current process is sketched in Fig. 3.

Weak neutral currents were first observed by the Gargamelle collaboration (Hasert *et al.* 1973), and since then they have been one of the main testing grounds of the GSW model (we discuss the existing data in Section 4). Neutral-current interactions do not modify the quark flavour; decays such as $K^+ \rightarrow \pi^+ \nu\bar{\nu}$ occur at most 10^{-7} times less frequently than their charged-current counterparts $K^+ \rightarrow \pi^0 e^+ \nu$. The justification of the GIM ansatz was that it predicted that neutral currents be flavour-conserving at least in models, such as the GSW, where the neutral current is the commutator of the charged ones:

$$J_\mu^{NC} \sim [J_\mu, J_\mu^\dagger].$$

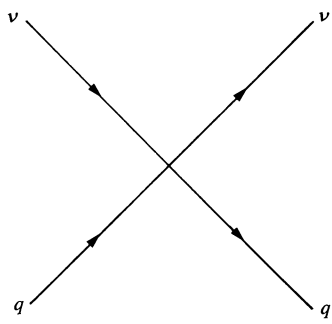

Fig. 3. Neutral-current reaction in which a neutrino scatters on a quark, shown here as a four-point coupling.

(2b) QED as a Gauge Theory

It is instructive to commence with a heuristic discussion of how a local gauge invariance (LGI) can prescribe the form of a well-known and well-tested theory, quantum electro-dynamics (QED). The Lagrangian field density for a free, massive, spin-$\frac{1}{2}$ fermion is

$$L_0 = \bar{f}[i\gamma_\mu \partial_\mu - m]f, \tag{7}$$

where the space–time dependence of the fermion field $f(x)$ has been omitted for conciseness, and where $\partial_\mu \equiv \partial/\partial x_\mu$. The familiar Dirac equation is directly obtainable from (7) via the Euler–Lagrange equations. The phase of f is unobservable. The central statement of LGI is that observers at different points in the Universe are free to choose the phase independently, while leaving the Lagrangian, and hence the 'physics', unchanged. If

$$f \rightarrow f' = Uf = e^{i\Lambda(x)}f, \tag{8}$$

then the corresponding change to L_0 is

$$L_0 \rightarrow L_0' = L_0 + \delta L,$$

where $\delta L = i\bar{f}\gamma_\mu[U^{-1}(\partial U/\partial x_\mu)]f$, and L_0 is not gauge invariant. The 'minimal', or

most economic, way to remedy this is to replace the derivative ∂_μ with the covariant derivative

$$D_\mu = \partial_\mu - icA_\mu(x) \tag{9}$$

and to require that the phase transformation on f be accompanied by a 'stretching' of the field A_μ in (9):

$$A_\mu \to A'_\mu = A_\mu + \delta A_\mu .$$

LGI is restored if

$$\delta A_\mu = -(i/c)[U^{-1}(\partial U/\partial x_\mu)] = (1/c)\partial\Lambda(x)/\partial x_\mu ,$$

and the revised Lagrangian becomes

$$L = \bar{f}[i\gamma_\mu \partial_\mu - m]f + c(\bar{f}\gamma_\mu f)A_\mu . \tag{10}$$

Comparing (7) and (10), one observes that the fermion f is no longer free, since the extra term in (10) represents its interaction with a vector field A_μ, at a strength determined by the coupling constant c. If this field A_μ is to be associated with a physical particle, or 'gauge boson', then a kinetic term must be introduced to describe its free propagation, and the final Lagrangian is

$$L = \bar{f}[i\gamma_\mu \partial_\mu - m]f + c(\bar{f}\gamma_\mu f)A_\mu - \tfrac{1}{4}F_{\mu\nu}F^{\mu\nu} , \tag{11}$$

where $F_{\mu\nu} = \partial_\mu A_\nu - \partial_\nu A_\mu$. This is just the familiar Lagrangian of QED, the middle term being an interaction of a fermion current with the photon field (see Fig. 4). If a particle mass is introduced, via a term $\frac{1}{2}M_A^2 A_\mu A_\mu$ in the Lagrangian, then the invariance is broken. The theory so far is therefore limited to massless gauge bosons, as is indeed the case for the photon, the gauge boson of QED.

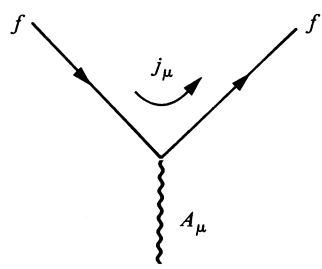

Fig. 4. Interaction term in the QED Lagrangian (10).

The important point is that the QED Lagrangian (11) has been derived by demanding a LGI (8), although historically the property of gauge invariance was remarked upon after the construction of the Lagrangian (11). Transformations of the type (8) are representations of the group U(1), which is Abelian as the elements of the group commute:

$$UU' = U'U .$$

The symmetry is easily extended to include many fermions, quarks and leptons, with fields $f_j(x)$ and electric charges q_j [measured in units of e, the magnitude of the

charge on the electron, i.e. $q(e) = -1$]. The Lagrangian (11) may be generalized to

$$L = \Sigma\{\bar{f}_j[\mathrm{i}\gamma_\mu \partial_\mu - m_j]f_j + eq_j(\bar{f}_j\gamma_\mu f_j)A_\mu\} - \tfrac{1}{4}F_{\mu\nu}F^{\mu\nu},$$

with local transformations

$$f_j \to f_j' = \mathrm{e}^{\mathrm{i}q_j\Lambda(x)} f_j, \qquad A_\mu \to A_\mu' = A_\mu + (1/e)\partial\Lambda(x)/\partial x_\mu .$$

Only one vector field A_μ is introduced, to which each fermion current couples with a strength eq_j, and the phase of the fermion fields at a common space–time point transform with a common phase $\Lambda(x)$, scaled by their charge q_j.

(2c) Basic Theoretical Ideas

In this review, we choose not to give a rigorous derivation of the standard model. Instead the ideas behind the model are shown to be plausible and the key tests of the model are highlighted. Firstly, the idea of LGI is extended, using one pair of massless fermions as an example, to SU(2)×U(1). Masses, for both fermions and gauge bosons, are then introduced via spontaneous symmetry breaking (SSB). The model is then extended to include all known fermions.

Non-Abelian Gauge Theories. The ideas of non-Abelian gauge theories are developed here using one pair of leptons (ν_l, l^-) as an example. Initially they are required to be massless, and the subscript on ν_l will be dropped for simplicity.

It is well known (see definitions 3 and 4) that the left-handed components of fermions couple to the charged weak field in pairs, while the right-handed components decouple. This suggests the grouping of the left-handed components into doublets, while the right-handed components remain as singlets:

$$\psi_1 = (\nu, l)_\mathrm{L}, \qquad \psi_2 = l_\mathrm{R}, \qquad \psi_3 = \nu_\mathrm{R},$$

where $f_\mathrm{L} = \frac{1}{2}(1-\gamma_5)f$ and $f_\mathrm{R} = \frac{1}{2}(1+\gamma_5)f$. Experimentally there is no evidence for the existence of a right-handed neutrino, but its presence causes no problems for the model, and it is retained here to facilitate the extension of the model to the quarks.

The grouping of fields into doublets immediately suggests the use of the familiar group SU(2), where ψ_1 is a doublet of weak isospin, while ψ_2 and ψ_3 are weak isospin singlets. The concept of fields undergoing local SU(2) transformations was first considered by Yang and Mills (1954) in the context of strong isospin, which is mathematically identical to weak isospin but physically quite distinct.

The starting point is the Lagrangian for the free fermion fields:

$$L_0 = \Sigma\,\bar{\psi}_\alpha[\mathrm{i}\gamma_\mu \partial_\mu]\psi_\alpha . \tag{12}$$

The basic physics principle is that L_0 is required to be invariant under local gauge transformations generated by the group SU(2)×U(1). It will soon become apparent that U(1) cannot be the familiar $\mathrm{U(1)_{em}}$ discussed earlier, but that a new 'charge' must be introduced to provide the couplings of the fermions to the corresponding field. This charge is hypercharge Y (or more properly, weak hypercharge Y_W) and the assignments of the GSW model are summarized in Table 2. For convenience, the quark quantum numbers, which will be discussed below, are included in Table 2.

What are the requirements of demanding that L_0 be invariant under local gauge transformations

$$\psi_a \to \psi_a' = \mathrm{U}_2\,\mathrm{U}_1\,\psi_a\,,$$

where U_1 and U_2 are, respectively, unitary matrices representing the groups $\mathrm{U}(1)_Y$ and SU(2)? The parametrizations of U_1 and U_2 are

$$\mathrm{U}_1 = \exp\{\mathrm{i}\,Y\Lambda(x)\}\,, \qquad \mathrm{U}_2 = \exp\{\mathrm{i}\,\boldsymbol{T}\,.\,\boldsymbol{\Theta}(x)\}\,.$$

The form of U_1 parallels the QED example discussed earlier. The three operators T_σ are the generators of weak isospin rotations and are related to the familiar Pauli matrices:

$$T_\sigma = \tfrac{1}{2}\tau_\sigma\,.$$

Further, $\boldsymbol{\Theta}(x)$ represents three phases, i.e. an isovector, all components of which may be freely chosen at each point in space–time. A feature of the SU(2) transformations is their non-commutability, i.e. $\mathrm{U}_2\,\mathrm{U}_2' \neq \mathrm{U}_2'\,\mathrm{U}_2$, which is reflected in the non-commutability of the generators,

$$[T_i, T_j] = \mathrm{i}\epsilon_{ijk}\,T_k\,,$$

and which has far-reaching consequences as discussed below.

Table 2. Weak quantum number assignments

The convention used here, $q = T^3 + Y$, is that of Jarlskog (1982) and Goggi (1984). Many authors (see e.g. Aitchison and Hey 1982) prefer to use $q = T^3 + \frac{1}{2}Y$ in analogy with strong isospin and hypercharge. The difference of convention leads to a subsequent difference in the definition of the covariant derivatives D_μ, but has no physical consequences

	q	T	T^3	Y
ν_L	0	$\frac{1}{2}$	$+\frac{1}{2}$	$-\frac{1}{2}$
l_L	-1	$\frac{1}{2}$	$-\frac{1}{2}$	$-\frac{1}{2}$
ν_R	0	0	0	0
l_R	-1	0	0	-1
q_L	$+\frac{2}{3}$	$\frac{1}{2}$	$+\frac{1}{2}$	$\frac{1}{6}$
q_L'	$-\frac{1}{3}$	$\frac{1}{2}$	$-\frac{1}{2}$	$\frac{1}{6}$
q_R	$+\frac{2}{3}$	0	0	$+\frac{2}{3}$
q_R'	$-\frac{1}{3}$	0	0	$-\frac{1}{3}$

LGI is restored by replacing the derivative ∂_μ appearing in (12) by a covariant derivative D_μ, and by a simultaneous 'stretching' of the fields appearing in D_μ:

$$\partial_\mu \to \mathrm{D}_\mu = \partial_\mu - \mathrm{i}g'\,Y B_\mu - \mathrm{i}g\boldsymbol{T}\,.\,\boldsymbol{W}_\mu\,,$$

$$B_\mu \to B_\mu' = B_\mu + (1/g')\partial\Lambda(x)/\partial x_\mu\,,$$

$$\boldsymbol{W}_\mu \to \boldsymbol{W}_\mu' = \boldsymbol{W}_\mu + (1/g)\partial\boldsymbol{\Theta}/\partial x_\mu - \boldsymbol{\Theta}\times\boldsymbol{W}_\mu\,.$$

The revised Lagrangian now couples the fermions to a new field B_μ via their hypercharge, and to a new triplet of fields W_μ via their isospin. Unknown constants, g' and g, describe the strengths of these couplings. The stretching term δB_μ exactly parallels that found for $U(1)_{em}$, but δW_μ contains a new ingredient, $\boldsymbol{\Theta} \times W_\mu$, arising from the non-Abelian nature of the group SU(2). If the new fields are to be associated with physical particles, kinetic terms must be added to L_0, which becomes

$$L_0 + \Sigma\, \overline{\psi}_\alpha[\mathrm{i}\gamma_\mu \partial_\mu + \gamma_\mu\, g\boldsymbol{T}\,.\, W_\mu + \gamma_\mu\, g'\, Y B_\mu]\psi_\alpha$$
$$-\tfrac{1}{4} B_{\mu\nu}\, B^{\mu\nu} - \tfrac{1}{4}\, \Sigma\, W^k_{\mu\nu}(W^{\mu\nu})^k, \tag{13}$$

where

$$B_{\mu\nu} = \partial_\mu\, B_\nu - \partial_\mu\, B_\nu,$$
$$W^k_{\mu\nu} = \partial_\mu\, W^k_\nu - \partial_\nu\, W^k_\mu + g\epsilon^{klm}\, W^l_\mu\, W^m_\nu\,.$$

and where k on W^k_μ is an isospin index.

The remarks made in Section 2*b* concerning the mass of the field A_μ are still valid. The Lagrangian (13) is only invariant if $M_B = M_W = 0$. Indeed, the introduction of a fermion mass term, $\overline{\psi}_\alpha\, m_\alpha\, \psi_\alpha$, would also break the invariance due to the non-Abelian nature of the SU(2) transformations. Given these restrictions, (13) is clearly not the required Lagrangian, and the essential question of the masses is discussed later. Before proceeding, however, an examination of the interaction terms in (13) is of great interest.

The interaction terms in (13) may be written as

$$g\boldsymbol{J}^{(T)}_\mu\, W_\mu + g' j^{(Y)}_\mu\, B_\mu, \tag{14}$$

where

$$\boldsymbol{J}^{(T)}_\mu = \Sigma\, \overline{\psi}_\alpha\, \gamma_\mu\, \boldsymbol{T}\psi_\alpha, \qquad j^{(Y)}_\mu = \Sigma\, \overline{\psi}_\alpha\, \gamma_\mu\, Y\psi_\alpha\,.$$

The fermion isospin and hypercharge currents couple to the W and B fields with strengths g and g' respectively. As usual, the physical charged particles associated with W are $W^\pm = \sqrt{\tfrac{1}{2}}(W^1 \mp \mathrm{i}\, W^2)$ and T is related to isospin raising and lowering operators, $T^\pm = \tfrac{1}{2}\tau^\pm$, where $\tau^\pm = \tau_1 \pm \mathrm{i}\tau_2$. Two of the terms in (14) may therefore be pictured as the interaction of a charged W with a charge-changing fermion current (see Fig. 5). This current is purely left-handed, because the right-handed fermions are assumed to be iso-singlets in this model.

The remaining terms in (14) may be described as the interactions of neutral fields with charge-conserving currents (see Fig. 6). Whereas the charged interactions agree precisely with our knowledge of the weak interaction, neither the W^0 nor the B^0 field can be associated with the photon, which couples equally to e_L and e_R and not at all to ν_L or ν_R. A key feature of the model is how a linear combination of the fields can be associated with the photon field A.

We define new fields (A_μ and Z_μ) as linear combinations of W^3_μ and B_μ, via an arbitrary unitary transformation

$$\begin{pmatrix} B \\ W^3 \end{pmatrix} = \begin{pmatrix} \cos\theta & -\sin\theta \\ \sin\theta & \cos\theta \end{pmatrix} \begin{pmatrix} A \\ Z \end{pmatrix}. \tag{15}$$

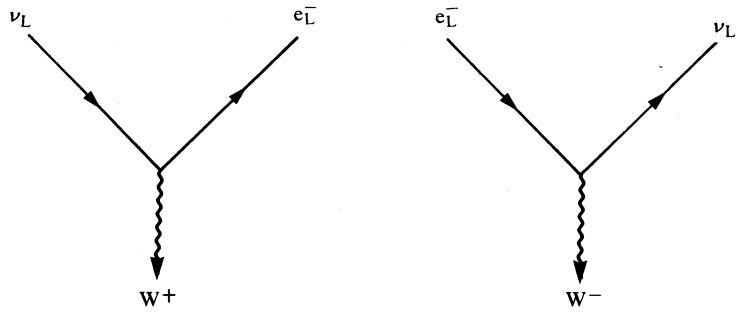

Fig. 5. Interaction terms in the GSW Lagrangian (13) corresponding to charged-current interactions.

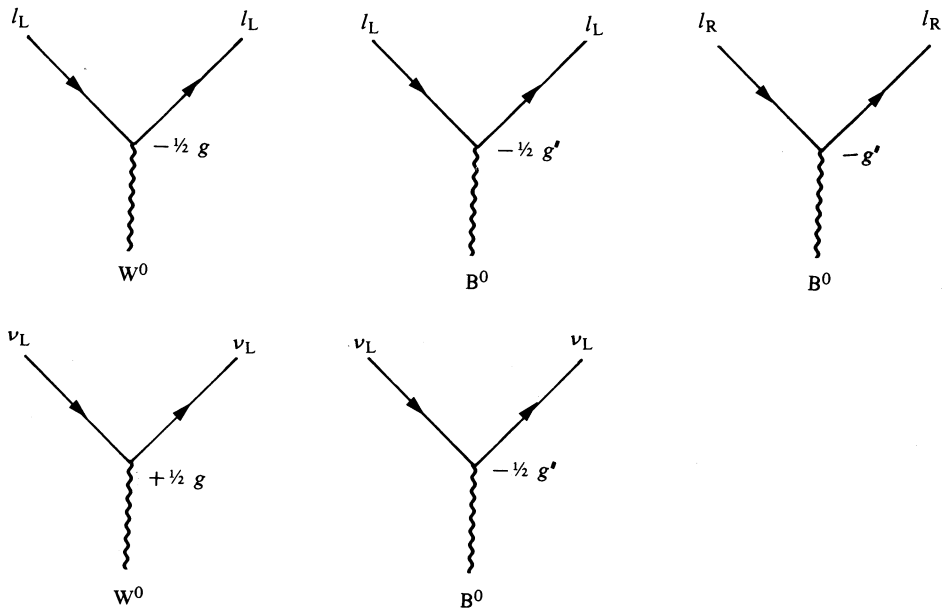

Fig. 6. Interaction terms in the GSW Lagrangian (13) corresponding to neutral-current interactions.

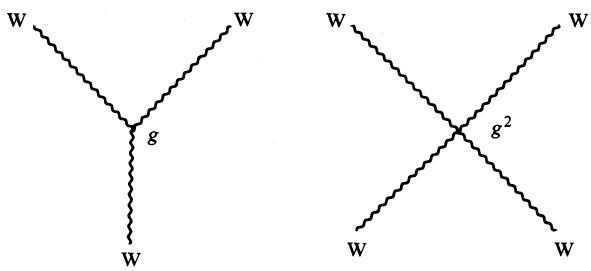

Fig. 7. The W self-coupling terms in the GSW Lagrangian (13).

The two neutral-current terms in (14) may be rewritten as

$$gJ_\mu^{(3)} W_\mu^3 + g' j_\mu^{(Y)} B_\mu$$
$$= (g \sin\theta\, J_\mu^{(3)} + g' \cos\theta\, j_\mu^{(Y)}) A_\mu + (g \cos\theta\, J_\mu^{(3)} - g' \sin\theta\, j_\mu^{(Y)}) Z_\mu . \quad (16)$$

The relationship between $J_\mu^{(3)}$, $j_\mu^{(Y)}$ and the electromagnetic current $j_\mu^{(\mathrm{em})}$ is given directly by the relationship between their operators $Q = T^3 + Y$:

$$j_\mu^{(\mathrm{em})} = J_\mu^{(3)} + j_\mu^{(Y)} .$$

Therefore, in order to equate the first term in (16) with the familiar interaction term of QED, one sets $\theta = \theta_\mathrm{W}$, where

$$g \sin\theta_\mathrm{W} = g' \cos\theta_\mathrm{W} = e . \quad (17)$$

This particular choice of θ was originally due to Glashow; θ_W is called the 'Weinberg angle' or 'weak angle'. The second term in (16) may be re-arranged to give

$$(g/\cos\theta_\mathrm{W})(J_\mu^{(3)} - \sin^2\theta_\mathrm{W}\, j_\mu^{(\mathrm{em})}) Z_\mu . \quad (18)$$

Thus, the coupling of fermions to the neutral weak field Z is exactly specified.

One other feature of the Lagrangian (13) deserves special attention. In the kinetic part for the W field there appears the term

$$W_{\mu\nu}^k \sim g\epsilon^{klm} W_\mu^l W_\nu^m .$$

This leads to self-couplings of the type shown in Fig. 7 which are novel and important features of non-Abelian gauge theories.

Spontaneous Symmetry Breaking. The concept of the generation of masses via spontaneous symmetry breaking (SSB), while obviously of great importance if the theory is to represent the real world, is only briefly summarized here. It is the most technical aspect of the GSW model and several excellent reviews exist (see e.g. Jarlskog 1982; Eichten *et al.* 1985).

Consider a complex scalar field, $\phi = \sqrt{\tfrac{1}{2}}(\phi_1 + \mathrm{i}\phi_2)$, and the potential $V(\phi)$ sketched in Fig. 8, which exhibits a clear symmetry. The 'vacuum', defined as the state of lowest energy, may be given without loss of generality as $\phi_0 = \sqrt{\tfrac{1}{2}}\, v$, where v is real. If the field $\phi(x)$ is expanded about ϕ_0,

$$\phi(x) = \sqrt{\tfrac{1}{2}}\{ v + h(x) + \mathrm{i}\xi(x)\} ,$$

then it is easy to demonstrate that the h field acquires a mass, while the ξ field remains massless. The underlying symmetry is not apparent in $h(x)$, i.e. the original symmetry is now 'spontaneously broken' or 'hidden'. Goldstone (1961) had shown that the spontaneous breaking of any continuous symmetry leads to an unwanted (because it is not observed), massless scalar particle, or 'goldstone boson'.

Higgs (1964, 1966) extended these ideas to the class of local gauge symmetries, and a 'miracle' occurred. The simplest case is the U(1) symmetry discussed in Section 2*b* together with a single complex scalar field $\phi(x)$. Then, for a particular choice of gauge, the Goldstone boson does not appear, the Lagrangian instead describing two massive interacting particles, namely a Higgs scalar and a massive vector gauge boson. The Goldstone boson has become the required longitudinal polarization of the massive vector boson. (This is clearly not desirable in QED where, indeed, the symmetry is not broken.)

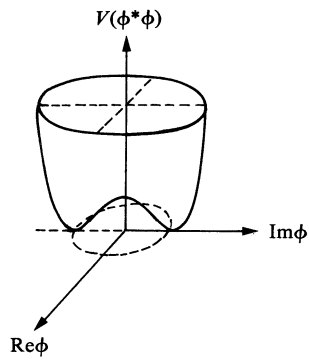

Fig. 8. Potential $V(\phi)$ relevant to the discussion of spontaneous symmetry breaking.

The extension of SSB to SU(2)×U(1) is more complicated. In view of the four generators involved [three for SU(2) and one for U(1)], then four real scalar fields θ must be introduced. The most economical way (Weinberg 1967) is a complex iso-doublet

$$\phi = \sqrt{\tfrac{1}{2}}\begin{pmatrix}\phi_1+\mathrm{i}\phi_2\\ \phi_3+\mathrm{i}\phi_4\end{pmatrix}, \tag{19}$$

with a real vacuum expectation value

$$\phi_0 = \sqrt{\tfrac{1}{2}}\begin{pmatrix}0\\ v\end{pmatrix}.$$

By this mechanism, the charged W fields acquire a mass

$$M_{\mathrm{W}} = \tfrac{1}{2}vg. \tag{20}$$

For the neutral fields, W^3 and B, one can find orthogonal linear combinations, A and Z, such that one field is massless ($M_A = 0$) while the other field acquires a mass

$$M_{\mathrm{Z}} = \tfrac{1}{2}v(g^2+g'^2)^{\frac{1}{2}}. \tag{21}$$

The required transformation from the W^3, B fields to the A, Z fields is that already specified in equations (15) and (17). This is not accidental; of the four generators of SU(2)×U(1), namely T and Y, only the combination $Q = T^3 + Y$ has the property that $Q.\phi_0 = 0$. The chosen vacuum is invariant under $\mathrm{U(1)_{em}}$ transformations and the photon remains massless.

The ratio of the gauge boson masses is independent of v. For the standard model, (20) and (21) combine to give

$$M_{\mathrm{W}} = \rho^{\frac{1}{2}} M_{\mathrm{Z}} \cos\theta_{\mathrm{W}}, \tag{22}$$

with $\rho \equiv 1$. [The parameter ρ here is precisely the relative strength of the charged and neutral weak couplings introduced in equation (6). Other, less economical, Higgs mechanisms are possible; these lead to $\rho \neq 1$.]

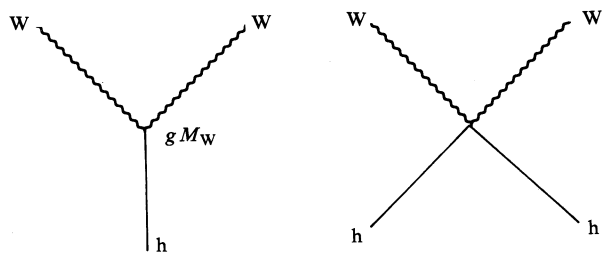

Fig. 9. Couplings of the Higgs boson to the W boson in the GSW Lagrangian after spontaneous symmetry breaking.

The problem of the fermion masses remains but, before addressing that problem, it is useful to summarize what has so far been achieved. By means of the Higgs mechanism, the Lagrangian has been extended to permit massive $W^{\pm}$ and Z fields, the photon remaining massless. The masses M_{W} and M_{Z} are predicted in terms of one new parameter v. The cost is the introduction of a neutral massive scalar field, $h(x)$. The mass of this Higgs particle is not given by the theory, but its couplings are. The modified Lagrangian (not given in full here) has terms

$$L \sim g^2(\tfrac{1}{2}vh+\tfrac{1}{4}h^2)\left(W_\mu^+ W_\mu^- + \frac{1}{2\cos^2\theta_{\mathrm{W}}} Z_\mu Z_\mu^\dagger\right),$$

corresponding to couplings of the type pictured in Fig. 9 (plus similar tri-linear and quadri-linear couplings to pairs of Z^0). The hWW vertex is strong, the coupling constant g being multiplied by M_{W}.

An attractive feature of the GSW model is that the same Higgs doublet (19) which 'generated' the boson masses, also allows fermion masses to be introduced. It is possible to introduce SU(2)×U(1) gauge invariant Higgs–fermion couplings into the Lagrangian which, after SSB, lead to the terms

$$L = -m_f \bar{f}f - (m_f/v)\bar{f}f\,h = -m_f \bar{f}f - \tfrac{1}{2}g(m_f/M_{\mathrm{W}})\bar{f}f\,h.$$

The theory does not give the fermion masses m_f, but it does predict that each fermion couples to the Higgs field with a strength proportional to the fermion mass.

Lastly, all of this theoretical work would have been in vain if it removed from the local gauge theory its key property of renormalizability. It was left to 't Hooft (1971*a*, 1971*b*) to show that this was not so.

Generalization to Many Fermions. The above discussion has been limited to a single pair of leptons (ν_l, l^-), differing in electric charge by one unit. The weak quantum number assignments for this pair are given in the top half of Table 2. Three

lepton families are well established: (ν_e, e^-), (ν_μ, μ^-) and (ν_τ, τ^-), and these are easily included in the model, by postulating the same weak quantum numbers for each family. All three lepton families are assumed to couple to the W and B fields with the same constants (g and g') respectively—this is termed lepton universality—and lepton-changing currents, for example $\bar{\nu}_e \gamma_\mu \tau^-$, are assumed not to exist.

In the standard model, the quarks are also grouped into pairs (q, q'), differing by one unit of electric charge, and are also assumed to occur as left-handed iso-doublets and right-handed iso-singlets. All known quarks have $q = -\frac{1}{3}$ or $+\frac{2}{3}$ and the standard assignments are given in the bottom half of Table 2. A more open question is how to choose (q, q') in terms of the known mass eigenstates revealed by hadron spectroscopy. Three quarks with $q = -\frac{1}{3}$ (namely d, s and b) are well established. It is widely believed (and is assumed here) that three $q = +\frac{2}{3}$ states also exist (u, c and t). Experimental evidence for the t quark has been reported, and is discussed in a later section. It has long been estalished that the charge-changing weak interactions do not respect quark flavour.

The most general possible assumption (Jarlskog 1982) is to relate the $q = -\frac{1}{3}$ weak eigenstates to the $q = -\frac{1}{3}$ mass eigenstates via a unitary transformation:

$$\begin{bmatrix} d' \\ s' \\ b' \end{bmatrix} = U_{KM} \begin{bmatrix} d \\ s \\ b \end{bmatrix}.$$

The 3×3 matrix U_{KM}, introduced by Kobayashi and Maskawa (1973), is characterized by three real angles (one of them the Cabbibo angle) and a complex phase which is responsible for CP violation. It is easy to demonstrate that the introduction of a second transformation, between the $q = +\frac{2}{3}$ weak and mass eigenstates is redundant, and can be absorbed into U_{KM}. The quark currents are assumed also to couple to the W and B fields, with strengths g and g' respectively. This is quark–lepton universality. The status of experimental investigations of this matrix has recently been reviewed by Chau (1983).

Neutral-current Couplings. The strengths of the couplings of fermions to the neutral Z field offer a method of measuring θ_W and of testing the model. The couplings implicit in equation (18) will be detailed here. We define

$$J_\mu^{(NC)} = J_\mu^{(3)} - \sin^2\theta_W j_\mu^{(em)} = \tfrac{1}{2} \Sigma \bar{f}\gamma_\mu(g_V - g_A\gamma_5)f.$$

It is a feature of the model that the neutral currents conserve flavour.

The constants g_V and g_A are related to the fermion charge q_f and to $T_L^{(3)}$, the third component of weak isospin of the left-handed fermion:

$$g_V = T_L^{(3)} - 2q_f \sin^2\theta_W, \qquad g_A = T_L^{(3)}.$$

Values of g_V and g_A are given in Table 3, with the caveat that many differing conventions exist in the literature. It is also useful to define chiral couplings via $g_{L,R} = \frac{1}{2}(g_V \pm g_A)$, and these are also tabulated.

Table 3. Weak neutral-current couplings ($x = \sin^2\theta_W$)

	$(\nu_e, \nu_\mu, \nu_\tau)$	(e^-, μ^-, τ^-)	(u, c, t)	(d, s, b)
$t_L^{(3)}$	$+\frac{1}{2}$	$-\frac{1}{2}$	$+\frac{1}{2}$	$-\frac{1}{2}$
q_f	0	-1	$+\frac{2}{3}$	$-\frac{1}{3}$
g_V	$+\frac{1}{2}$	$-\frac{1}{2}+2x$	$\frac{1}{2}-\frac{4}{3}x$	$-\frac{1}{2}+\frac{2}{3}x$
g_A	$+\frac{1}{2}$	$-\frac{1}{2}$	$+\frac{1}{2}$	$-\frac{1}{2}$
g_L	$+\frac{1}{2}$	$-\frac{1}{2}+x$	$\frac{1}{2}-\frac{2}{3}x$	$-\frac{1}{2}+\frac{1}{3}x$
g_R	0	x	$-\frac{2}{3}x$	$\frac{1}{3}x$
$g_V^2+g_A^2$ *	0·50	0·25	0·29	0·38

* For $x = 0{\cdot}217$.

(2d) Testing the Model

One would like to test the model as completely as possible. Two important tests of the model have of course already been satisfied. Neutral-current interactions have been observed at about the expected rates, and the W and Z gauge bosons have been discovered with about the correct masses. It is now important to determine if the neutral-current couplings and the boson masses are exactly as predicted by the minimal GSW model, or if more exotic couplings and particles are required. In Sections 3 and 4 of this review, we discuss in detail predictions of the model for the gauge bosons and for neutral currents respectively, and confront them with the existing experimental data. Two other important predictions of the GSW model are unlikely to be tested in the near future. The non-Abelian nature of the SU(2) gauge transformations leads to gauge boson self-couplings as pictured in Fig. 7, and the mechanism of SSB requires the existence of a Higgs scalar where mass is undetermined in the model.

An eventual discrepancy between experiment and the model predictions may be fundamental, or may be due simply to the neglect of radiative corrections. Higher order diagrams, in both the weak and electromagnetic interactions, can be important. These corrections will be discussed in the relevant sections below.

In addition to the masses of the fermions, the mass of the Higgs scalar and the elements of the KM matrix, the model requires three parameters (or four if $\rho \neq 1$ is considered). These are v, and any two of g, g', e and $\sin^2\theta_W$. The value of e is well known through the fine structure constant of atomic physics, $\alpha = e^2/4\pi$, and the Fermi constant G_F is best measured in μ-decay. The accepted values, as listed by the Particle Data Group (1984), are $\alpha^{-1} = 137{\cdot}03604(11)$ and $G_F = 1{\cdot}16637(2)\times 10^{-5}\ \mathrm{GeV}^{-2}$, where the numbers in parentheses are the uncertainties in the last significant figures. The constant G_F is directly related to v; equations (5) and (20) may be combined to yield $v = (\sqrt{2}\,G_F)^{-1/2}$, and hence $v = 246$ GeV. The third and only new parameter, $\sin^2\theta_W$, was initially measured in a number of experiments at low q^2, which will be discussed later, and these measurements enabled the masses of the W and Z gauge bosons to be predicted. However, it is logical to define $\sin^2\theta_W$ at the natural mass scale of the weak interactions, via

$$\sin^2\theta_W \equiv 1-(M_W/M_Z)^2\,. \tag{23}$$

Radiative corrections must then be applied to values of $\sin^2\theta_W$ measured at the values of $q^2 \ll M_W^2$.

The predicted masses and branching fractions of the gauge bosons, their expected production cross sections and the asymmetries expected for their decay products motivated the design of the CERN $\bar{p}p$ Collider, and of the UA1 and UA2 experiments at the Collider. We summarize these properties here, prior to a description of the Collider and the experiments in Section 3.

Masses of the W and Z. The masses of the bosons are given by

$$M_W = 0{\cdot}5vg = 0{\cdot}5ve/\sin\theta_W, \qquad M_Z = M_W/\cos\theta_W. \tag{24}$$

Using the values of e and v given above, taking $\sin^2\theta_W = 0{\cdot}220$ from low energy experiments, and making the necessary radiative corrections, the predicted masses from Marciano and Sirlin (1984) are 83·0 and 93·8 GeV respectively for the W and Z bosons.

Widths of the W and Z. The partial width for $W \to e\nu$, for massless leptons, follows from the interaction Lagrangian, and is

$$\Gamma(W{\to}e\nu) = \Gamma_0 = G_F M_W^3/6\pi\sqrt{2} \sim 0{\cdot}250\ \text{GeV},$$

where the predicted mass given above was used. If one of the final-state fermions is massive, this width is modified by a factor

$$F = (1-x)^2(1+\tfrac{1}{2}x); \qquad x = (m_f/M_W)^2.$$

Even for the τ lepton, F is close to unity, and hence lepton universality predicts equal rates for the three leptonic decay modes $W{\to}e\nu, \mu\nu, \tau\nu$. The W also decays into qq' pairs, and the quarks will normally fragment to produce jets of hadrons, at a rate $\Gamma(W \to qq') = 3\Gamma_0$, where the factor 3 arises from colour. The experimental determination of the total W decay rate into pairs of jets is feasible. For three families of massless quarks, $\Gamma(W{\to}\text{jets}) = 9\Gamma_0$. The factor 9 is an important prediction, arising mainly from lepton–quark universality and the existence of colour. A comparison of $\Gamma(W{\to}\text{jets})$ and $\Gamma(W{\to}e\nu)$ would have to consider radiative corrections, the mass of the t quark, and QCD effects which enhance $\Gamma(W{\to}\text{jets})$ by a factor $\{1+\alpha_s(M_W)/\pi\}$, i.e. about 5%. The predicted total W width, for a top-quark mass of 40 GeV, is $\Gamma(W{\to}\text{all}) = 2{\cdot}83$ GeV.

The partial widths of the Z^0 are given in terms of

$$\Gamma_0' = G_F M_Z^3/6\pi\sqrt{2} \sim 0{\cdot}361\ \text{GeV}.$$

Neglecting fermion masses and radiative corrections, we then have

$$\Gamma(Z^0{\to}ll) = \Gamma_0'\{g_V^2(l)+g_A^2(l)\},$$

$$\Gamma(Z^0{\to}qq) = 3\Gamma_0'\{g_V^2(q)+g_A^2(q)\}.$$

Values of g_V and g_A have been given in Table 3 in terms of $\sin^2\theta_W$. Using $\sin^2\theta_W = 0{\cdot}220$, the model predicts a total width $\Gamma(Z^0{\to}\text{all})$ of between 3·10 GeV (for $m_{top} = 0$) and 2·77 GeV (for $m_{top} > 0{\cdot}5M_Z$). The Z^0 total width has been

measured at the Collider, and the measurements have sufficient precision that we can begin to test the assumptions made in the above derivation. For example, the existence of other lepton or quark families, or of supersymmetric particles (for a recent review see Nanopoulos and Savoy-Navarro 1984), would all lead to larger widths than those given here.

Charge Asymmetry and V–A Coupling. The standard model was constructed such that only left-handed fermions couple to the charged W fields, in accord with the V–A phenomenological model of the weak interactions. It predicts an asymmetry in leptons, or indeed any pair of fermions, produced via $\bar{p}p \rightarrow W \rightarrow l\nu_l$. Only left-handed quarks and right-handed antiquarks (generally valence quarks in $\bar{p}p$ interactions) in the beam projectiles can fuse to form a $W^{\pm}$, which is therefore completely longitudinally polarized. The subsequent decay $W^+ \rightarrow e^+_R \nu_L$, or its charge conjugate, therefore favours configurations in which an e^+ is emitted in the direction of the incident $\bar{p}$ or an e^- in the proton direction. Unfortunately, a V+A coupling at both vertices would yield the same prediction. With polarized p and/or $\bar{p}$ beams, more stringent tests would be possible. Alternatively, a third weak decay (e.g. $W \rightarrow \tau\nu$, $\tau \rightarrow e\nu\nu$) would permit a distinction between V+A and V−A couplings (see also Section 4*a* and Goggi 1979).

3. Results from the CERN Proton–Antiproton Collider

A considerable body of data, existing before operation of the $\bar{p}p$ Collider, was in outstanding agreement with predictions of the GSW model. These data involved processes resulting from the exchange of a virtual W or Z^0 (see Section 4). However, it was only after construction of the CERN $\bar{p}p$ Collider (Billinge *et al.* 1979; Staff of CERN $\bar{p}p$ Project 1981) that centre-of-mass collision energies ($\sqrt{s}$) permitting the production of real intermediate vector bosons (IVBs) became available. The UA1 and UA2 experiments provided evidence for the existence of these particles, and since then the two experiments have measured W and Z^0 properties that are in good agreement with predictions of the GSW model.

Following a summary of the $\bar{p}p$ Collider and its performance, we describe the UA1 and UA2 detectors with an emphasis on the capability of each detector to investigate the validity of the GSW model. We then describe aspects of the data that are relevant to the model. We conclude this section with a discussion of future measurements at the $\bar{p}p$ Collider which may provide either additional or more stringent tests of the model.

In this review we discuss those data collected at the Collider which are relevant to the electroweak theory; this is a small fraction of the available data. The recent lectures of Darriulat (1984), Dowell (1984) and DiLella (1985*a*) described other aspects of the data in detail. Also the reports of Wahl (1984) and Radermacher (1984) provided a concise summary of IVB data collected until 1983.

Kinematic variables relevant to this section are discussed in Appendix 1.

(3a) The CERN $\bar{p}p$ Collider

The CERN $\bar{p}p$ Collider was proposed by Rubbia *et al.* (1977) as a realistic means of achieving the $\bar{p}p$ collision energies required to produce W and Z^0 bosons. Using QCD-evolved nucleon structure functions that are measured at lower energy, and

assuming the validity of both the GSW electroweak model and the QCD gauge theory of strong interactions, the W and Z^0 cross sections are expected to vary with $\sqrt{s}$ approximately as in Fig. 10. The most recent calculations are from Altarelli *et al.* (1985). This implies that at the chosen Collider energies of $\sqrt{s} = 546$ GeV and in 1984 $\sqrt{s} = 630$ GeV (these energies being defined by the maximum magnet power dissipation), luminosities of $\mathscr{L} \sim 5\times10^{28}\ \mathrm{cm}^{-2}\,\mathrm{s}^{-1}$ are required to produce W and Z^0 at a measurable rate.* Such luminosities are only obtainable if high intensity, monoenergetic and highly collimated bunches of protons and antiprotons are able to circulate and collide in the CERN SPS.

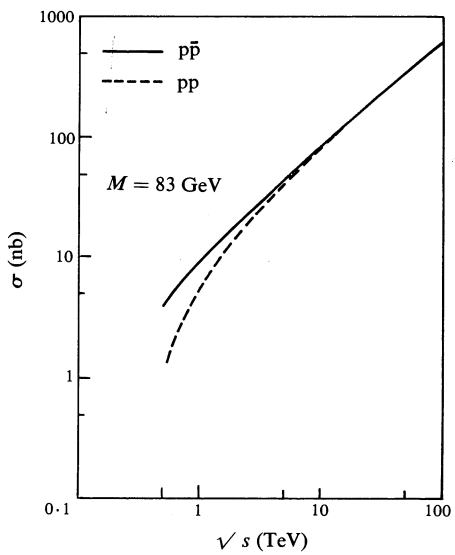

Fig. 10. Predicted cross section for production of an IVB of mass 83 GeV, plotted as a function of $\sqrt{s}$. [From Altarelli *et al.* (1984).]

The original contribution by Rubbia *et al.* (1977) was to recognize that high-intensity $\bar{p}$ bunches could be practically obtained by using the principle of either 'electron cooling' (Budker 1967) or 'stochastic cooling' (Van der Meer 1972). The 'electron cooling' technique uses monoenergetic electron beams to cool a beam, which is disordered in phase-space and momentum, but which travels with the same average velocity. The 'stochastic cooling' technique measures fluctuations about the mean of a disordered beam over a fixed time interval. It then generates from these measurements corrections to the beam trajectory. After repeated applications both the momentum spread and the phase-space spread of the beam is reduced. A review of the stochastic cooling technique has been given by Mohl *et al.* (1980). Each cooling technique was experimentally demonstrated soon after its invention [for electron cooling by Budker *et al.* (1975) and for stochastic cooling by Bramham *et al.* (1975)]. Prior to approval of the $\bar{p}p$ Collider, it was known (Carron *et al.* 1978; Bregman *et al.* 1978) that either technique could be used to produce a nearly monoenergetic $\bar{p}$ beam. The stochastic cooling technique was chosen for technical reasons.

* The luminosity relates the event rate for a given process to the cross section for that process by $N(\mathrm{s}^{-1}) = \mathscr{L}(\mathrm{cm}^{-2}\,\mathrm{s}^{-1})\,\sigma(\mathrm{cm}^2)$.

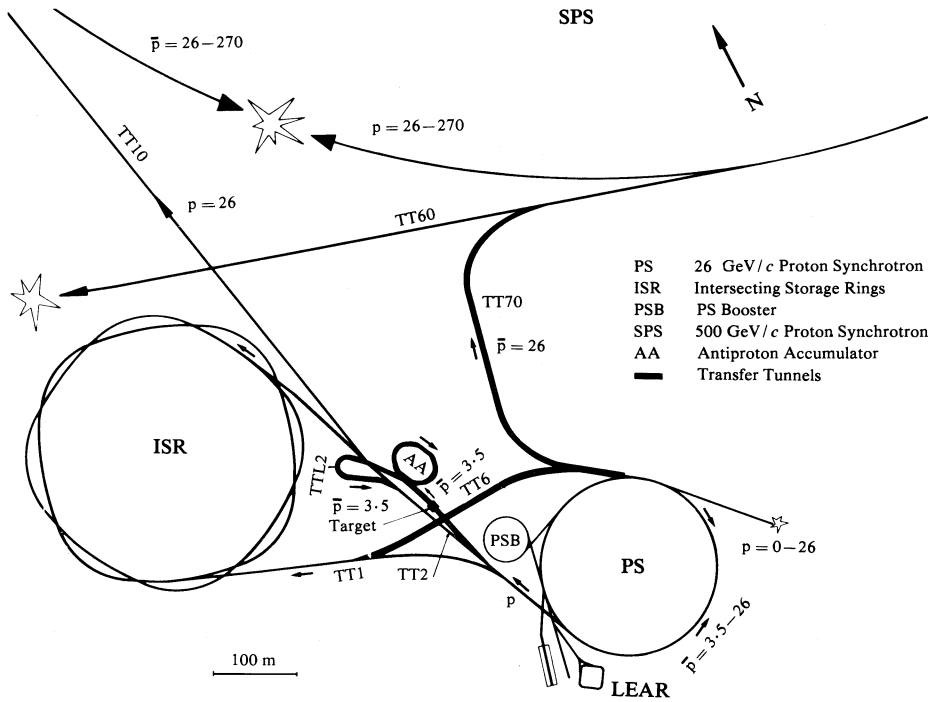

Fig. 11. Overall site layout of the machines used at CERN (PSB, PS and AA) to supply antiprotons to the ISR and the SPS. Proton and antiproton values are in units of GeV/c.

Antiproton–proton collisions are obtained in practice at CERN using a complex of three accelerator rings, shown in the layout of Fig. 11:

(i) At $\sim 2\cdot 4$ s intervals, bunches of $\sim 10^{13}$ protons (p) are extracted from the CERN PS at an energy of 26 GeV, and focussed onto a beryllium target. About 10^7 $\bar{p}$ are produced per bunch, but with large angular and momentum spreads. The maximum $\bar{p}$ yield occurs at a momentum of $3\cdot 5$ GeV/c.

(ii) The $\bar{p}$ produced are electrostatically focussed, and injected into the Antiproton Accumulator (AA). In the $2\cdot 4$ s prior to the following bunch, the $\bar{p}$ are stochastically cooled (from $\delta p/p \sim 0\cdot 015$ to $\sim 0\cdot 002$), then decelerated and added to an existing $\bar{p}$ stack obtained from previous bunches. A stacking capacity of about 5×10^9 $\bar{p}$ per hour is possible, with a maximum stack intensity of about 5×10^{11} $\bar{p}$. The $\bar{p}$ stack is itself continually cooled and a net reduction of $\sim 10^9$ in the product of phase-space and momentum spread is achieved. Intense $\bar{p}$ stacks have been maintained in the AA for as long as one month.

(iii) In successive PS cycles, three p and three $\bar{p}$ bunches are loaded into the SPS. First, bunches of $\sim 10^{11}$ p are injected from the PS at 26 GeV. Then bunches of $\sim 10^{10}$ $\bar{p}$ are extracted from the AA, accelerated in the PS to 26 GeV, and injected into the SPS.

(iv) The six bunches, each 2 ns in duration and about 1 mm in transverse dimension, are accelerated to 273 GeV (more recently 315 GeV) and allowed to

circulate in the SPS for typically 12–24 h. During this time the beam intensity drops exponentially in the SPS with a lifetime of $\tau \sim 15$ h. The maximum lifetime so far achieved is 24 h. The beams collide at six points around the machine, and at the two points used for experimentation the beam is laterally contracted to increase the luminosity. In standard operation, bunch crossings occur every $7 \cdot 7$ μs.

The $\bar{p}p$ Collider has achieved a maximum luminosity of $\mathscr{L} = 3 \cdot 5 \times 10^{29}$ cm^{-2} s^{-1} and since its first operation in 1981 has delivered the following integrated luminosity:

Period	$\sqrt{s}$ (GeV)	$\int \mathscr{L}\, dt$ (nb^{-1})
Dec. 1981	546	$\sim 0 \cdot 023$
Oct.–Dec. 1982	546	~ 28
Apr.–Jun. 1983	546	~ 150
Sep.–Dec. 1984	630	~ 395

The quality of the machine construction and subsequent operation was crucial to the success of the CERN W and Z^0 search. Future improvements, which were recently reviewed by de Raad (1984) and Billinge (1984), will significantly increase the Collider intensity.

A similar machine complex, designed to operate at $\sqrt{s} = 2$ TeV, is scheduled to start operation at FNAL in 1987 [see Harrison (1984) for a status report].

(3b) Design of the UA1 and UA2 Detectors

A total of six experiments have collected data at the $\bar{p}p$ Collider. They have been located in two large underground areas, at $\bar{p}p$ interaction regions in the long straight sections LSS4 and LSS5 of the SPS. Two of the detectors, UA1 (Arnison *et al.* 1978) and UA2 (Banner *et al.* 1978), were designed to study W and Z^0 production and decay.

To fully test the GSW model, all IVB decay modes should be identified with their predicted rates (see Section 2). Possible features of their production and decay which are incompatible with the GSW model should also be identified. Of course, neither detector completely fulfills these requirements.

Prior to the design of the UA1 and UA2 detectors, considerable data on hadronic processes existed at lower energies. Nucleon structure functions were measured using neutrino, muon, electron and hadron probes. At the CERN ISR, data existed showing the dependence of charged multiplicity on $\sqrt{s}$, and the pseudo-rapidity (η) and transverse momentum (p_T) distributions for charged-particle production. These data, together with the predictive power of the GSW model and the QCD gauge theory, enabled an extrapolation of typical event characteristics to energies of the Collider which was, in retrospect, remarkably accurate. The predictions were essential to the design of the UA1 and UA2 detectors. To illustrate this, we can now use $\bar{p}p$ data collected by the UA1, UA2, UA4 and UA5 experiments:

(i) The total $\bar{p}p$ interaction cross section is $\sigma_T = 61 \cdot 9 \pm 1 \cdot 5$ mb at $\sqrt{s} =$ 546 GeV (Bozzo *et al.* 1984). Only about one interaction in 10^7 results in the production of a W or Z^0.

(ii) In a typical 'minimum bias' interaction, particles are produced with a mean charged-particle multiplicity $\langle n_{ch} \rangle = 28 \cdot 9 \pm 0 \cdot 4$ (Arnison *et al.* 1983*b*; Alner *et al.* 1984) and with large event-by-event fluctuations about this value. Particle production

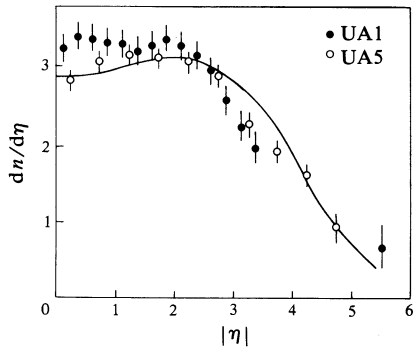

Fig. 12. Pseudo-rapidity density for non-single diffractive inelastic events measured in UA1 and UA5. The superimposed curve is the expectation of cylindrical phase space, for $\langle p_T \rangle = 0{\cdot}5$ GeV/c.

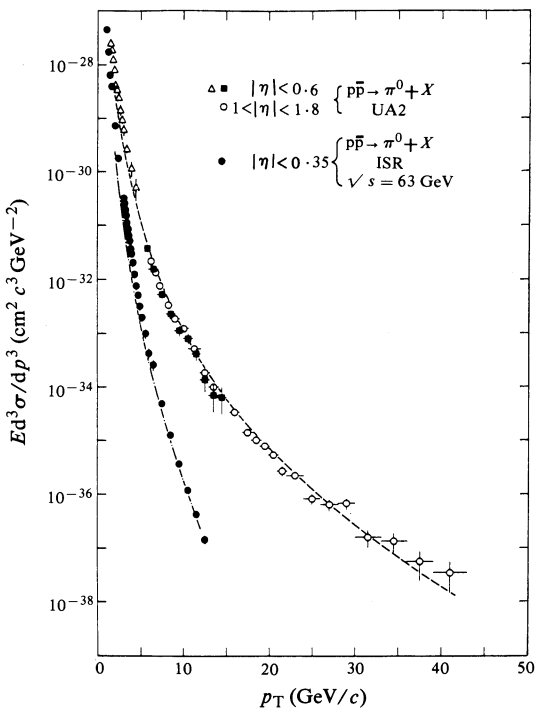

Fig. 13. Comparison of the invariant cross section for inclusive π^0 production in UA2 (Banner *et al.* 1985) and at the ISR (Kourkoumelis *et al.* 1980). The superimposed curves are QCD-based predictions, using structure and fragmentation functions from Baier *et al.* (1979).

is approximately uniformly distributed in the central rapidity region (see Fig. 12), and is characterized by a low p_T with respect to the beam axis. Averaged over all multiplicities, we get $\langle p_T \rangle \approx 0{\cdot}4$ GeV/c (Arnison *et al.* 1982; Banner *et al.* 1982, 1983*a*). However, particles can be produced, rarely, with very high p_T. Superimposed on the data (Banner *et al.* 1985) of Fig. 13 is a QCD prediction for π^0 production at p_T values between 0·25 and 40 GeV/c.

(iii) Typical high-p_T processes for the production of quarks and gluons from $\bar{p}p$ collisions are shown in lowest order in Fig. 14. In general, the outgoing quarks (gluons) are detected experimentally as clusters of highly collimated particles, or 'jets', that result from the quark (gluon) fragmentation. The high-p_T π^0 noted in (ii) results from that small fraction of jet fragmentations for which most of the momentum is carried by a single particle, in this case a π^0.

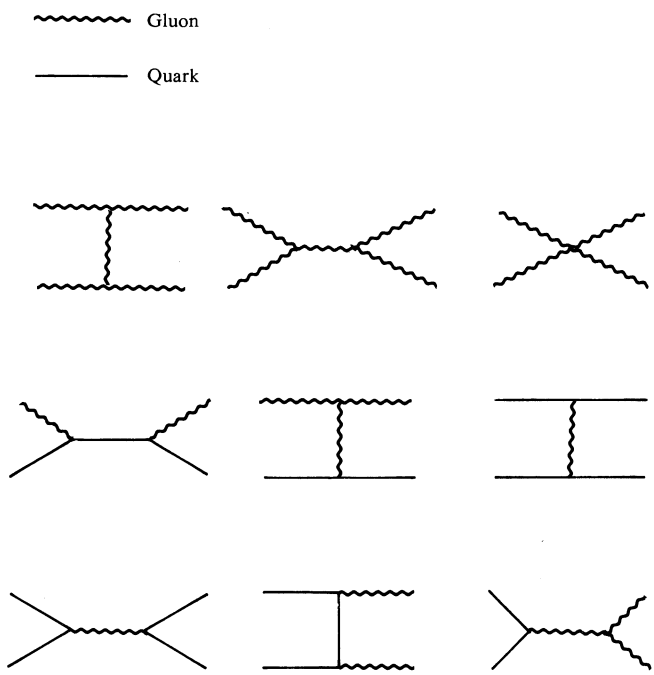

Fig. 14. Lowest order graphs for quark–quark, quark–gluon and gluon–gluon interactions in $\bar{p}p$ collisions.

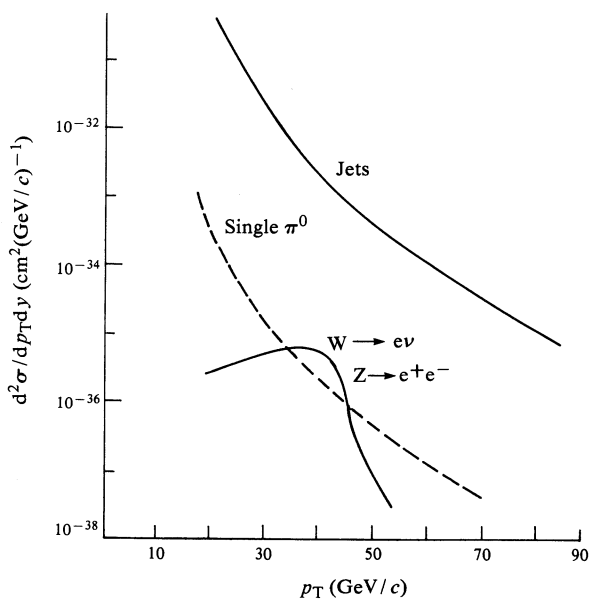

Fig. 15. Inclusive cross section for jet production at the $\bar{p}p$ Collider, compared with the yield of high-p_T single hadrons and high-p_T leptons expected from the decay of W or Z^0.

(iv) Typical high-p_T processes are characterized by two jets at opposite azimuth (back-to-back) in the plane transverse to the beam direction, though not necessarily back-to-back longitudinally since the centre-of-mass of the interacting constituents is not generally at rest in the laboratory. In addition to the jets, typically four or five charged and neutral hadrons per rapidity unit, characteristic of a minimum bias event, will be superimposed on the two-jet structure.

(v) Events in which an IVB is produced with a subsequent quark–antiquark decay are topologically indistinguishable from two-jet events resulting from QCD processes. However, their expected rate is much lower (see Fig. 15). If a two-jet mass peak is to be identified as a superposition on the dominant QCD continuum, the two-jet mass resolution should be small.

(vi) To test predictions of the GSW model, it is essential to detect leptonic decay products of the IVBs. Furthermore, they provide the cleanest signature for identification of IVBs. If leptons are to be identified experimentally, good rejection is required against a background of low-multiplicity jets or isolated hadrons that fake the experimental lepton signature. For electrons, this background is mainly from the Dalitz decay of π^0 and from external photon conversion ('conversion background'), or from the overlap of a high-momentum π^0 or γ with a nearby charged track ('overlap background'). For muon identification, the background sources include the decay of high-p_T $\pi^\pm$ and $K^\pm$, as well as low-p_T K decays which fake a high-p_T track.

As suggested in (i), the detectors must be designed to filter out IVB events from those that might fake the experimental signature. Both the UA1 and UA2 detectors are designed to detect leptons with good efficiency, with good rejection power against events faking the lepton signature, and all of this in an environment of high track multiplicity. Each detector identifies electrons, and in addition the UA1 detector is equipped to identify muons. Both detectors identify jets and measure their energies and directions. This enables QCD processes to be studied and should allow the identification of hadronic decay modes of IVBs when sufficient statistics are available. For W and Z^0 leptonic decays, the lepton(s) are expected to be well isolated from substantial hadronic activity. At the expense of some efficiency, such a requirement can be used to increase the rejection of jets faking the lepton signature. It should be noted that neither detector is well equipped to detect leptons in the proximity of substantial hadronic activity (e.g. a jet).

In the case of the identification of leptonic decay products of the IVBs, additional rejection against misidentified hadrons or jets can be obtained from topological constraints. A good example is the decay $W \rightarrow e\nu_e$. The electron produced has a p_T^e distribution with Jacobian peak at $p_T^e \approx \frac{1}{2}M_W$, smeared by the finite W width and by the p_T of the W produced, p_T^W. The dominant background will be from a misidentified jet; in that case a second jet should be identified at opposite azimuth in the transverse plane. However, the W signal should be characterized by having no signal back-to-back, since the neutrino does not interact in the detector. It is therefore important to measure all particle momenta over the maximum possible solid angle to identify the lack of signal in the detector. In this example, the existence of a neutrino can subsequently be inferred, and its transverse momentum p_T^ν measured. Independent of the event topology, we call the undetected transverse momentum 'missing p_T', or p_T^{miss}.

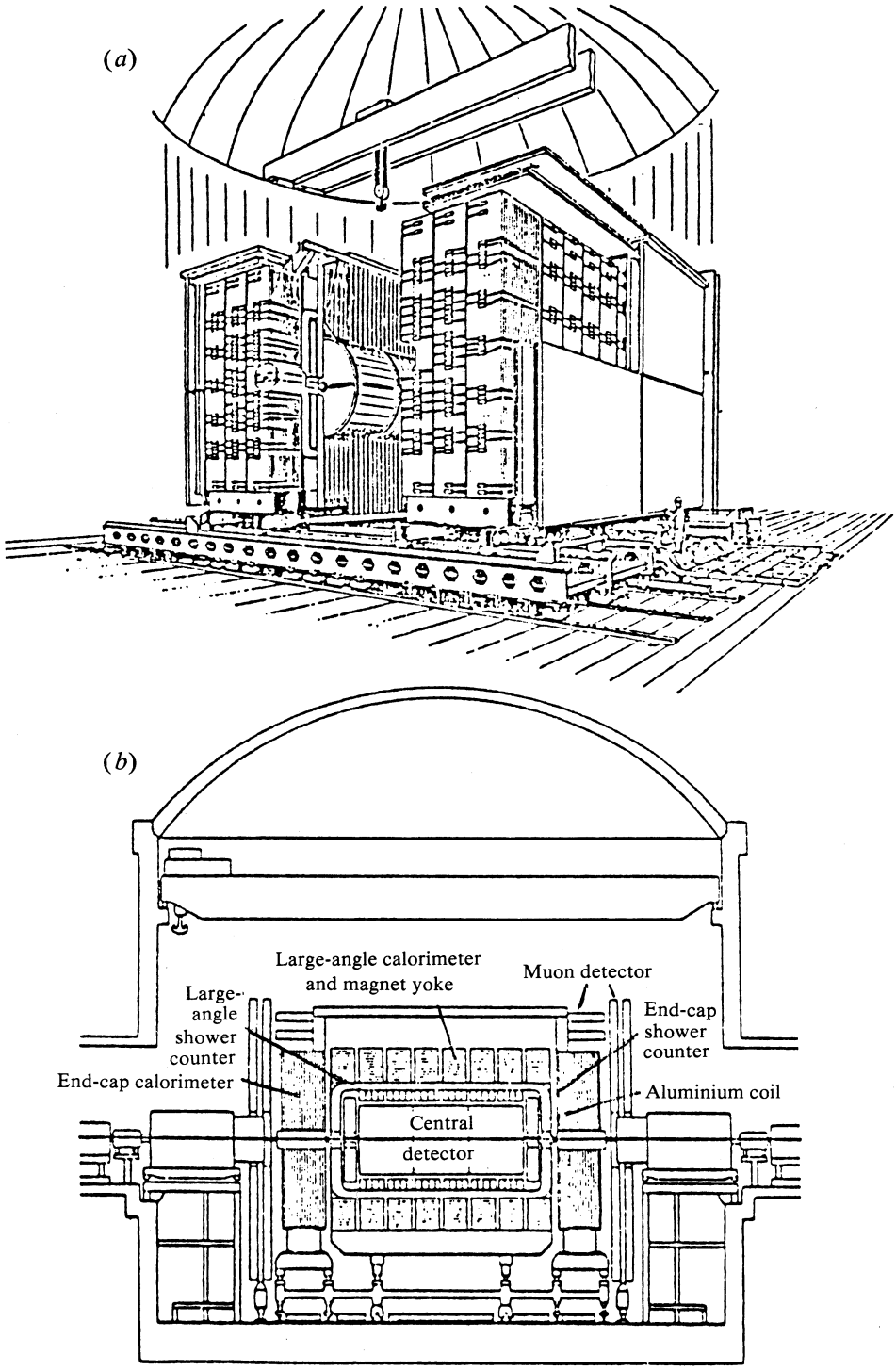

Fig. 16. UA1 detector: (*a*) general view and (*b*) side view.

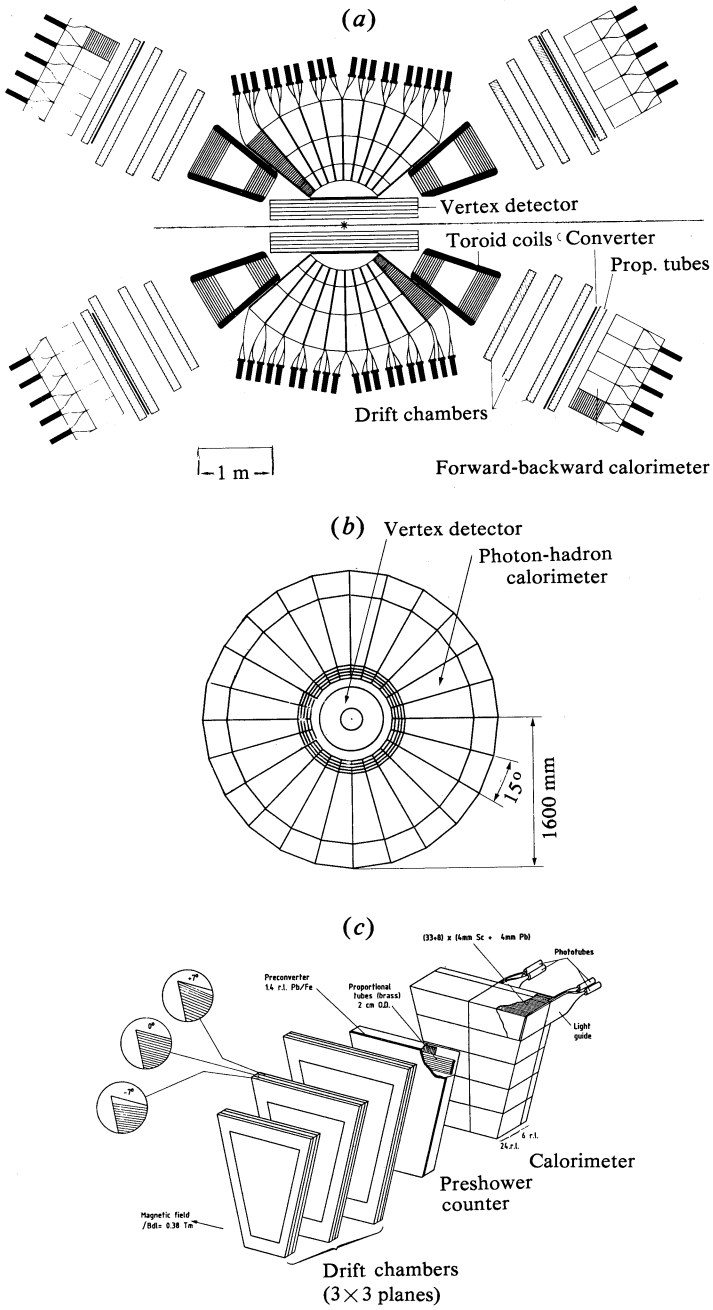

Fig. 17. Views of the UA2 detector: (*a*) cross-section in the vertical plane containing the beam axis; (*b*) cross-section of the central detector normal to the beam axis; and (*c*) exploded view of a sector in one of the forward detectors.

The UA1 detector is general purpose with an almost 4π sr coverage about the $p\bar{p}$ interaction region (see Fig. 16). In addition to the UA1 proposal, recent descriptions were given by Timmer (1983, and references therein). Particles first traverse a large drift chamber (6 m long and 2·4 m diameter), which allows the reconstruction of charged tracks, and subsequently the event vertex. A 0·7 T dipole magnetic field in this region allows the momentum measurement of charged tracks with a precision of typically $\delta p/p \sim 0{\cdot}005p$ (p measured in GeV/c). The drift chamber is surrounded by a total of 112 electromagnetic (EM) calorimeter cells, covering a polar angle range of $5° < \theta < 175°$, and with full azimuthal coverage. Though the spatial segmentation of the calorimeter is limited, four independent longitudinal EM samplings allow a measurement of the profile of deposited energy. The energy resolution for electrons and photons is $\Delta E/E \sim 0{\cdot}15/\sqrt{E}$ (E in GeV), with a quoted energy-scale uncertainty of $\sim\pm 3\%$, and a cell-to-cell calibration uncertainty of $\sim\pm 3\%$. The energy is less well measured within $\pm 15°$ of the vertical direction because of the space taken by light-guides of the EM calorimeter. By rejecting events having missing energy in this direction, UA1 quoted a resolution on the evaluation of missing transverse energy of $\Delta E_{\mathrm{T}}^{\mathrm{miss}}/E_{\mathrm{T}} \sim 0{\cdot}7/(\Sigma E_{\mathrm{T}}^{\epsilon})^{1/2}$ [$\Sigma E_{\mathrm{T}}^{\epsilon}$ being the (scalar) summed transverse energy deposited in each cell of the calorimeters]. Additional chambers and calorimeters also cover the small-angle region ($|\theta| > 0{\cdot}2°$). Beyond the EM calorimeters, a hadron calorimeter measures the energy leakage from the EM calorimeters for electrons and photons, and the energy deposition for single hadrons or jets. The energy resolution for hadrons is $\delta E/E \sim 0{\cdot}80/\sqrt{E}$ (E in GeV). Outside the hadron calorimeter, eight layers of drift chambers are used to identify muons.

The UA2 detector (see Fig. 17) is a smaller detector more specifically adapted to the search for W and Z^0, and to studies of jet production. A full description has been given by Mansoulié (1983). A small drift- and proportional-chamber system is used to reconstruct tracks and the event vertex in a region of no magnetic field. In the angular range $40° < \theta < 140°$, and with full azimuthal coverage, a highly segmented EM and hadronic calorimeter of 240 cells measures the energy of electrons and photons with resolution $\delta E/E \sim 0{\cdot}15/\sqrt{E}$ (E in GeV). The resolution for the detection of single hadrons and jets varies as $E^{-1/4}$ between 32% at 1 GeV and 11% at 70 GeV. For the EM calorimeter cells, the energy-scale uncertainty is $\pm 1{\cdot}5\%$, and the cell-to-cell calibration uncertainty is $\pm 2{\cdot}5\%$. The energy-scale uncertainty for hadronic-calorimeter cells is $\pm 4\%$. Again with full azimuthal coverage in the forward regions with respect to the beam axis ($20° < \theta < 40°$ and $140° < \theta < 160°$) a series of 12 magnetic spectrometers provides a charged-particle momentum measurement of accuracy $\delta p/p \sim 0{\cdot}007p$ (p in GeV/c). In the same angular range an additional 240 individual EM calorimeter cells follow the spectrometers. No hadron calorimeters exist in this region. Before each EM calorimeter, a converter of thickness about 1·5 radiation lengths is followed by proportional chambers to measure the position of the produced shower, and consequently to reject 'overlap' background. No particle coverage exists for $|\theta| < 20°$, and limited identification is available ($\sim 20\%$ dead space from the spectrometer coils, and no neutral-hadron identification) in the forward spectrometer region. Consequently, the accurate measurement of $p_{\mathrm{T}}^{\mathrm{miss}}$ in UA2 is limited to event topologies such as $W \to e\nu$ for which unidentified large-p_{T} activity in the forward directions is kinematically disfavoured.

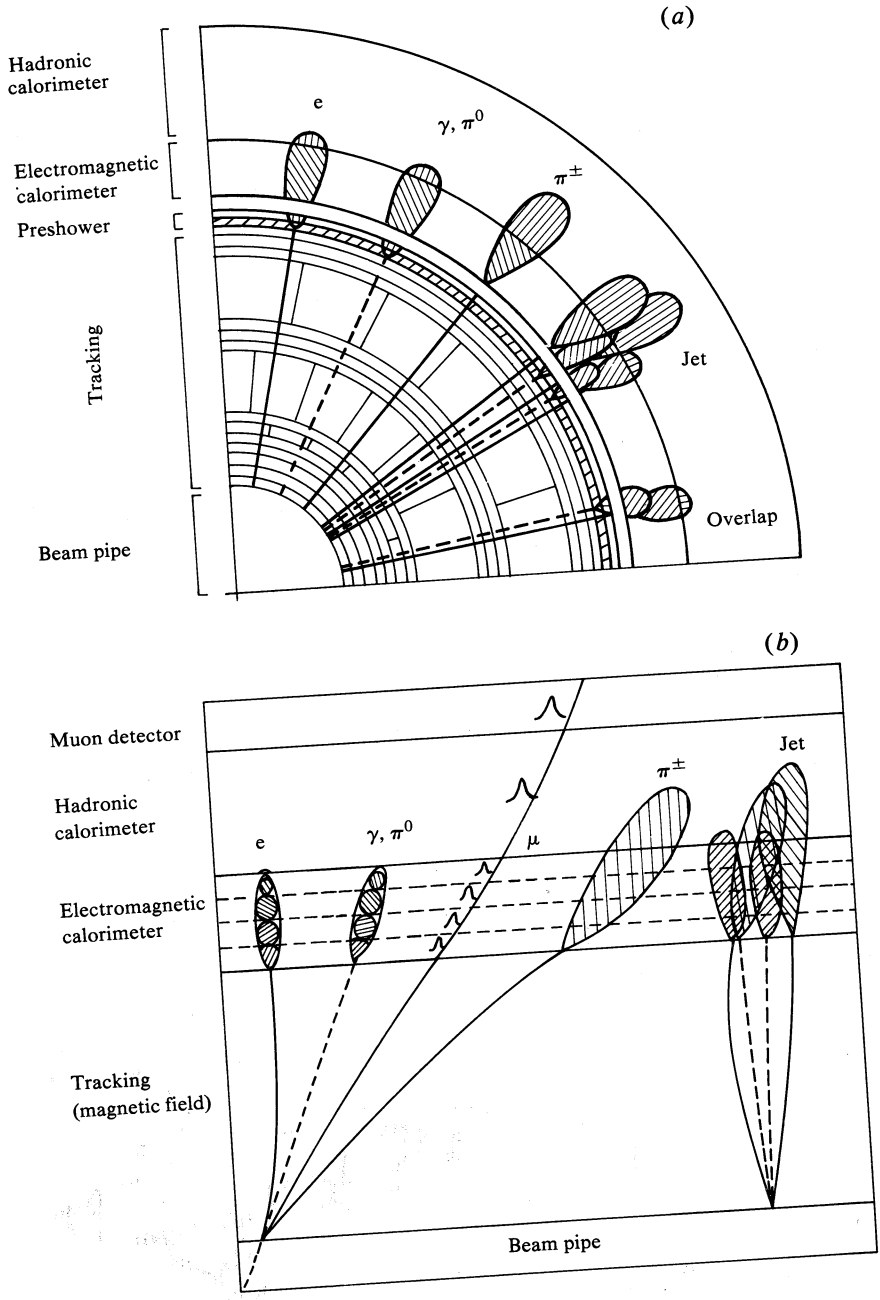

Fig. 18. Schematic representation of particle signatures in (*a*) a quadrant of the UA2 detector and (*b*) a central section of the UA1 apparatus. Dashed lines in the tracking detectors represent neutral particles, while full lines represent charged particles. The curvature illustrated in (*b*) represents the momentum analysis capability of the UA1 detector in the central rapidity region. The existence of longitudinal sampling in the calorimeters is shown qualitatively. Also illustrated pictorially are the minimum-ionizing signals characteristic of a muon detected in the UA1 apparatus.

The principle of detection is shown for each of the UA1 and UA2 detectors and for different particle types in Fig. 18. For electrons, the presence of a charged track must match in position an energy deposition in the EM calorimeter that is characteristic in lateral and longitudinal profile of an electron, and in particular has small hadronic leakage. Where possible, momentum information is used (UA1 and the forward regions of UA2). The presence of a pre-shower signal (UA2) characteristic of an electron and with a good spatial match to the charged track is required.

Muons (UA1 only) are identified by matching track segments before and after the EM and hadronic calorimeters with a signal in the calorimeters characteristic of a minimum-ionizing particle.

Prior to topology selections, the rejection obtainable by each detector for electrons against misidentified jets, using 'standard' analysis criteria described by each collaboration, is in the order of 5×10^4, with an associated electron detection efficiency of typically 75%. Of course, for each detector the rejection can be significantly improved at the expense of detection efficiency. In the case of the UA1 detector, similar rejection factors are obtainable for muon detection.

As emphasized in Section 2, a precise measurement of the IVB masses is important to test the validity of the GSW model. The best mass measurements presently result from the decays $Z^0 \to e^+e^-$ and $W \to e\nu$, and are dominated in each experiment by systematic uncertainties of the electron energy calibration. Any future $\bar{p}p$ experiment should maintain a significantly better calibration.

Table 4. UA1 and UA2 event samples for $W \to e\nu_e$ and $W \to \mu\nu_\mu$

	UA1(e)	UA2(e)	UA1(μ)
Luminosity (nb^{-1})	399	452	362
p_T^l cut (GeV/c)	15	25	15
Candidates	172 (148)[A]	119	44
QCD background	$5\cdot3\pm1\cdot9$	$5\cdot6\pm1\cdot7$	2–3
$Z^0 \to l^+ l^-$	—	$4\cdot4\pm0\cdot8$	
$W \to \tau\nu_\tau;\ \tau \to l\nu_l\nu_\tau$	$9\cdot1\pm0\cdot5$	$1\cdot7\pm0\cdot2$	Not quoted
$W \to \tau\nu_\tau;\ \tau \to$ hadrons	$2\cdot7\pm0\cdot4$	—	
Signal	155 ± 13	107 ± 11	≈41

[A] Event sample with good p_T^{miss} measurement.

Table 5. UA1 and UA2 event samples for $Z^0 \to e^+e^-$ and $Z^0 \to \mu^+\mu^-$

	UA1(e)	UA2(e)	UA1(μ)
Luminosity (nb^{-1})	399	452	362
Candidates	18	16	10
QCD background	Small	$<0\cdot2$[A]	Small
Events used for mass evaluation	14	13	10

[A] $M^{ee} > 70$ GeV.

(3c) The W and Z^0 Data Samples

At the conclusion of the 1984 $\bar{p}p$ Collider run, the UA1 (UA2) experiments had collected data corresponding to a luminosity of 399 (452) nb^{-1}, including 263 (310) nb^{-1} at $\sqrt{s} = 630$ GeV. The total event samples for W and Z^0 leptonic

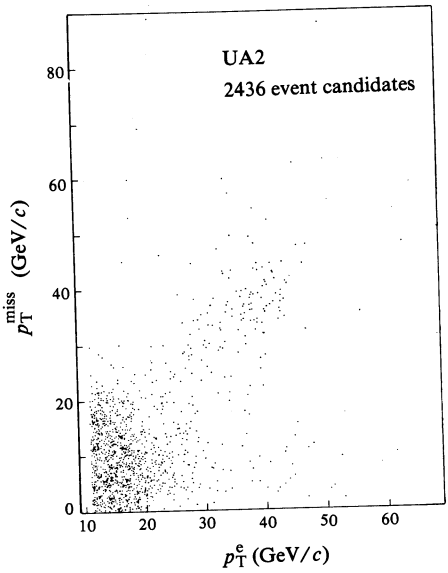

Fig. 19. Distribution of p_T^{miss} versus p_T^e for the highest p_T electron candidate of $p_T^e > 11$ GeV/c, identified by the standard analysis criteria of UA2 (1983 + 1984 data).

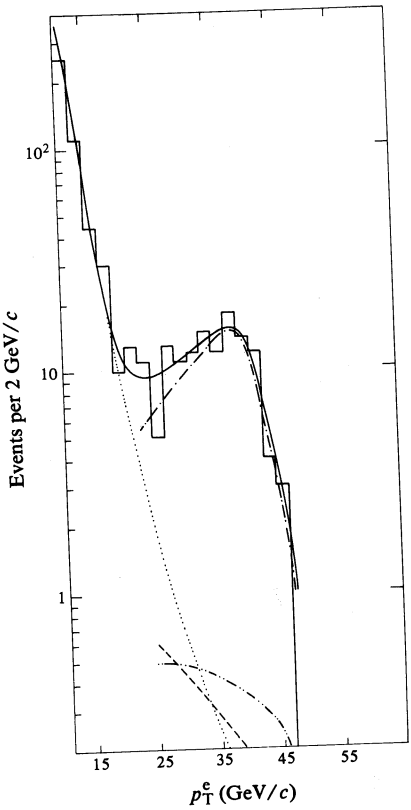

Fig. 20. Distribution of p_T^e (UA2, 1983 + 1984) for 593 electrons of $p_T^e > 11$ GeV/c satisfying topology selections for $W \to e\nu_e$ decay. Superimposed are expected contributions from misidentified hadrons (dots), decays $W \to \tau\nu_\tau$ (dashes), and decays $Z^0 \to e^+e^-$ where one electron is not detected (dash-dot-dot). Also shown is the expectation for $W \to e\nu_e$ decay (dash-dot), and the sum of all contributions (solid curve).

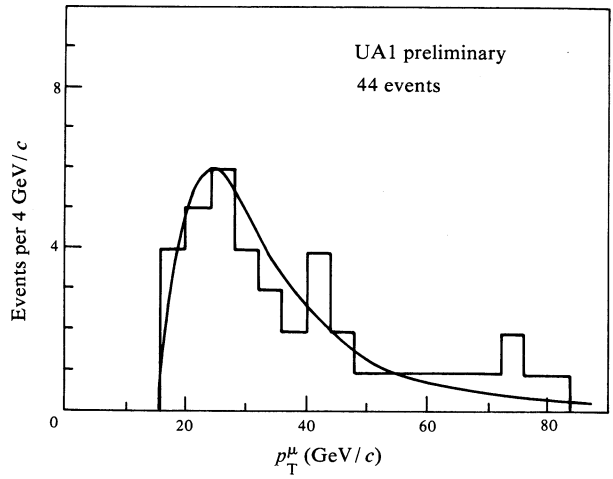

Fig. 21. Distribution of p_T^μ (UA1, 1983 + 1984) for muons with $p_T^\mu >$ 15 GeV/c identified as W decays. The expectation for $W \rightarrow \mu\nu_\mu$ decay is shown by the superimposed curve.

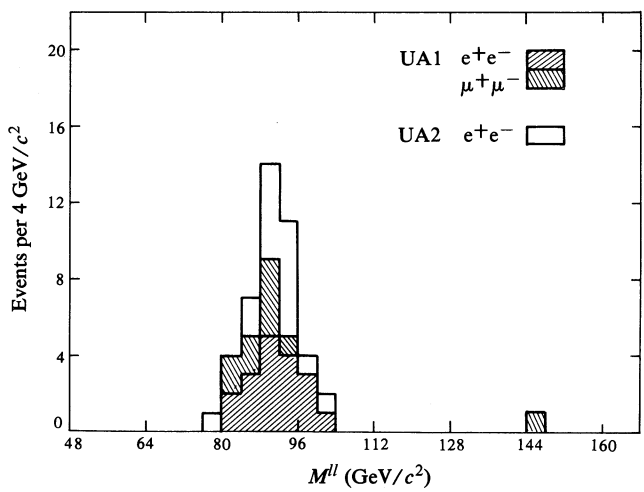

Fig. 22. Combined UA1 and UA2 data sample (1983 + 1984) of all lepton pairs identified with mass $M^{ll} > 50$ GeV. The highest mass $\mu^+ \mu^-$ pair is compatible within errors with Z^0 decay.

decay are shown in Tables 4 and 5 respectively. Publications describing the leptonic decay modes of Z^0 and W data collected before 1984 include those of Banner *et al.* (1983*b*), Bagnaia *et al.* (1983, 1984*a*, 1984*b*) and Arnison *et al.* (1983*a*, 1983*c*, 1984*a*, 1984*b*, 1984*c*). Data from 1984 are in general published as conference reports, which are referred to as appropriate in the following sections. The data have most recently been reviewed by Froidevaux (1985), DiLella (1985*b*) and Levi (1985). Some UA1 data from 1984 have also recently been published (Arnison *et al.* 1985).

Fig. 19 shows, by example, the p_T^{miss} versus p_T^e distribution of all electron candidates satisfying the UA2 'standard' cut criteria with $p_T^e > 11$ GeV/c^{-1} (Bagnaia *et al.*

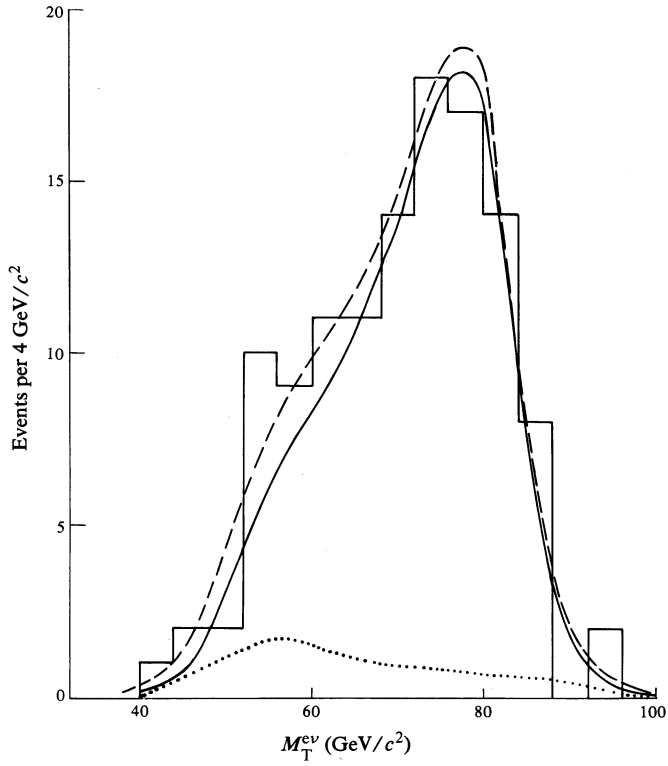

Fig. 23. Transverse mass distribution (UA2: 126 events) for events satisfying $p_T^e > 15$ GeV/c and $p_T^\nu > 25$ GeV/c. The expectation from $W \to e\nu_e$ decay is superimposed (solid curve), together with other contributions that include misidentified hadrons, $W \to \tau\nu_\tau$ decay, and $Z^0 \to e^+e^-$ decay (dotted curve). The sum of all contributions is shown as the dashed curve.

1984*a*). Already at this stage a significant event population exists at large p_T^e and p_T^{miss}, as expected from W-decay. After making topological selections described by Bagnaia *et al.*, the p_T^e distribution is shown for W candidates in Fig. 20. Superimposed are the background contributions from hadrons that are misidentified as electrons, and as well genuine electrons from

(i) $W \to \tau\nu$; $\tau \to e\nu_e\,\nu_\tau$ decays, and

(ii) $Z^0 \to e^+e^-$ decays for which one electron is not detected (primarily the UA2 detector).

In Fig. 21, the p_T^μ distribution is shown for $W \to \mu\nu_\mu$ events from the UA1 experiment. The expected distribution, which takes into account the muon momentum resolution, is superimposed. Because of the poor momentum resolution, a Jacobian peak is not expected.

The invariant mass distribution of the decay $Z^0 \to l^+l^-$ is shown in Fig. 22, for the combined UA1 and UA2 data sample, for $M^{ll} > 50$ GeV. Because rejection criteria can be applied to both lepton candidates of the Z^0-decay, the background from hadrons and jets that are misidentified as leptons is negligible; no other lepton pair event satisfying $M^{ll} > 50$ GeV is measured.

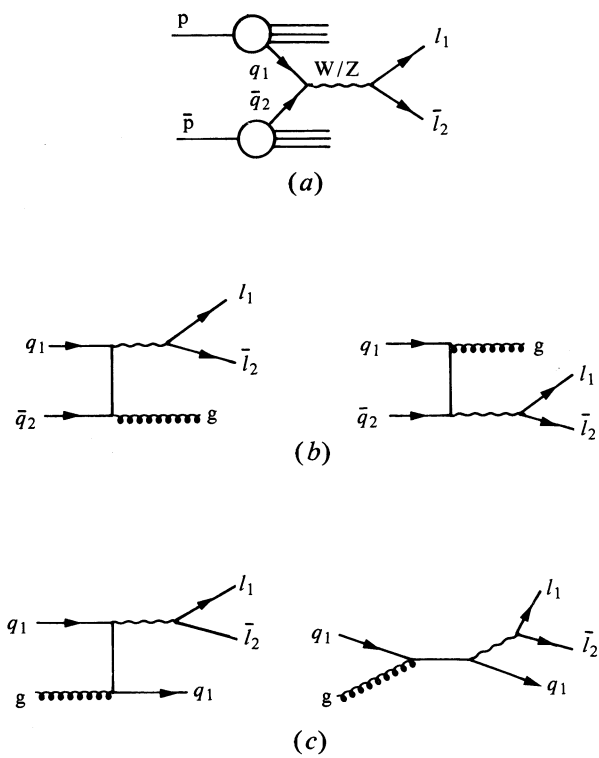

Fig. 24. Some of the parton-scattering diagrams which contribute to the total W and Z^0 production cross section, either with or without associated jet production.

The Z^0 mass can be evaluated directly from the distribution of Fig. 22. However, the W mass cannot be directly measured because of the lack of knowledge of the longitudinal neutrino momentum p_L^ν. The mass value must be inferred from either a fit to the p_T^e distribution of Fig. 20, of all known contributing processes, or of a similar fit to the transverse mass distribution, shown for UA2 data in Fig. 23 $[M_T^2(W) = 2p_T^e p_T^\nu(1 - \cos\Delta\phi^{e\nu})]$. Such fits are model-dependent, since the distributions are smeared by the lepton energy resolution, by $\Gamma(W)$, and by the longitudinal and transverse motion of the W.

The dominant IVB production process is via the Drell–Yan (1970) mechanism shown in Fig. 24*a*. In addition, higher order diagrams (examples of which are shown in Figs 24*b* and 24*c*) contribute to the total IVB production cross section. This last category is characterized by associated jet production that balances transversely the high-p_T IVBs produced. In Appendix 2, the basic elements of the cross-section evaluation for the diagram of Fig. 24*a* are outlined. In addition to the electroweak coupling parameters, a knowledge is required of the nucleon structure functions and their QCD evolution to $M_{W,Z}$. For higher order contributions, detailed QCD evaluations are required; the most recent calculations are from Altarelli *et al.* (1984, 1985). Ellis *et al.* (1985) have recently calculated the contribution to the IVB cross section of associated jet and multi-jet production.

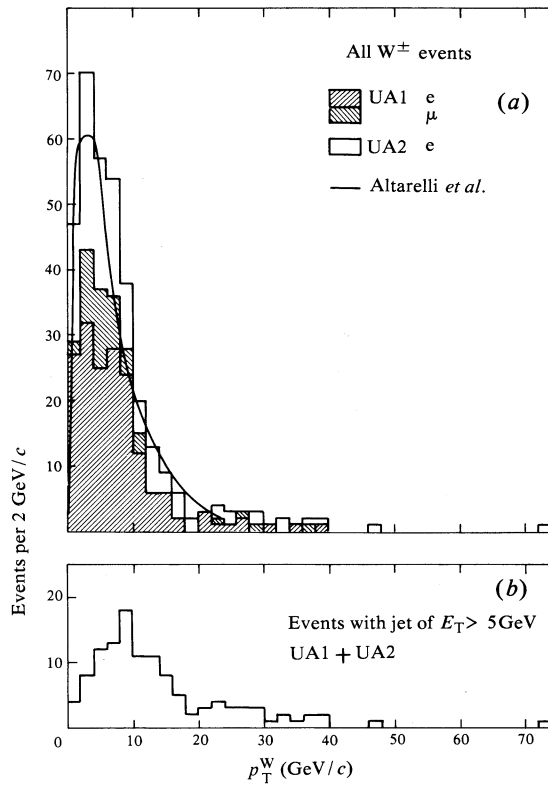

Fig. 25. (*a*) p_T^W distribution for UA1 and UA2 (total 1983 + 1984 data sample). Superimposed is the QCD expectation from Altarelli *et al.* (1984, 1985), using the Duke and Owens (1984) structure functions with $\Lambda = 0{\cdot}2$ GeV. (*b*) A sub-sample of events having at least one jet of $E_T > 5$ GeV.

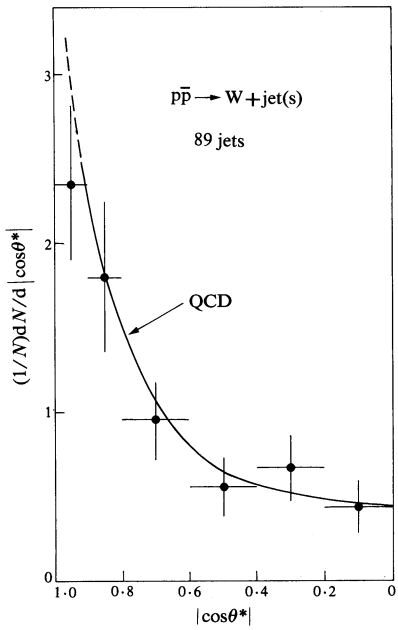

Fig. 26. The $\cos\theta^*$ distribution for UA1 data in the W-jet centre-of-mass. The superimposed curve is that expected from gluon bremsstrahlung processes.

Before discussing the measured IVB properties, and their agreement with predictions of the GSW model, it is useful to discuss some properties of IVB production that can be compared with predictions of the QCD model for strong interactions:

(a) *Transverse motion.* Higher order processes may result in the production of one or more associated jets, with a consequent increase of the mean p_T for W and Z^0 production. Fig. 25 shows the p_T^W distribution for UA1 and UA2 data, and compares this with the QCD calculations of Altarelli *et al.* The agreement is excellent. Similar agreement is obtained for Z^0 production. Mean transverse momenta are typically 7–9 GeV/c. The produced jet(s) are distributed in angle with respect to the beam axis (in the W-jet rest frame) according to $dN/d(\cos\theta^*) \propto (\sin\frac{1}{2}\theta^*)^{-2}$, as expected from gluon bremsstrahlung, and as shown in Fig. 26 (Arnison *et al.* 1985).

Some events collected by the UA2 collaboration during the 1983 run were characterized by large p_T^W, large p_T^{miss} and large transverse jet energy (Bagnaia *et al.* 1984*b*). At that time, these events were judged to be inconsistent with W+jet production from QCD processes. Similar event topologies were not observed during the 1984 run, and it is now considered most likely that the event configurations were in fact produced via QCD processes (Plothow-Besch 1985).

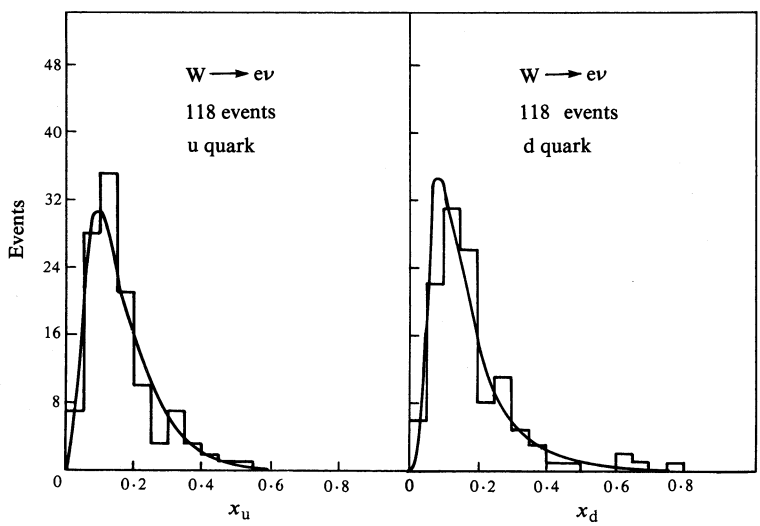

Fig. 27. Longitudinal momentum fractions x_u and x_d carried by u and d quarks in the nucleon, assuming W production as in Fig. 24*a*. The data shown are events from the UA1 experiment for which the electron charge is known to better than 3σ. Superimposed expectations use the structure functions of Eichten *et al.* (1985).

(b) *Longitudinal motion.* In the leptonic decays $W \to l\nu_l$, the neutrino longitudinal momentum p_L^ν cannot be measured and, as a result, M_W cannot be directly evaluated. However, from a knowledge of $\boldsymbol{p}^e$ and $\boldsymbol{p}_T^\nu$, p_L^ν can be evaluated if the condition $M^{l\nu} \equiv M_W$ is imposed. Two values of p_L^ν are allowed, corresponding to two values of p_L^W. In practice, one solution is often unphysical (70–80% of the time). For events such that two p_L^ν values are kinematically allowed, the solution with the smallest absolute value of p_L^W is the most likely (see below).

The fractional beam momentum $x_W = 2p_L^W/\sqrt{s}$ carried by the W bosons can be used, if p_T^W is small, via the relations

$$x_W = x_q - x_{\bar{q}}, \qquad M_W^2 = x_q x_{\bar{q}} s, \tag{25}$$

to determine the fractional momentum of the quarks involved in the W production. For small p_T^W, the dominant diagram is that of Fig. 24*a*. If a lepton charge measurement is available, the processes $u\bar{d} \to W^+$ and $\bar{u}d \to W^-$ can be separated, resulting in measurements of x_u and x_d (assuming $dn/dx_q = dn/dx_{\bar{q}}$). Fig. 27 shows dn/dx_u and dn/dx_d from the UA1 experiment (Arnison *et al.* 1985), together with expectations from QCD-evolved structure function measurements at low energy. It is because small values of x_u and x_d are favoured, that the smaller $|p_L^W|$ value evaluated is the most likely.

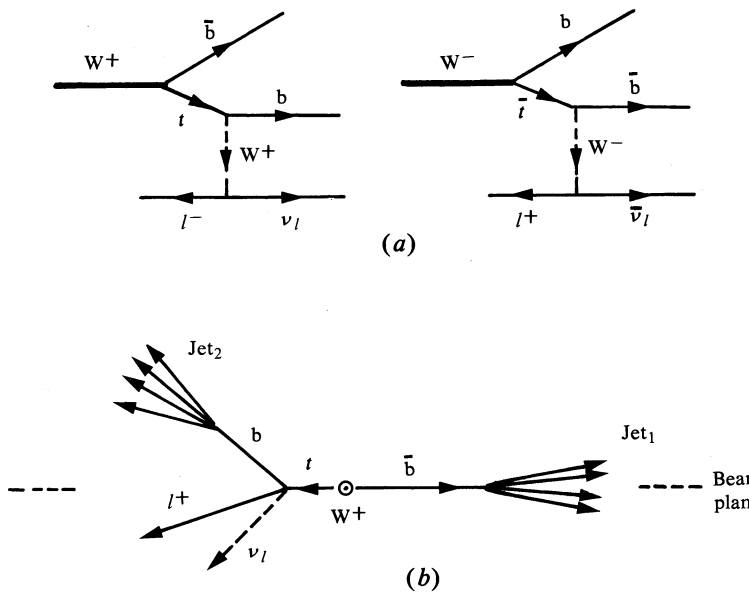

Fig. 28. (a) Diagrams showing the final-state fermions in the semi-leptonic decays $W^+ \to t\bar{b}$ and $W^- \to \bar{t}b$. (b) Resulting event topology as it would appear in the UA1 or UA2 detectors.

(3d) Searches for Other IVB Decay Modes

Strenuous efforts have been made to identify other decay modes of the Z^0 and W:

(a) $W, Z^0 \to \text{jet}_1 + \text{jet}_2$. No significant signal has been observed. The best limits come from the UA2 collaboration (Weidberg 1984), which measured an excess $N_W = 108 \pm 80$ events with respect to the QCD continuum at $\sqrt{s} = 546$ GeV. The expected number is $N_W \sim 150$.

(b) $W \to \tau\nu_\tau$. The UA1 collaboration has provided evidence using data at $\sqrt{s} = 546$ GeV (Savoy-Navarro 1985) for the decays

$$\tau^\pm \to \pi^\pm(n\pi^0)\nu_\tau, \qquad \tau^\pm \to \pi^\pm\pi^\mp\pi^\pm(n\pi^0)\nu_\tau. \tag{26}$$

Respectively, five and three events were isolated with the expected characteristics of these topologies. The corresponding background estimates for misidentified τ-decays are respectively $0\cdot5\pm0\cdot1$ and $0\cdot6\pm0\cdot2$ events. It is estimated that

$$R = \sigma(\mathrm{W}\rightarrow\tau\nu)/\sigma(\mathrm{W}\rightarrow\mathrm{e}\nu) = 0\cdot96\pm0\cdot48\ (\mathrm{stat}).$$

The statistical error on this ratio should be significantly improved when the 1984 data are available.

(c) $\mathrm{W}^+ \rightarrow \mathrm{t\bar{b}}$ and $\mathrm{W}^- \rightarrow \mathrm{\bar{t}b}$. The UA1 collaboration (Arnison *et al.* 1984*d*) has investigated event topologies which contain a high-p_T lepton, in association with at least two high-E_T jets. Such configurations would be expected for the decay $\mathrm{W}^+ \rightarrow \mathrm{t\bar{b}}$; $\mathrm{t} \rightarrow l^+\nu_l\mathrm{b}$ and the corresponding W^- decay, as illustrated in Fig. 28.

An event sample with $p_\mathrm{T}^\mathrm{e} > 15$ GeV, $E_\mathrm{T}(\mathrm{jet}_1) > 8$ GeV and $E_\mathrm{T}(\mathrm{jet}_2) > 7$ GeV was selected and stringent selection criteria were applied (at the expense of efficiency) to the identified lepton. This is necessary because, while in the W search the large measured $p_\mathrm{T}^\mathrm{miss}$ values of W-decay can be utilized as a powerful discriminant against hadronic background processes, the $p_\mathrm{T}^\mathrm{miss}$ values of this sample are expected to be small.

In the 1983 data sample a total of ten events of the lepton+2 or more jet category were identified. Fig. 29 shows the distribution for the ten events of $E_\mathrm{T}^\mathrm{out}$ versus $\cos\theta^*_{\mathrm{j}_2}$, where $E_\mathrm{T}^\mathrm{out}$ is the transverse lepton energy relative to the plane defined by the beam axis and jet_1, and $\cos\theta^*_{\mathrm{j}_2}$ is the centre-of-mass angle of jet_2 with respect to the beam axis. The ten events are approximately uniformly distributed in $\cos\theta^*_{\mathrm{j}_2}$ and have large $E_\mathrm{T}^\mathrm{out}$ values. In similar event topologies from QCD processes, one would expect the lepton candidate to be non-isolated, and $\cos\theta^*_{\mathrm{j}_2}$ to be peaked near $\cos\theta^*_{\mathrm{j}_2} \approx \pm1$, with a distribution in $\cos\theta^*_{\mathrm{j}_2}$ as for bremsstrahlung. This is indeed the case for an event sample in which the electron selection requirements are replaced by criteria to select the π^0 (see Fig. 30).

In the region $|\cos\theta^*_{\mathrm{j}_2}| < 0\cdot8$, UA1 inferred a background due to QCD processes with a fake lepton of $0\cdot1\pm0\cdot04$ events for the electron sample, and a similar value for the muon sample. One obvious background event and three events each with three jets were discarded, leaving six events for further analysis.

Fig. 31 shows for the six events $m(l\nu_\mathrm{T}\mathrm{j}_1\mathrm{j}_2)$ versus $m(l\nu_\mathrm{T}\mathrm{j}_2)$. If the events are interpreted as resulting from $\mathrm{W}^+ \rightarrow \mathrm{t\bar{b}}$ or $\mathrm{W}^- \rightarrow \mathrm{\bar{t}b}$ decay, it implies $30 \leqslant m_\mathrm{t} \leqslant 50$ GeV. However, limitations of the analysis are the requirements of both a high-p_T lepton, and high-E_T jets, which kinematically favour configurations peaked as in Fig. 31 (though the distributions are somewhat broader).

Preliminary results for the 1984 run have been presented by Dobrzynski (1985), and six additional e+2 jet candidates have so far been identified. Analysis of the data from the muon channel is still in progress. From the standard model about three events would have been expected for the process $\mathrm{W}^+ \rightarrow \mathrm{t\bar{b}}$; $\mathrm{t} \rightarrow l^+\nu_l\mathrm{b}$ and its charge conjugate. Additional physical processes must be invoked to account for the excess of events (for example, gluon $\rightarrow \mathrm{t\bar{t}}$). The UA2 collaboration (Mansoulié 1985) has however not confirmed these data.

(d) $\mathrm{Z}^0 \rightarrow \mathrm{e}^+\mathrm{e}^-\gamma$. The UA1 and UA2 experiments identified, in the 1983 run, two events consistent with $\mathrm{Z}^0 \rightarrow \mathrm{e}^+\mathrm{e}^-\gamma$ (see Fig. 32). An additional event consistent with $\mathrm{Z}^0 \rightarrow \mu^+\mu^-\gamma$ was identified by the UA1 experiment but the mass uncertainty of

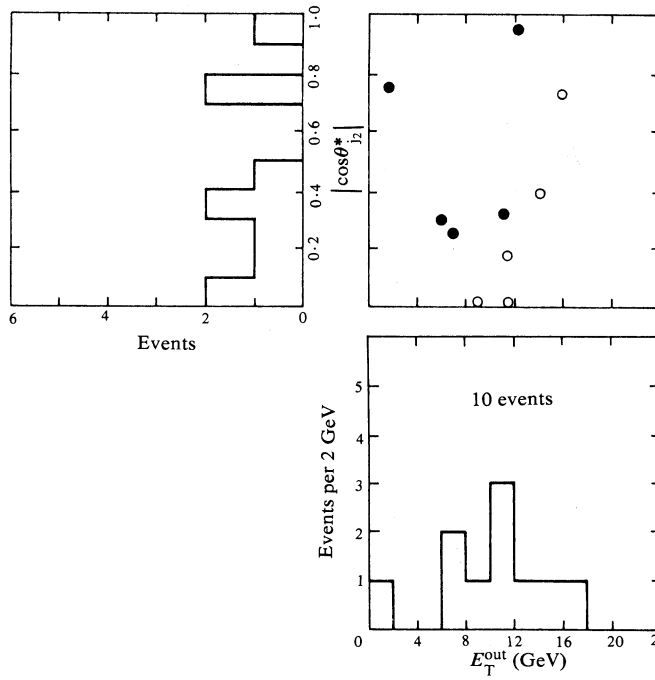

Fig. 29. Distribution (UA1, 1983) of E_T^{out} versus $|\cos\theta^*_{j2}|$ (see text) for 10 events in which the electron (open circles) or muon (closed circles) is associated with at least two jets.

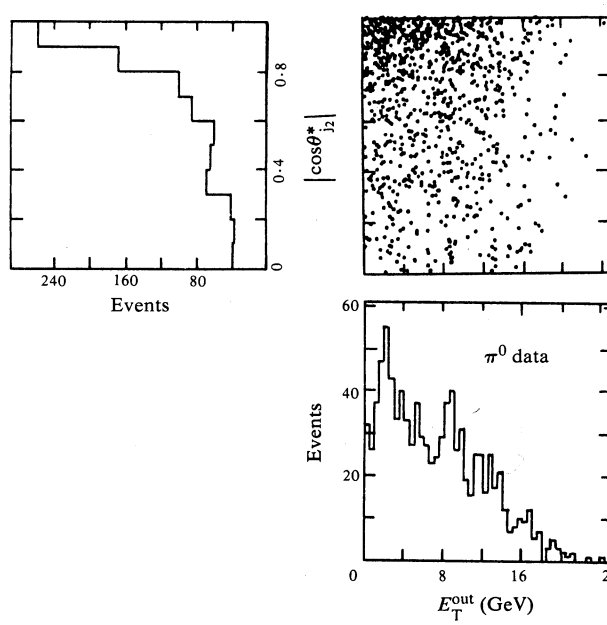

Fig. 30. Distribution (UA1, 1983) of E_T^{out} versus $|\cos\theta^*_{j2}|$ (see text) for QCD processes in which a π^0 is produced in association with at least two jets.

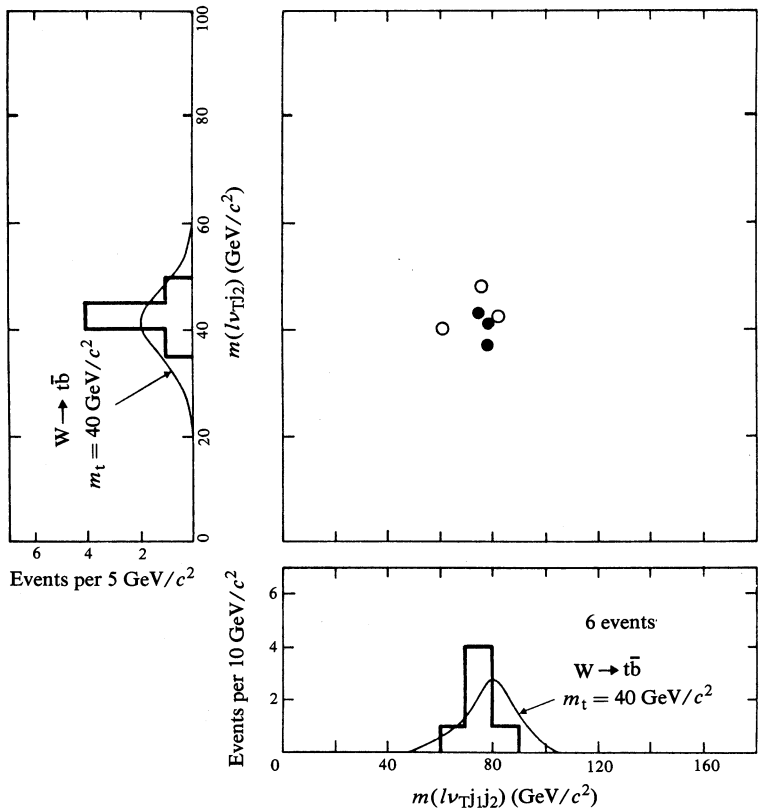

Fig. 31. Distribution (UA1, 1983) of the four-body mass $m(l\nu_T j_1 j_2)$ versus the three-body mass $m(l\nu_T j_2)$ for the six $W \to tb$ candidates, in which the electron (open circles) or muon (closed circles) is associated with two jets.

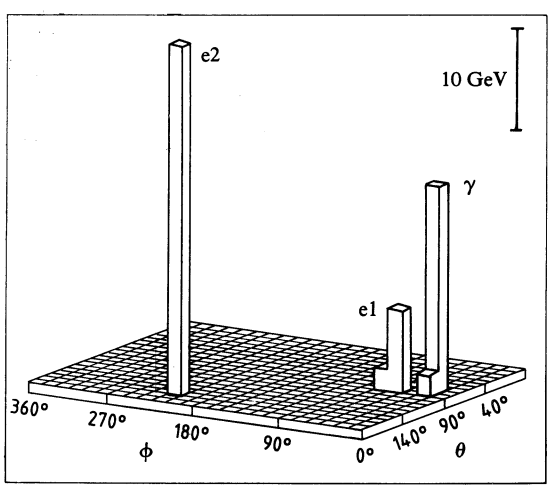

Fig. 32. The $Z^0 \to e^+e^-\gamma$ event observed in the UA2 experiment. The distribution shown is the transverse energy associated with each of 480 calorimeter cells in the detector, plotted as θ versus ϕ.

this event is such that the decay $Z^0 \rightarrow \mu^+\mu^-$ cannot be excluded. The probability that such event configurations resulted from internal bremsstrahlung was typically $\approx 1\cdot 5\%$ per event, making the observation of two such events unlikely. Many attempts (see Ellis 1984) were made to interpret the events in terms of unexpected decay modes of the Z^0, but no alternative explanation could explain the observed collinearity of the photon with one of the leptons. Since no new events have been reported in the 1984 run, the interpretation of these events as internal bremsstrahlung remains most likely.

(3e) Measurement of $\sin^2\theta_W$ and ρ at the $\bar{p}p$ Collider

As discussed in Section 2*d*, all parameters of the GSW model are defined following measurements of G_F, α_{EM}, M_W and M_Z. In practice, it is usual to evaluate the quantities $\sin^2\theta_W$ and ρ. Using mass measurements from the Collider, $\sin^2\theta_W$ can be defined in a scale-independent way (see equation 23) by

$$\sin^2\theta_W = 1 - M_W^2/M_Z^2, \quad \text{with } \rho \equiv 1. \tag{27}$$

This definition is in principle powerful, since experimental and theoretical uncertainties largely cancel, and the inclusion of radiative corrections is implicit. At present, however, the accuracy of the measurement is limited statistically.

Alternatively, $\sin^2\theta_W$ can be evaluated in the minimal GSW model from equation (24), with

$$\sin\theta_W(M_W) = A/M_W, \qquad \sin 2\theta_W(M_W) = 2A/M_Z, \tag{28}$$

$$A = \{\pi\alpha/\sqrt{2}\, G_F(1-\Delta r)\}^{\frac{1}{2}} = (37\cdot 2810 \pm 0\cdot 0003)/(1-\Delta r)^{\frac{1}{2}}\ \text{GeV}.$$

The radiative corrections Δr are dominantly electromagnetic but include purely weak effects ($\sim 0\cdot 5\%$ if $m_t \sim 40$ GeV). Marciano and Sirlin (1984) estimated $\Delta r = 0\cdot 0696 \pm 0\cdot 0020$. These radiative corrections were originally worked out by Veltman (1977, 1980), and are sensitive to m_t but relatively insensitive to m_{Higgs}. The quoted value of Δr used $m_t = 36$ GeV and $m_{Higgs} \approx 100$ GeV. If $m_{Higgs} \sim M_Z$ the two definitions are almost equivalent; $\sin^2\theta_W = 1\cdot 006 \sin^2\theta_W(M_W)$.

As discussed in Section 2*c*, the GSW model makes the most economical choice for the Higgs sector (that is, an isodoublet Higgs field resulting in a single neutral scalar Higgs particle). As a consequence of this choice, the parameter ρ in equation (22) is required to be unity; in fact, the existence of such additional isodoublet fields will not change the value of ρ. If the calculation of radiative effects is assumed to be correct then ρ can be evaluated. We rewrite equation (22) as

$$\rho = (M_W/M_Z \cos\theta_W)^2 = (M_W/M_Z)^2/\{1-(A/M_W)^2\}. \tag{29}$$

The quantity ρ is only weakly dependent on the mass of the Higgs particle, but is sensitive to the isospin structure of the Higgs fields.

Alternatively, taking $\rho = 1$, we can measure Δr in (27) and (28) from either the W and Z^0 masses alone, or from a combination of those measurements, and low-energy measurements of $\sin^2\theta_W(M_W)$ (see Section 4).

Table 6 lists the measured values of M_W and M_Z, and shows the derived measurements of $\sin^2\theta_W$, ρ and Δr. The most accurate data so far are from the UA2 collaboration; the data are compared with expectations of the GSW model in Fig. 33.

Table 6. Standard-model parameters measured in the UA1 and UA2 experiments

Parameter	UA1(e)	UA1(μ)	UA2(e)	Prediction[A]
M_W (GeV)	$83\cdot1^{+1\cdot3}_{-0\cdot8}\pm3\cdot0$[B]	$81\cdot0^{+6}_{-7}$[C]	$81\cdot2\pm1\cdot1\pm1\cdot3$	$82\cdot4\pm1\cdot1$
M_Z (GeV)	$93\cdot0\pm1\cdot6\pm3\cdot0$	$88\cdot8^{+5\cdot5}_{-4\cdot6}$	$92\cdot5\pm1\cdot3\pm1\cdot5$	$93\cdot3\pm0\cdot9$
$\sin^2\theta_W$	$0\cdot202\pm0\cdot036$		$0\cdot229\pm0\cdot030$	$0\cdot22\pm0\cdot006$
$\sin^2\theta_W(M_W)$	$0\cdot216^{+0\cdot005}_{-0\cdot008}\pm0\cdot01$		$0\cdot227\pm0\cdot006\pm0\cdot008$	$0\cdot22\pm0\cdot006$
ρ	$1\cdot018\pm0\cdot041\pm0\cdot021$		$0\cdot996\pm0\cdot024\pm0\cdot009$	$1\cdot006$
Δr[D]			$0\cdot08\pm0\cdot10\pm0\cdot03$	$0\cdot0696\pm0\cdot002$
Δr[E]			$0\cdot05\pm0\cdot03\pm0\cdot03$	$0\cdot0696\pm0\cdot002$

[A] From Marciano (1985), with $\sin^2\theta_W = 0\cdot22$ being determined as the average of existing measurements excluding UA1 and UA2 data.
[B] In all cases the first error is statistical and the second error represents the systematic uncertainty.
[C] 1983 data.
[D] Single experiment.
[E] With low energy data.

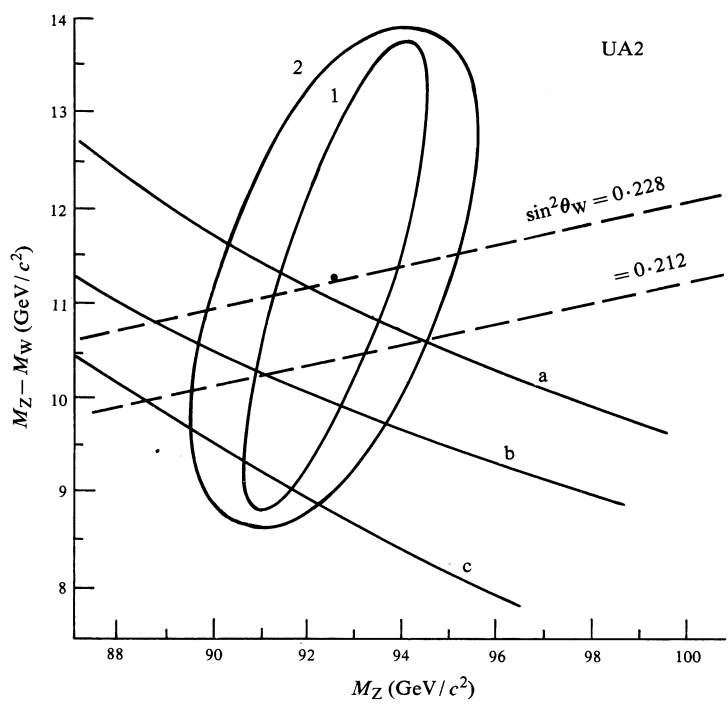

Fig. 33. Contours of 68% confidence in the plot of $M_Z - M_W$ versus M_Z taking into account the statistical error only (1), and with statistical and systematic errors combined in quadrature (2). Curve a (curve b) is the standard-model prediction for $\rho = 1$ with (without) radiative corrections. The band defined by curves a and c corresponds to the region allowed by the low energy result $\rho = 1\cdot02\pm0\cdot02$. The dashed lines corresponding to two different values of $\sin^2\theta_W$ define the region allowed by the world average of low energy results $\sin^2\theta_W = 0\cdot220\pm0\cdot008$.

The following comments can be made on the basis of Collider data:

(i) There is no evidence of any deviation from standard-model predictions. The agreement of $\sin^2\theta_W$ and $\sin^2\theta_W(M_W)$ with predictions is outstanding.

(ii) Assuming the validity of radiative-correction evaluations, there is no evidence for a deviation of the GSW model prediction $\rho = 1$, expected for a single neutral Higgs particle of known coupling.

(iii) Assuming the validity of the GSW model, the expected radiative corrections are consistent with measured values. However, the existing experimental accuracy is marginal, and the result is sensitive to systematics.

(3f) W Spin and V–A Coupling

As noted in Section 2*d*, a significant lepton charge asymmetry is expected for $W \to l\nu_l$ decay, if a left-handed coupling of the W occurs at the production and decay vertices (we assume W production via the process of Fig. 24*a*). Furthermore, the angular distribution (for a fully polarized spin-1 W) of the lepton with respect to the incident quarks in the W centre-of-mass should take the form

$$\mathrm{d}N/\mathrm{d}(Q\cos\theta^*) \propto (1+Q\cos\theta^*)^2\,, \tag{30}$$

where Q is the charge of the decay electron and θ^* is its angle, defined with respect to the direction of the incoming anti-quark in the W rest frame. Data from the UA1 experiment are shown in Fig. 34 and are compatible with expectations.

The UA2 detector is restricted in its charge measurement to the forward regions. A sample of 28 W candidates exists for $p_T^e > 20$ GeV/c. Fig. 35 shows the measured charge asymmetry. Defining N_p^+ ($N^-\bar{p}$) as the number of e^+ (e^-) on the side of incoming p ($\bar{p}$), and equivalently N_p^- ($N^+\bar{p}$), the UA2 collaboration has measured

$$\alpha = \{(N_p^+ + N^-\bar{p}) - (N^+\bar{p} + N_p^-)\}/N_{tot} = 0{\cdot}43 \pm 0{\cdot}17\,. \tag{31}$$

This is in good agreement with the value $\alpha = 0{\cdot}52 \pm 0{\cdot}06$ expected from their detector, in the case of pure V–A coupling.

(3g) The W and Z^0 Widths and the Number of Additional Neutrinos

Both $\Gamma(Z^0 \to \text{all})$ and Γ $(W \to \text{all})$ are determined by the number of fermions kinematically allowed in the decay. If kinematically allowed, decays to additional (l, ν_l) or (q, q') doublets would result in an increase of $\Gamma(W \to \text{all})$, and $(l, \bar{l})$, $(\nu_l, \bar{\nu}_l)$ or $(q, \bar{q})$ decays would result in an increase of $\Gamma(Z^0 \to \text{all})$.

Setting $\sin^2\theta_W = 0{\cdot}22$, using the W and Z^0 masses measured by the UA2 experiment, and $m_t = 40$ GeV, we get

$$\begin{aligned}
\Gamma(Z^0 \to l^+ l^-) &= 0{\cdot}088 \text{ GeV} \quad (l = e, \mu \text{ or } \tau)\,,\\
\Gamma(Z^0 \to \nu\bar{\nu}) &= 0{\cdot}177 \text{ GeV} \quad (l = \nu_e, \nu_\mu \text{ or } \nu_\tau)\,,\\
\Gamma(Z^0 \to q\bar{q}) &= 0{\cdot}319 \text{ GeV} \quad (q = \text{u or c})\,,\\
\Gamma(Z^0 \to q\bar{q}) &= 0{\cdot}068 \text{ GeV} \quad (q = \text{t}, m_t = 40 \text{ GeV})\,,\\
\Gamma(Z^0 \to q'\bar{q}') &= 0{\cdot}409 \text{ GeV} \quad (q' = \text{d, s or b})\,.
\end{aligned} \tag{32}$$

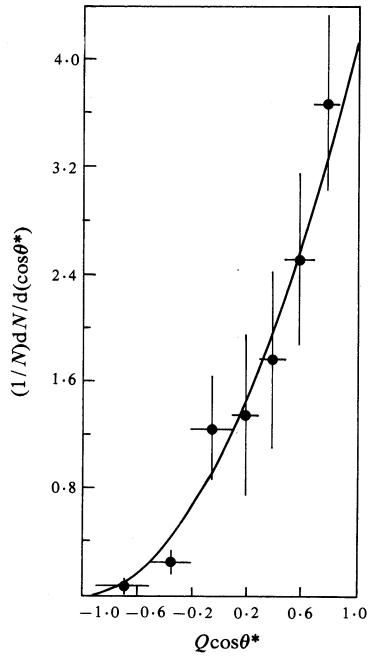

Fig. 34. Acceptance-corrected electron asymmetry for the decay $W \to e\nu$ from the UA1 experiment (118 events). The superimposed curve is of the form $(1 + Q\cos\theta^*)^2$, where Q and $\cos\theta^*$ are defined in the text.

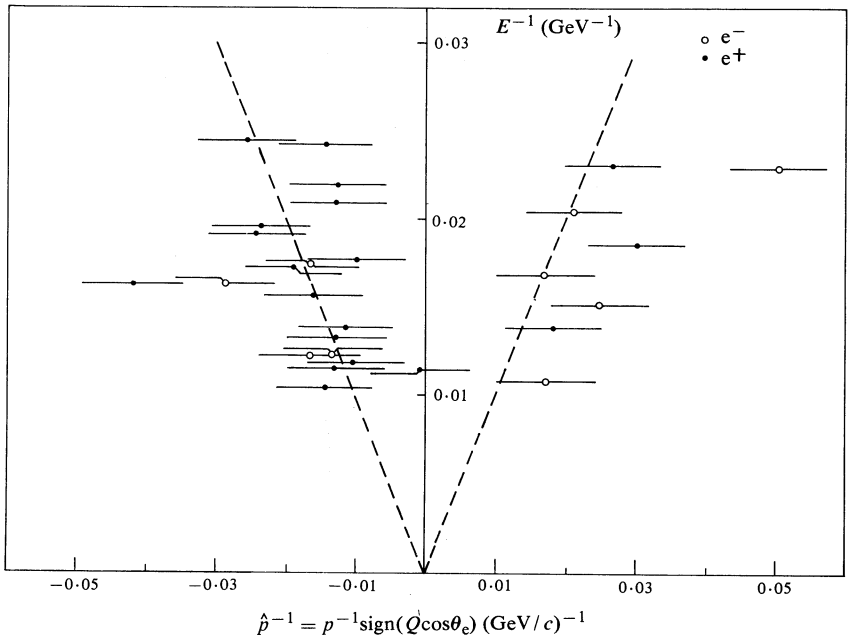

Fig. 35. The $W \to e\nu$ charge asymmetry in the UA2 experiment for 28 $W \to e\nu$ candidates in the range $20° < \theta < 40°$ and $140° < \theta < 160°$ with respect to the beam line, and with $p_T^e > 20$ GeV/c.

Within the GSW model, therefore, with three families of leptons and quarks, the total width $\Gamma(\mathrm{Z}\to\mathrm{all})$ is predicted to be 2·73 GeV. Suppose, however, that additional lepton doublets exist for which the decay $\mathrm{W}\to l\nu_l$ is kinematically disallowed, but for which the neutrino mass is light ($m_\nu \ll \frac{1}{2}M_\mathrm{W}$). The decays of Z^0 into the new light neutrino ($\mathrm{Z}^0 \to \nu_l\bar{\nu}_l$) would increase the Z^0 width:

$$\Gamma_\mathrm{Z}(\mathrm{meas}) = \Gamma_\mathrm{Z}(\mathrm{GSW})+(n_\nu-3)\Delta\Gamma_\nu; \qquad \Delta\Gamma_\nu = 0\cdot177\ \mathrm{GeV}. \tag{33}$$

Other new decays, for example supersymmetric decays $\mathrm{Z}^0 \to \tilde{\mathrm{e}}^+\tilde{\mathrm{e}}^-$ (Baer *et al.* 1985), could also contribute to $\Gamma(\mathrm{Z}^0)$.

Experimentally, $\Gamma(\mathrm{W}\to\mathrm{all})$ is difficult to measure since the mass M_W is not fully reconstructed; any limit must result from a fit of the p_T^e or M_T^W distribution to all known contributions, as already discussed. The best limit so far is $\Gamma(\mathrm{W}\to\mathrm{all}) < 7$ GeV (90% CL).

The width $\Gamma(\mathrm{Z}^0)$ can be directly measured (method 1), or can be obtained from the ratio of the production cross section for Z^0 and W into leptons (method 2):

$$\begin{aligned} R &= \sigma(\mathrm{Z}^0\to\mathrm{e}^+\mathrm{e}^-)/\sigma(\mathrm{W}\to\mathrm{e}\nu) \\ &= (\sigma_\mathrm{Z}/\sigma_\mathrm{W})\{\Gamma(\mathrm{Z}^0\to\mathrm{e}^+\mathrm{e}^-)/\Gamma(\mathrm{W}\to\mathrm{e}\nu)\}\{\Gamma(\mathrm{W}\to\mathrm{all})/\Gamma(\mathrm{Z}^0\to\mathrm{all})\}. \end{aligned} \tag{34}$$

This ratio R is measured experimentally, and the cross-section ratio $\sigma_\mathrm{Z}/\sigma_\mathrm{W}$ is evaluated from QCD. A recent calculation by Altarelli *et al.* (1985) predicted $\sigma_\mathrm{Z}/\sigma_\mathrm{W} = 0\cdot30\pm0\cdot02$. Taking $\Gamma(\mathrm{W}\to\mathrm{all})$, $\Gamma(\mathrm{W}\to\mathrm{e}\nu)$ and $\Gamma(\mathrm{Z}^0\to\mathrm{e}^+\mathrm{e}^-)$ from the GSW model, $\Gamma(\mathrm{Z}^0\to\mathrm{all})$ can be measured. The main advantage of this method is that most detector-dependent systematic uncertainties cancel, meaning that data from different experiments, and different decay channels, can be directly compared.

Table 7. Measurements of the Z^0 width

Quoted errors represent theoretical uncertainties

Width	UA1(e) (Levi 1985)	UA2(e) (DiLella 1985 *b*)
Γ_Z (GeV) (Method 2)	—	$2\cdot19^{+0\cdot7}_{-0\cdot5}\pm0\cdot22$ $<3\cdot17\pm0\cdot03$ (90% CL)
Γ_Z (GeV) (Method 1)	$<8\cdot5$ (90% CL) (1983 data)	$<3\cdot3$ (90% CL)

The current status of the $\Gamma(\mathrm{Z}^0\to\mathrm{all})$ measurements, and subsequent limits on the number of additional light neutrinos, is given in Table 7 for the UA1 and UA2 experiments.

(3h) Production Cross Section and Lepton Universality

Table 8 lists the measured production cross sections for the reactions

$$\begin{aligned} &\bar{\mathrm{p}}\mathrm{p}\to\mathrm{W}+X; \qquad \mathrm{W}\to l\nu_l; \qquad l = \mathrm{e}\ \mathrm{or}\ \mu, \\ &\bar{\mathrm{p}}\mathrm{p}\to\mathrm{Z}^0+X; \qquad \mathrm{Z}^0\to l^+l^-; \quad l = \mathrm{e}\ \mathrm{or}\ \mu. \end{aligned} \tag{35}$$

We have already noted (Section 3*d*) the report from UA1 of the decay $\mathrm{W}\to\tau\nu$.

Table 8. W and Z^0 production cross sections

$\sigma_Z \equiv \sigma(\bar{p}p \to Z^0 + X) B(Z^0 \to l^+ l^-)$, $\sigma_W \equiv \sigma(\bar{p}p \to W^\pm + X) B(W^\pm \to l^\pm \nu_l)$

Process	$\sqrt{s}$ (GeV)	Data (pb)	Prediction[A] (pb)
		UA1 collaboration	
$Z^0 \to e^+e^-$	546	$40 \pm 20 \pm 6$	42^{+13}_{-6}
$Z^0 \to \mu^+\mu^-$		$100 \pm 50 \pm 15$	
$Z^0 \to e^+e^-$	630	$79 \pm 21 \pm 12$	51^{+16}_{-10}
$Z^0 \to \mu^+\mu^-$		$51 \pm 17 \pm 9$	
$W \to e\nu_e$	546	$550 \pm 80 \pm 90$	360^{+110}_{-50}
$W \to \mu\nu_\mu$		$670 \pm 170 \pm 150$	
$W \to e\nu_e$	630	$630 \pm 50 \pm 90$	460^{+140}_{-80}
$W \to \mu^\pm\nu_\mu$		$610 \pm 110 \pm 130$	
		UA2 collaboration	
$Z^0 \to e^+e^-$	546	$110 \pm 39 \pm 9$	42^{+13}_{-6}
	630	$52 \pm 19 \pm 4$	51^{+16}_{-10}
$W \to e\nu_e$	546	$500 \pm 90 \pm 50$	360^{+110}_{-50}
	630	$530 \pm 60 \pm 50$	460^{+140}_{-80}

[A] From Altarelli *et al.* (1985).

Table 9. Measurements of lepton and quark coupling strengths at the Collider (UA1 experiment)

For example, $B(W \to e\nu_e)$ is the branching ratio for decay of a W into an e and ν_e

Coupling	Measured	Prediction
$W^\pm$: $\sigma_W B(W^\pm \to \mu^\pm \nu_\mu)/\sigma_W B(W^\pm \to e^\pm \nu_e)$	$1{\cdot}07 \pm 0{\cdot}17 \pm 0{\cdot}13$	1·0
$\sigma_W B(W^\pm \to \tau^\pm \nu_\tau)/\sigma_W B(W^\pm \to e^\pm \nu_e)$	$0{\cdot}96 \pm 0{\cdot}48$[A]	1·0
$\sigma_W B(W^\pm \to t\bar{b})/\sigma_W B(W^\pm \to e^\pm \nu_e)$	—	1·89
Z^0: $\sigma_Z B(Z^0 \to \mu^+\mu^-)/\sigma_Z B(Z^0 \to e^+e^-)$	$0{\cdot}73 \pm 0{\cdot}37$	1·0

[A] 1983 data.

This means that all known lepton doublets have been identified at the Collider. With the exception of $W \to t\bar{b}$, no direct observation of quark couplings has been reported (this is not the case for data reported in Section 4). Of course, if the u- and d-quark coupling to IVBs differed significantly from expectation, most results of the previous sections would be drastically affected.

Table 9 summarizes our knowledge from the $\bar{p}p$ Collider of tests on lepton universality. No results are quoted for the decays $W^+ \to t\bar{b}$ and $W^- \to \bar{t}b$ because the analysis of UA1 data is not yet complete.

We conclude that all leptonic decay modes have been reported, but that the quark coupling strengths have not been verified. Existing measurements at the Collider have limited accuracy, and improved statistics are necessary, as well as an improved control of systematic uncertainties.

(3i) Important Future Measurements at $\bar{p}p$ Colliders

With the measurement of M_W and M_Z at values predicted by the GSW model and the measurement of $\rho = 1$, evidence for the validity of the GSW model, with a single

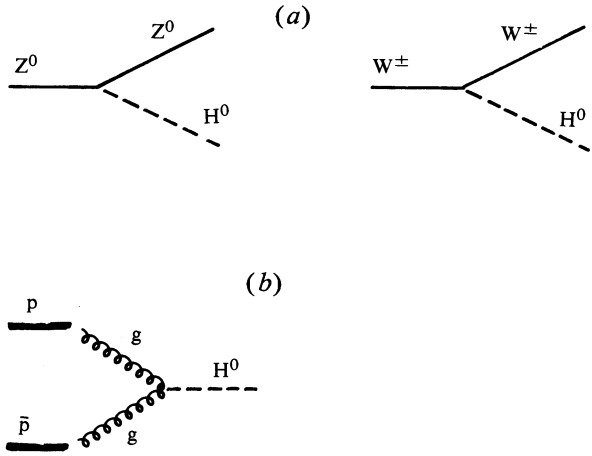

Fig. 36. Mechanisms for Higgs production at $\bar{p}p$ Colliders: (*a*) production via bremsstrahlung from a real or virtual Z^0 or W; and (*b*) direct production from gluon fusion.

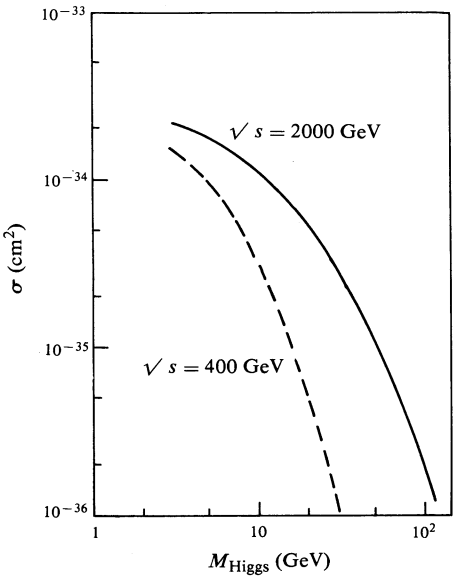

Fig. 37. Cross section for the inclusive production of Higgs particles as a function of the mass M_{Higgs}. [From Goggi (1984).]

neutral Higgs particle being the manifestation of mass generation, is overwhelming. Obviously, the search for significant deviations from the GSW model by more accurate mass measurements remains an important priority, both with regard to the identification of the effects of the Higgs boson from accurate measurements of ρ, and for the study of higher order radiative processes from accurate measurements of Δr.

As noted in Section 2*b*, the Higgs particle couples, with strength proportional to m_f, to the final-state fermion pairs. Production mechanisms which are relevant to the Collider include bremsstrahlung from W or Z^0 and gluon fusion (see Fig. 36).

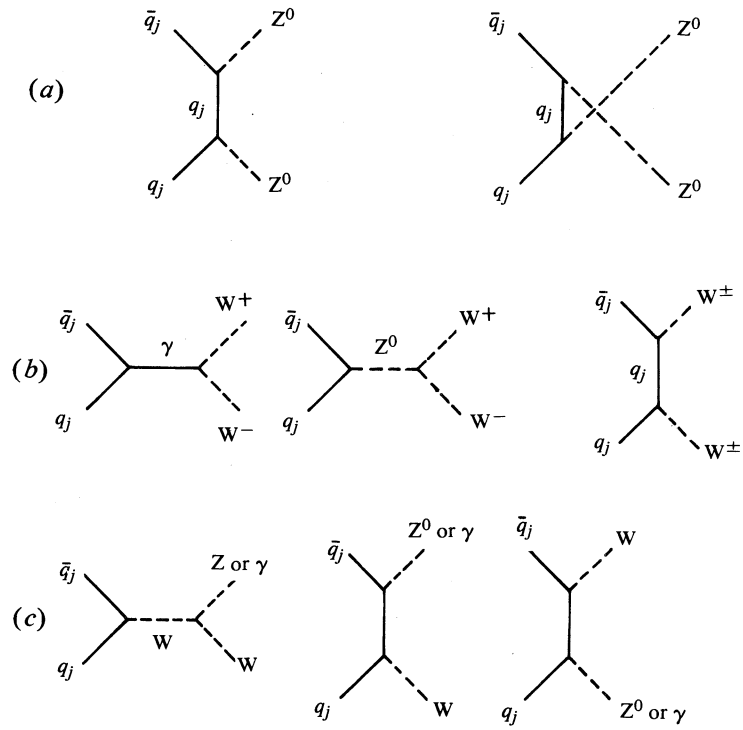

Fig. 38. Lowest order Feynman diagrams for the production of gauge pairs: (*a*) $q_j\bar{q}_j \to Z^0Z^0$, (*b*) $q_j\bar{q}_j \to W^+W^-$, and (*c*) $q_j\bar{q}_j \to WZ^0$ and $W^\pm\gamma$.

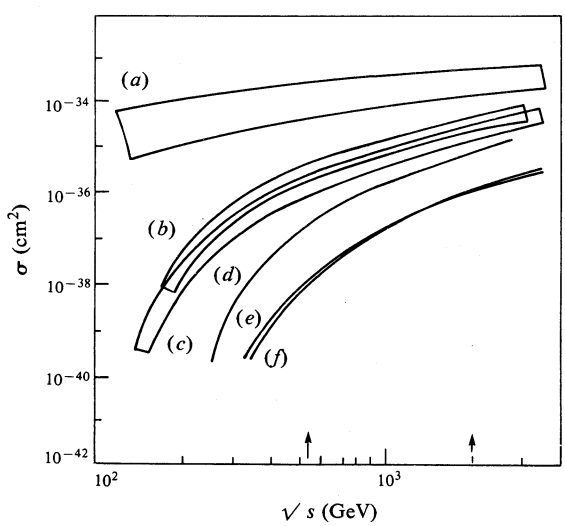

Fig. 39. Estimates of the production cross section for gauge-boson pairs plotted as a function of $\sqrt{s}$: (*a*) $\gamma\gamma$ production, (*b*) γZ^0 production, (*c*) γW production, (*d*) W^+W^- production, (*e*) Z^0Z^0 production, and (*f*) W^-Z^0 production. [From Humpert (1984).]

Unfortunately, the direct observation of the Higgs particle is unlikely at the $\bar{p}p$ Collider, because of its small production cross section (see Fig. 37). The production cross section increases with $\sqrt{s}$, and its observation is more likely at the proposed supercolliders ($\sqrt{s} \geqslant 10$ TeV). The whole question of Higgs particle production at these energies has been treated in detail by Eichten *et al.* (1985).

Another crucial measurement is the observation of self-coupling of the IVBs, with the expected rate. Typical lowest order diagrams for gauge-boson production are shown in Fig. 38. Large statistics are required because of cancellations between different contributions to the pair-production cross section. The cross-section predictions of Humpert (1984) are shown in Fig. 39; though W^+W^- production may be observable at the upgraded CERN $\bar{p}p$ Collider, measureable W^+W^- production is more likely at the Fermilab Collider ($\sqrt{s} \sim 2$ TeV) (the energies of these accelerators are indicated by arrows in Fig. 39).

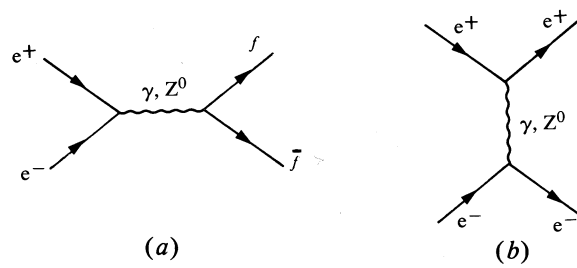

Fig. 40. Diagrams for (*a*) the s-channel process $e^+e^- \to f\bar{f}$, where f is a fermion of Table 1; and (*b*) the additional allowed t-channel process for the reaction $e^+e^- \to e^+e^-$.

4. Tests of the GSW Model in Other Interactions

In this review, attention has so far been placed on tests of the GSW model in the kinematic regime where physical IVBs exist and are detected. However, as already noted, extensive experimentation following the discovery of neutral currents in 1973 placed the GSW model on a firm footing even before $\bar{p}p$ Collider results were available.

Most of the work carried out has involved the validation of the predicted neutral-current axial and vector coupling constants noted in Table 3. From these couplings (sometimes with additional assumptions), $\sin^2\theta_W$ can be evaluated. If radiative corrections (which are process-dependent) are made, the resultant value $\sin^2\theta_W(M_W)$ can be compared with Collider results.

We concentrate here on quantitative tests of the GSW model involving neutral-current processes. With an obvious exception (the $W^\pm$), most experimentally observable consequences of charged-current processes can equally well be described by developments (which include for example the KM matrix) of the Fermi model. The charged-current data, which are of high precision, have recently been reviewed by Bertin and Vitrale (1984).

In this section we discuss e^+e^-, νe, νN and lepton–N interactions in Sections 4*a* to 4*d* respectively. As noted in the Introduction, we frequently utilize the recent review by Pullia (1984), and also that by Panman (1985). Where important new results have post-dated their reviews, we have included them in this section.

(4a) Tests of the GSW Model in e^+e^- Interactions

As shown in Fig. 40*a*, the reactions $e^+e^- \to f\bar{f}$ may proceed via the s-channel exchange of a photon or a Z^0. The interference between the two reactions produces a forward–backward asymmetry of the produced f ($\bar{f}$), allowing a measurement of certain coupling constants. For Bhaba scattering ($e^+e^- \to e^+e^-$), the situation is more complicated because of additional diagrams of the type shown in Fig. 40*b*. Nevertheless, comparisons can be made with predictions of the model.

So far, data are available at centre-of-mass energies up to $\sqrt{s} = 46\cdot8$ GeV from PEP ($\sqrt{s} = 29$ GeV) and Petra ($\sqrt{s} \leqslant 46\cdot8$ GeV). All fermion pairs have been produced, with the exception of $t\bar{t}$, therefore placing a mass limit of $m_t > 22\cdot7$ GeV (see Section 3*d* for $\bar{p}p$ results). At Petra, the following experiments have collected data: TASSO, PLUTO, CELLO, MARKJ and JADE. At PEP, the relevant experiments are MAC, HRS and MARK2.

The differential cross section (excluding Bhaba scattering) can be written as

$$d\sigma(e^+e^- \to f\bar{f})/d\Omega = (\alpha^2/4s)\{B(1+\cos^2\theta^*)+C\cos\theta^*\}, \tag{36}$$

where θ^* is the angle, measured in the centre-of-mass system, between the incident electron and the produced fermion.

The total cross section is therefore $\sigma(ee \to f\bar{f}) = (4\pi\alpha^2/3s)B$, and the forward–backward asymmetry is $A_{FB} = \frac{3}{8}C/B$. The term B, which measures the ratio of the actual cross section to the 'point-like' cross section, is often designated R^{ff}. The terms B and C depend on the couplings, and on a kinematic variable χ defined by

$$\chi = (G_F\rho/2\sqrt{2}\,\pi\alpha)sM_Z^2/\{(s-M_Z^2)+i\Gamma_Z M_Z\}. \tag{37}$$

For $s \ll M_Z^2$ and $\Gamma_Z \ll M_Z$, one finds that

$$\chi = -(G_F\rho/2\sqrt{2}\,\pi\alpha)s \sim -1\cdot8\times10^{-4}\,s. \tag{38}$$

At the highest available energies, $\sqrt{s} = 46\cdot8$ GeV, χ is about $0\cdot4$.

The expressions for B and C in (36) read

$$B = N_C[q_f^2 - 2q_f\,g_V(e)\,g_V(f)\,\mathrm{Re}(\chi) + \{g_A^2(e)+g_V^2(e)\}\{g_A^2(f)+g_V^2(f)\}\chi^2], \tag{39}$$

$$C = N_C\{4q_f\,g_A(e)\,g_A(f)\,\mathrm{Re}(\chi) + 8g_A(e)\,g_A(f)\,g_V(e)\,g_V(f)\chi^2\}. \tag{40}$$

The factor N_C in these definitions of B and C is 1 for leptons and 3 for quarks. Given the relatively modest values of χ presently obtainable, and the standard-model prediction that $g_V(e) \sim 0$ for the measured $\sin^2\theta_W$ (see Table 3), then the increase in the total cross section due to weak neutral currents is small, and $B \sim N_C\,q_f^2$ will be used. If χ^2 terms are neglected then the expected asymmetry is

$$A_{FB} = \tfrac{3}{2}\{g_A(e)\,g_A(f)/q_f\}\chi. \tag{41}$$

A measurement of A_{FB} in (41) determines the product of the axial couplings of the electron and the final-state fermion. In the GSW model (see Table 3) all axial couplings take the value $\pm\frac{1}{2}$ and the sign and magnitude of the expected asymmetries are precisely predicted, independent of $\sin^2\theta_W$. These measurements provide a strong test of the 'universality' of the axial couplings. Because of the existence of χ in (41), the asymmetry is $\sqrt{s}$ dependent, and it is important to measure A_{FB} at different $\sqrt{s}$ values.

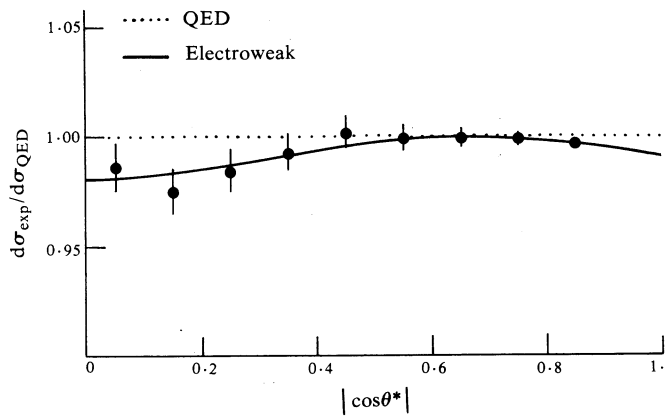

Fig. 41. Data from the MAC experiment (Prepost 1984) for the process $e^+e^- \rightarrow e^+e^-$. The deviation from the expected QED cross section is shown as a function of $\cos\theta^*$, with θ^* being the angle between the outgoing e^+ (e^-) and the incoming e^+ (e^-). Superimposed is the expectation from the GSW model with $\sin^2\theta_W = 0{\cdot}23$.

Measurements of the Reaction $e^+e^- \rightarrow e^+e^-$. As noted above, the simplicity of this reaction is masked by t-channel exchange contributions (see Fig. 40*b*). Recent data from the MAC experiment at PEP (Prepost 1984) is shown in Fig. 41, together with expectations from QED and the GSW model. Agreement with the GSW model is satisfactory, but significantly improved data are needed.

Combining these data with data of similar quality from PLUTO (Berger *et al.* 1985*a*) and using measurements of R^{ee}, one obtains

$$g_V^2(e) = 0{\cdot}09 \pm 0{\cdot}09\,, \qquad g_A^2(e) = 0{\cdot}36 \pm 0{\cdot}15\,.$$

The expected values, for $\sin^2\theta_W = 0{\cdot}22$, are $0{\cdot}004$ and $0{\cdot}25$ respectively.

Measurements of the Reaction $e^+e^- \rightarrow \mu^+\mu^-$. Since no t-channel exchange is involved, the asymmetry is given by equation (41), apart from small effects due to QED radiative corrections. Furthermore, from (41), the expected asymmetry A_{FB} should increase with s.

Data have been collected by all of the above experiments (see Pullia 1984, and cited references) at energies extending to $\sqrt{s} = 44{\cdot}7$ GeV. The data are shown in Fig. 42, and a comparison is made with expectations of the GSW model; the agreement is reasonable.

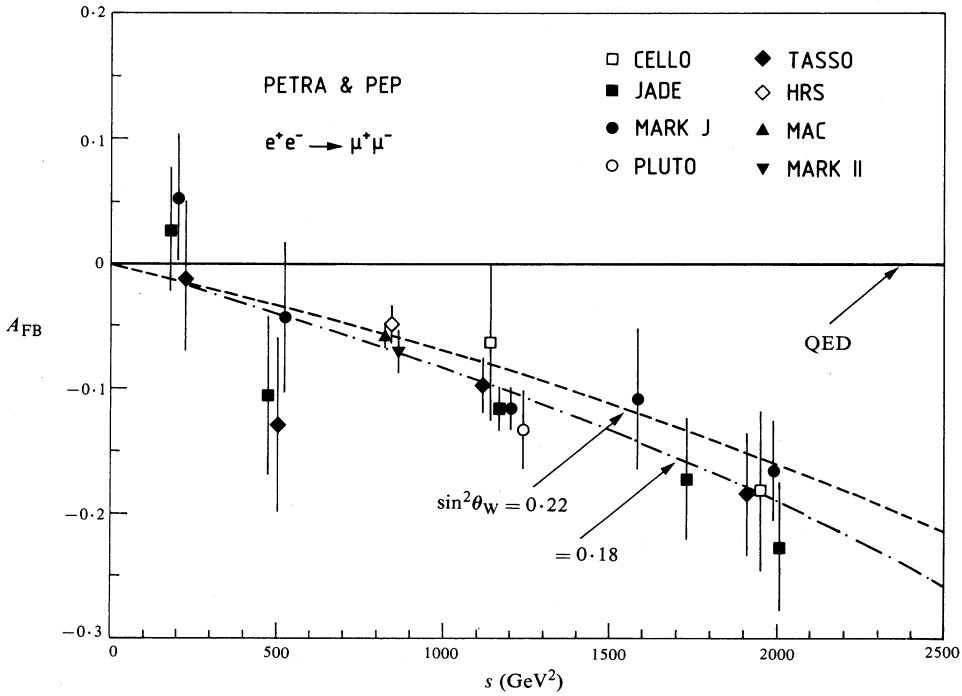

Fig. 42. Measured forward–backward asymmetry A_{FB} plotted as a function of the squared centre-of-mass energy s. Superimposed are expectations from QED, and from the GSW model with $\sin^2\theta_W = 0{\cdot}18$ and $\sin^2\theta_W = 0{\cdot}22$ (from A. Böhm, personal communication 1985).

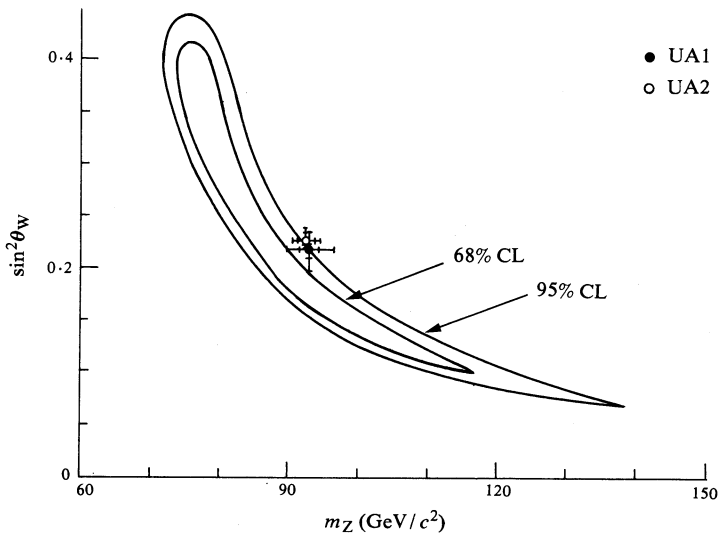

Fig. 43. The 68% and 95% confidence limits for the measurement of M_Z and $\sin^2\theta_W$, using combined PETRA and PEP data for the reaction $e^+e^- \to \mu^+\mu^-$. Superimposed are the limits obtained from UA1 and UA2 data (shown are statistical errors and the errors when statistical and systematic errors are added in quadrature).

From measurements of A_{FB} the quantity $g_A(e)\,g_A(\mu)$ can be evaluated (strictly speaking for given values of M_Z and ρ). If measurements of $R^{\mu\mu}$ are also included, the quantity $g_V(e)\,g_V(\mu)$ can be evaluated. A compilation of existing data has been given by Berger *et al.* (1985*a*). Averaging their values gives

$$g_A(e)\,g_A(\mu) = 0{\cdot}25 \pm 0{\cdot}02\,, \qquad g_V(e)\,g_V(\mu) = 0{\cdot}02 \pm 0{\cdot}02\,,$$

which can be compared with GSW model predictions of 0·25 and 0·004 respectively.

By assuming the validity of the GSW model, a fit can be made to M_Z and $\sin^2\theta_W$. The resulting contour enclosing allowed M_Z and $\sin^2\theta_W$ values is shown in Fig. 43, where it is compared with measurements from the UA1 and UA2 experiments (Böhm 1985 and personal communication).

Measurements of the Reaction $e^+e^- \to \tau^+\tau^-$. A measurement of $R^{\tau\tau}$ and A^{τ}_{FB} allows a determination of $g_A(e)\,g_A(\tau)$ and $g_V(e)\,g_V(\tau)$ exactly as for the muon case described above. A comparison of $g_A(e)\,g_A(\tau)$ provides a test of lepton universality in the axial neutral-current sector of the GSW model. The data were recently reviewed by Langacker (1984), but since then accurate new data have become available from MAC (Fernandez *et al.* 1985), HRS (Gan *et al.* 1985), TASSO (Althoff *et al.* 1985) and PLUTO (Berger *et al.* 1985*b*).† An average of existing data results in the measurement of (to be compared with 0·25 in the GSW model)

$$g_A(e)\,g_A(\tau) = 0{\cdot}22 \pm 0{\cdot}04\,.$$

Measurements of $g_V(e)\,g_V(\tau)$, which are difficult because of the need to accurately measure $R^{\tau\tau}$, are consistent with zero but with a large uncertainty. The ability to determine the τ helicity state from its weak decay enables, in principle, a sensitive test of the neutral-current vector couplings, and a determination of the relative signs of the vector and axial couplings. So far the data are inadequate. However, for studies near the Z^0 pole at the LEP and SLC machines, such an analysis will be of interest (Goggi 1979).

Measurements of the Reactions $e^+e^- \to c\bar{c}$ *and* $e^+e^- \to b\bar{b}$. It is evident from equation (41), and Table 3, that the expected asymmetry is larger in these reactions than for purely leptonic processes, because of the fractional quark charge q_f. It is also obvious from Table 3 that the quantities derived from a measurement of $A_{FB}(c)$ or $A_{FB}(b)$, and $g_A(e)\,g_A(c)$ or $g_A(e)\,g_A(b)$ respectively, have opposite sign.

The latter fact has important implications. If for example the sample of events compatible with the process $e^+e^- \to c\bar{c}$ is contaminated by d-quark or b-quark backgrounds, then the measured value of $g_A(e)\,g_A(c)$ is drastically affected. Similar arguments apply for the b-quark sample.

The asymmetry must further be corrected for the effect of higher order QCD processes, for example, the exchange of a virtual gluon between the outgoing q and $\bar{q}$.

† See also the recent data from PLUTO (Berger *et al.* 1985*a*), TASSO (Althoff *et al.* 1984), JADE (Bartel *et al.* 1984, 1985), CELLO (Behrend *et al.* 1982), MARKJ (Adeva *et al.* 1982, 1985), MAC (Fernandez *et al.* 1983*a*, 1983*b*), HRS (Bender *et al.* 1984; Derrick *et al.* 1985), MARK2 (Levi *et al.* 1984) and TPC (Aihara *et al.* 1985).

In practice, c-quark decays are identified by the direct observation of the decay of a D* resonant state, or from the lepton following a semileptonic decay of the c quark. (The latter method is also used for b-quark identification.) Because of the difficulties of isolating clean c-quark and b-quark samples (which we do not discuss here), the data are so far sparse. When averaged over all available data, $g_A(e)\,g_A(c)$ and $g_A(e)\,g_A(b)$ are measured with large statistical errors. The average values given by Langacker (1984) were

$$\begin{aligned} g_A(c) &= 0{\cdot}5 \pm 0{\cdot}2 && \text{(PETRA)} \\ &= 0{\cdot}6 \pm 0{\cdot}15 && \text{(PEP)} \\ &= 0{\cdot}5 && \text{(GSW model)}, \\ g_A(b) &= -0{\cdot}47 \pm 0{\cdot}11 && \text{(PETRA)} \\ &= -0{\cdot}57 \pm 0{\cdot}12 && \text{(PEP)} \\ &= -0{\cdot}5 && \text{(GSW model)}. \end{aligned}$$

Preliminary data by Böhm (1985) have slightly improved the errors; considerable efforts are being made to improve the accuracy of these data at both PETRA and PEP.

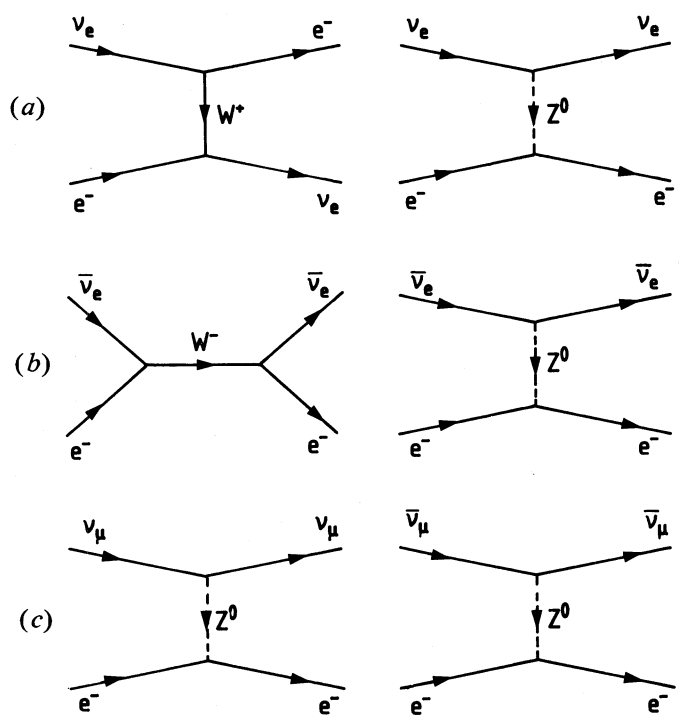

Fig. 44. Diagrams for the processes (*a*) $\nu_e e \to \nu_e e$, (*b*) $\bar{\nu}_e e \to \bar{\nu}_e e$, and (*c*) $\nu_\mu e \to \nu_\mu e$ and $\bar{\nu}_\mu e \to \bar{\nu}_\mu e$.

No similar asymmetry data exist for u-, d- and s-quark processes, since experimentally the quark flavour is difficult to unambiguously identify. Finally, we once again note that the process $e^+e^- \rightarrow t\bar{t}$ has not been observed at energies $\sqrt{s} \leqslant 47$ GeV.

(4b) Neutrino–Electron Scattering

The class of neutral-current reactions $\nu e \rightarrow \nu e$ (see Fig. 44) is studied using relatively high energy ν_μ and $\bar{\nu}_\mu$ beams from accelerators, using low energy $\bar{\nu}_e$ from reactors and, recently, using intermediate energy ν_e from a LAMPF beam stop experiment. These experiments yield valuable information on the neutral coupling of the Z^0 to the electron.

The cross sections for all four reactions can be put in the form

$$d\sigma/dy = (G_F^2 s/\pi)\{A + B(1-y)^2 + Cy\}, \tag{42}$$

where $s = 2M_e E_\nu$ and $y = (E_\nu - E_\nu')/E_\nu$. Here E_ν (E_ν') is the energy of the incident (outgoing) ν, measured in the rest frame of the target electron. Equivalently, y is the fractional energy given to the electron $y = E_e/E_\nu$. The coefficient C is proportional to M_e/E_ν and is dropped here, although it should not be neglected in reactor experiments. The coefficients A and B are simplest when expressed in terms of helicity couplings, assuming $g_L(\nu) = \frac{1}{2}$ and $g_R(\nu) = 0$:

	A	B
$\nu_\mu e$	$g_L^2(e)$	$g_R^2(e)$
$\bar{\nu}_\mu e$	$g_R^2(e)$	$g_L^2(e)$
$\nu_e e$	$\{g_L(e)+1\}^2$	$g_R^2(e)$
$\bar{\nu}_e e$	$g_R^2(e)$	$\{g_L(e)+1\}^2$

The more easily studied ν_μ induced reactions (Fig. 44*c*) measure the square of couplings, while the ν_e induced reactions contain a neutral-current charged-current interference term (Figs 44*a* and 44*b*), and can be used to determine the signs of the couplings.

Given the many systematic uncertainties inherent in the cross-section evaluations in these experiments, a measurement of the ratio

$$R = \sigma(\nu_\mu e)/\sigma(\bar{\nu}_\mu e) = (1+\eta+\eta^2)/(1-\eta+\eta^2), \tag{43}$$

where $\eta = 1 - 4\sin^2\theta_W$, gives a sensitive measurement of $\sin^2\theta_W$ in which many systematic errors cancel. Using this method, $\sin^2\theta_W$ is measured independently of ρ, which cancels in the ratio. If we use in addition the relation

$$\sigma(\bar{\nu}_\mu e)_{meas} = \rho^2\sigma(\bar{\nu}_\mu e)_{th}, \tag{44}$$

then ρ can be estimated. Because of their theoretical simplicity, attempts are at present under way to make the most precise possible measurements using these reactions.

A compilation of recent $\nu_\mu e$ and $\bar{\nu}_\mu e$ scattering experiments is shown in Table 10. It is evident that, especially for the reaction $\bar{\nu}_\mu e \rightarrow \bar{\nu}_\mu e$, the data are dominated by the E734 experiment at BNL and the CHARM experiment at CERN.

Table 10. Compilation of ν_μ e and $\bar{\nu}_\mu$ e scattering experiments

Experiment	Signal	Background	σ/E (10^{-42} cm^2 GeV^{-1})	Reference
			ν_μ e	
Aachen–Padova	7	$3\cdot9\pm0\cdot5$	$1\cdot1\pm0\cdot6$	Faissner *et al.* (1978)
GGM-SPS	9	$0\cdot5\pm0\cdot2$	$2\cdot4^{+1\cdot2}_{-0\cdot9}$	Armenise *et al.* (1979)
Columbia	11	$0\cdot8\pm0\cdot8$	$1\cdot8\pm0\cdot8$	Cnops *et al.* (1978)
VPI-M	34	12 ± 3	$1\cdot4\pm0\cdot3\pm0\cdot2$	Heisterberg *et al.* (1980)
E734	51	25 ± 3	$1\cdot6\pm0\cdot55\pm0\cdot49$	Murtagh (1984)
	46	64 ± 10		
CHARM	37	48 ± 10	$1\cdot8\pm0\cdot3\pm0\cdot4$	Panman (1984)
			$\bar{\nu}_\mu$ e	
Aachen–Padova	6	$1\cdot7\pm0\cdot3$	$2\cdot2\pm1\cdot0$	Faissner *et al.* (1978)
GGM-PS	3	$0\cdot4\pm0\cdot3$	$1\cdot0^{+1\cdot3}_{-0\cdot6}$	Blietschau *et al.* (1976)
E734	59		$1\cdot16\pm0\cdot2\pm0\cdot14$	Ahrens *et al.* (1985)
CHARM	77	174 ± 19	$1\cdot4\pm0\cdot3\pm0\cdot3$	Panman (1984)
	35	81 ± 10		

To minimize systematic errors resulting from cross-section normalization and background-subtraction uncertainties, both the CHARM (Panman 1984) and E734 (Ahrens *et al.* 1985) experiments used equation (43) to evaluate $\sin^2\theta_W$, and the coupling constants $g_V(e)$ and $g_A(e)$. The current status of these measurements is

	$\sin^2\theta_W$	$\lvert g_V(e)\rvert$	$\lvert g_A(e)\rvert$
CHARM	$0\cdot215\pm0\cdot032\pm0\cdot012$	$0\cdot08\pm0\cdot07\pm0\cdot03$	$0\cdot54\pm0\cdot05\pm0\cdot06$
BNL	$0\cdot209\pm0\cdot029\pm0\cdot013$		
Mean	$0\cdot212\pm0\cdot023$		

From the existing ν_μ e and $\bar{\nu}_\mu$ e data alone, $|g_V(e)|$ and $|g_A(e)|$ are interchangeable solutions. However, when these data are combined with results from e^+e^- interactions (see the previous subsection), only the solution shown in Fig. 45 is acceptable.

The estimation of $\sin^2\theta_W$ above is independent of ρ, since equation (43) is used. Using equation (44) ρ can be estimated, though with large systematic uncertainties. The CHARM experiment quoted

$$\rho = 1\cdot09\pm0\cdot09(\text{stat})\pm0\cdot11(\text{syst}).$$

With an expected ten-fold increase in statistics from the CHARM2 experiment, which is now in preparation, $\sin^2\theta_W$ should be measured to an accuracy of $\sim0\cdot005$, an accuracy similar to that of measurements from the $\bar{p}p$ Collider.

Because of the interference term existing in ν_e e scattering the sign ambiguities of $g_V(e)$ and $g_A(e)$ measurements can be resolved. Wang (1984) described such an experiment at LAMPF. In this important experiment, ν_e of energy $0 \leqslant E_\nu \leqslant 50$ MeV are produced by the decay of π^+ mesons, produced at the dump of an 800 MeV/c proton beam. Roughly equal proportions of ν_e, ν_μ and $\bar{\nu}_\mu$ are produced, but the ν_μ and $\bar{\nu}_\mu$ momentum spectra are different. The preliminary results given by Wang were

$$\sigma(\nu_e\,e) = (10\cdot6\pm4\cdot6\pm1\cdot9)E_\nu\times10^{-42}\,\text{cm}^2 \quad (E_\nu \text{ in GeV}),$$

$$\sin^2\theta_W = 0\cdot27\pm0\cdot17.$$

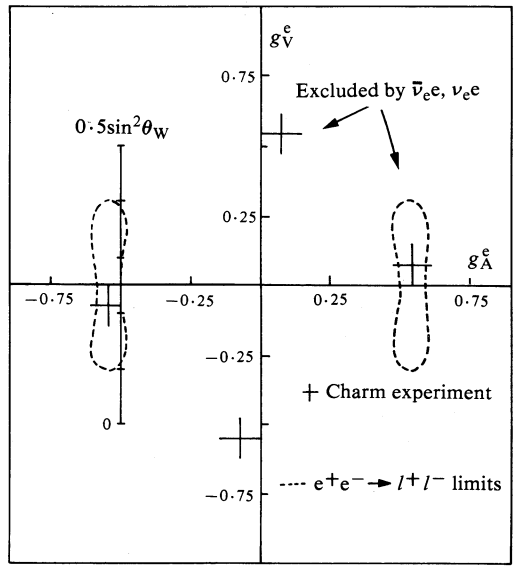

Fig. 45. Measurements of g_A^e and g_V^e from the reactions ν_μ e $\rightarrow$ ν_μ e and $\bar{\nu}_\mu$ e $\rightarrow$ $\bar{\nu}_\mu$ e in the CHARM experiment. Superimposed are results from e^+e^- annihilation experiments. Solutions of g_A^e and g_V^e, which are excluded by ν_e e and $\bar{\nu}_e$ e scattering measurements, are also marked.

This precision is sufficient to resolve the sign ambiguity of g_A(e) and g_V(e). The number of ν_e e candidates in the data was $17\cdot0\pm7\cdot4$ events, compared with $15\pm2\cdot7$ events expected from the GSW model, and $30\cdot8\pm5\cdot5$ events if no interference existed. The accuracy of the data, as summarized by Haidt (1985), has since significantly improved, but the latest analysis is not yet published.

The process $\bar{\nu}_e$ e $\rightarrow$ $\bar{\nu}_e$ e has also been reported (Reines *et al.* 1976). This experiment was of sufficient precision to exclude constructive interference, but the zero-interference case could not be excluded.

(4c) Neutrino–Hadron Interactions

The cross section for ν or $\bar{\nu}$ scattering from a nucleon (see Fig. 46) is a simple extension of the previously given cross-section formulae for νe and $\bar{\nu}$e scattering; the ν cross section is

$$\begin{aligned} d\sigma^{NC}/dy(\nu N\rightarrow\nu X) = (G_F^2\, s/\pi) \int x\, dx\, [u^N(x)\{g_L^2(u)+g_R^2(u)(1-y)^2\} \\ + d^N(x)\{g_L^2(d)+g_R^2(d)(1-y)^2\} \\ + \text{corrections}], \end{aligned}$$

where $s = 2M_N E_\nu$ and y is the fractional energy loss of the neutrino, $y = (E_\nu - E_\nu')/E_\nu$, measured in the rest frame of the target nucleon. The functions $u^N(x)$ and $d^N(x)$ are the quark momentum distributions for the nucleon, and x is the Bjorken scaling variable (Bjorken and Paschos 1969). The equivalent cross section for $\bar{\nu}$ scattering is obtained by interchanging g_L and g_R.

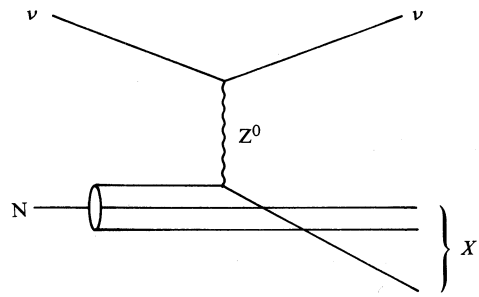

Fig. 46. Neutral-current reaction $\nu N \to \nu X$. The diagram is unchanged for the reaction $\bar{\nu} N \to \bar{\nu} X$.

Contrary to the case of νe scattering discussed in Section 4*b*, additional corrections must be applied:

(i) QCD effects and uncertainties of the structure-function measurement;

(ii) sea-quark contributions to the nucleon momentum; and

(iii) the creation of new reaction channels with increasing energy.

Measurements of νN or $\bar{\nu} N$ scattering have been made using hydrogen or deuterium-filled bubble chambers, and they provide determinations of $g_L^2(u)$, $g_L^2(d)$, $g_R^2(u)$ and $g_R^2(d)$. Because of the small measured νN cross sections, isoscalar targets are frequently used; for example, iron (CDHS), SiO_2 (CHARM), or ^{18}Ne (bubble chambers). In these experiments, only the combinations $g_L^2(u)+g_L^2(d)$ and $g_R^2(u)+g_R^2(d)$ can be measured, though with good statistical precision. However, the associated theoretical uncertainties are less well known (for example, differences between the quark structure functions measured in iron and in hydrogen, and higher order QCD processes). In all experiments, the non-observation of scattered neutrinos makes a measurement of the momentum transfer given to the Z^0 exchange difficult. Furthermore, measurements of the cross sections alone have normalization uncertainties. For a summary of the experimental problems, the review by Pullia (1984) is recommended.

Many experimental uncertainties (especially cross-section normalizations) are reduced when the above neutral-current processes are compared with the charged-current reactions:

$$d\sigma^{CC}/dy(\nu N \to l^- X) = (G_F^2\, s/\pi) \int x\, dx\, \{ d^N(x) + \text{corrections} \},$$

$$d\sigma^{CC}/dy(\bar{\nu} N \to l^+ X) = (G_F^2\, s/\pi) \int x\, dx\, \{ u^N(x)(1-y)^2 + \text{corrections} \}.$$

For isoscalar targets (similar expressions are available for nucleon targets), we have

$$R_\nu = \sigma^{NC}(\nu)/\sigma^{CC}(\nu)$$

$$= \{ g_L^2(u)+g_L^2(d) \} + r\{ g_R^2(u)+g_R^2(d) \} + \text{corr.}, \tag{45a}$$

$$R_{\bar{\nu}} = \sigma^{NC}(\bar{\nu})/\sigma^{CC}(\bar{\nu})$$

$$= \{ g_L^2(u)+g_L^2(d) \} + r^{-1}\{ g_R^2(u)+g_R^2(d) \} + \text{corr.}, \tag{45b}$$

where $r = \sigma^{CC}(\bar{\nu})/\sigma^{CC}(\nu)$, and $r = \frac{1}{3}$ in the naive valence-quark treatment of νN

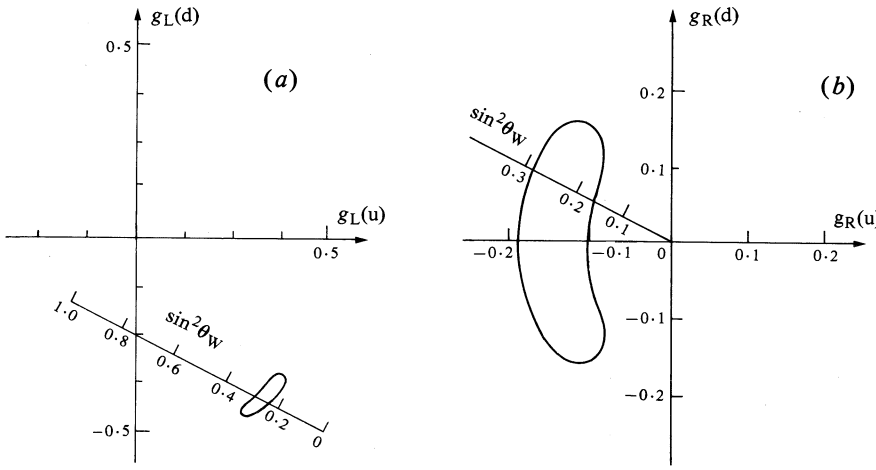

Fig. 47. The 68% confidence limits for (*a*) g_L(d) versus g_L(u) and (*b*) g_R(d) versus g_R(u) measured in neutrino–nucleon and antineutrino–nucleon interactions. [From the review by Pullia (1984).]

scattering. A direct measurement of $\sin^2\theta_W$ can be made from the ratio (Paschos and Wolfenstein 1973)

$$R^{\pm} = \{\sigma^{NC}(\nu)\pm\sigma^{NC}(\bar{\nu})\}/\{\sigma^{CC}(\nu)\pm\sigma^{CC}(\bar{\nu})\}\,. \tag{46}$$

For an isoscalar target, we have

$$R^- = \rho^2(\tfrac{1}{2}-\sin^2\theta_W)\,, \qquad R^+ = \rho^2(\tfrac{1}{2}-\sin^2\theta_W+\tfrac{10}{9}\sin^4\theta_W)\,.$$

In addition to the above inclusive measurements, a measurement of some exclusive processes, for example $\nu p \to \nu n\pi^+$ and $\nu p \to \nu p\pi^0$, separates the isospin structure of the neutral currents and allows the measurement of a unique solution for g_L(u), g_L(d), g_R(u) and g_R(d).

The most recent published values for the chiral couplings to light quarks have been taken from Pullia (1984) and are given by (see also Fig. 47)

$$g_L(\mathrm{u}) = 0{\cdot}344\pm0{\cdot}026\,, \qquad g_L(\mathrm{d}) = -0{\cdot}419\pm0{\cdot}022\,,$$

$$g_R(\mathrm{u}) = -0{\cdot}153\pm0{\cdot}022\,, \qquad g_R(\mathrm{d}) = 0{\cdot}076\pm0{\cdot}041\,.$$

Also shown in Fig. 47 are the GSW predictions as a function of $\sin^2\theta_W$.

A measurement of $\sin^2\theta_W$ is best extracted from these data via the ratios R_ν and $R_{\bar{\nu}}$ (or $R^{\pm}$) given in equations (45) and (46). Fig. 48, taken from Abramowicz *et al.* (1985), summarizes the results with the caveat that the measured ratios from the various experiments have been corrected to allow for their different kinematic acceptances. The values of $\sin^2\theta_W$ determined from these measurements are presented in Table 11. It is apparent from Fig. 48 that of the two ratios (45) R_ν is much more sensitive to $\sin^2\theta_W$. Moreover, available ν beam fluxes are about six times more intense than $\bar{\nu}$ fluxes. Three experiments have recently measured R_ν to good precision, and their preliminary results represent the best determination of $\sin^2\theta_W$

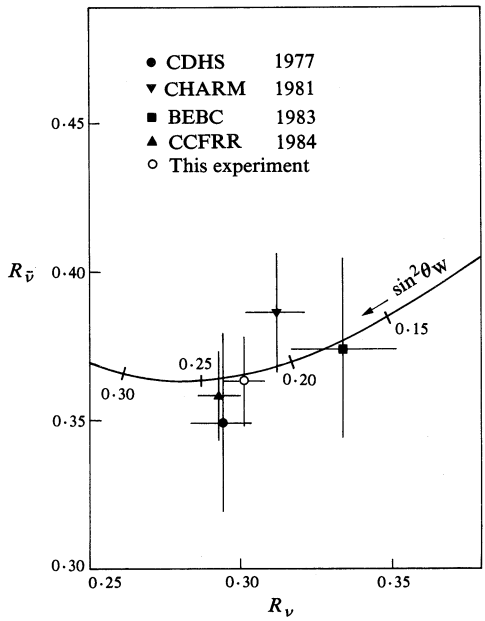

Fig. 48. Ratios R_ν and $R_{\bar{\nu}}$ for recent data from neutrino(antineutrino)-nucleon interactions. [From Abramowicz *et al.* (1985).]

Table 11. Measurements of $\sin^2\theta_W$ from νN scattering

Definitions of the radiatively corrected values of $\sin^2\theta_W$ differ slightly from experiment to experiment (see Section 4*c*)

Experiment (Reference)	$\sin^2\theta_W$ Measured	$\sin^2\theta_W$ Corrected	ρ
BEBC (Bosetti 83)	0·182±0·020±0·012 (stat) (syst)		
CDHS (Abramowicz 85)	0·239±0·012	0·226±0·012±0·006 (exp) (th)	1
CDHS (Blondel 85)		0·217±0·007±0·006 (exp) (th)	1
CHARM (Jonker 81)		0·220±0·014±0·009 (exp) (th)	1
		0·247±0·038	1·027±0·023
CHARM (Bergsma 85)	0·224±0·010	0·215±0·010 (exp)	1
CCFRR (Reutens 85)		0·242±0·011±0·005 (exp) (th)	1
		0·234±0·026±0·010	0·991±0·025±0·009

in νN scattering. Results have been presented by the CDHS collaboration (Blondel 1985), by the CHARM experiment (Bergsma *et al.* 1985) and by CCFRR (Reutens *et al.* 1985). Their values of $\sin^2\theta_W$ are given in Table 11. All three experiments are dominated by systematic errors, and the quoted uncertainties are conservative, reflecting the preliminary nature of the results.

A study of the reactions $\bar{\nu}N \rightarrow \bar{\nu}V^0X$, where V^0 is a neutral strange particle, has been reported by Asratyan *et al.* (1984). They measured the strange-quark couplings

to be $g_L^2(s)+g_R^2(s) = 0\cdot30\pm0\cdot11$, a value in agreement with the GSW expectation (see Table 3).

In some exclusive channels, for example

$$\nu N \rightarrow \nu\Psi + X; \qquad \Psi \rightarrow \mu^+\mu^-,$$

limited information is available on the $c\bar{c}Z^0$ vertex coupling. Abramowicz *et al.* (1982) have observed the diffractive production of the Ψ in the above reaction, and concluded that their measured cross section is consistent with the hypothesis that the $c\bar{c}Z^0$ and $u\bar{u}Z^0$ couplings are equal.

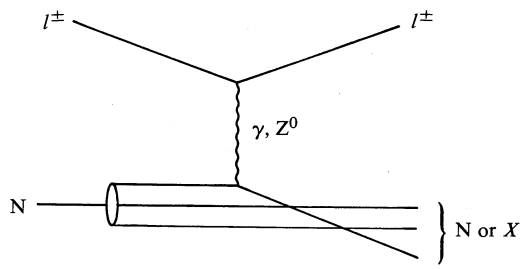

Fig. 49. Neutral currents in charged-lepton-hadron scattering.

(4d) Charged-lepton–Hadron Scattering

Three kinds of experiment have probed the weak neutral currents using γ–Z^0 interference effects in charged-lepton–hadron scattering (see Fig. 49). In the scattering of polarized electrons from deuterium ($e\uparrow D \rightarrow eX$), a left–right asymmetry of the cross section can be defined (Cahn and Gilman 1978). Defining σ_L (σ_R) to be the cross section for the scattering of left-handed (right-handed) electrons, measured in a given interval of q^2 and y, the expected asymmetry is

$$\epsilon = (\sigma_R-\sigma_L)/(\sigma_R+\sigma_L) = (3G_F/5\sqrt{2}\,\pi\alpha)\{A+BF(y)\}q^2,$$

where

$$A = g_A(e)\{2g_V(u)-g_V(d)\}, \qquad B = g_V(e)\{2g_A(u)-g_A(d)\},$$

$$F(y) = \{1-(1-y)^2\}/\{1+(1-y)^2\},$$

and where y is the fractional energy loss of the electron, and q^2 is the square of the four-momentum transferred from the electron via the exchanged Z^0 or γ.

Experimentally one measures A and B and so determines products of coupling constants of the type $g_A(e)\,g_V(q)$. This experiment has been performed at SLAC (Prescott *et al.* 1979), where the asymmetry was fitted to the form $\epsilon/q^2 = a+bF(y)$, and $a = (-9\cdot7\pm2\cdot6)\times10^{-5}$ GeV^{-2} and $b = (4\cdot9\pm8\cdot1)\times10^{-5}$ GeV^{-2} were obtained. From these values $\sin^2\theta_W = 0\cdot224\pm0\cdot012(\text{stat})\pm0\cdot008(\text{syst})$ was deduced, taking $\rho = 1$. When radiatively corrected to the W mass, the result becomes $\sin^2\theta_W = 0\cdot218\pm0\cdot020$ (Marciano 1985).

The same processes have been studied in a different q^2 range [$|q^2| \sim 10^{-12}$ (GeV/c)^2] from atomic transitions in heavy nuclei. It can be shown that the parity violating interaction Lagrangian takes the form

$$L = (G_F/\sqrt{2})(\boldsymbol{\sigma}\,.\,\boldsymbol{p}/m)_e\, Q_W\, g_A(e),$$

where $Q_W = 2\{N_u\, g_V(u) + N_d\, g_V(d)\}$, N_u and N_d are the numbers of u and d quarks in the nucleus, and $\boldsymbol{\sigma}$ is the Pauli operator. As $N_u \approx N_d$ for heavy nuclei, these experiments measure a different combination of $g_V(u)$ and $g_V(d)$ than in polarized electron scattering. The main uncertainty in these measurements is the knowledge of the electron density within the heavy nucleus. The experiments are also relatively insensitive to $\sin^2\theta_W$, as will be demonstrated below.

Experiments have been made on bismuth, lead, thallium and cesium with similar precision. As an example, we quote the most recent results for cesium atoms (Bouchiat *et al.* 1982, 1984) which give

$$\sin^2\theta_W = 0{\cdot}205 \pm 0{\cdot}034(\text{stat}) \pm 0{\cdot}025(\text{syst}) \pm 0{\cdot}045(\text{th}).$$

The data were reviewed by Fortson and Lewis (1984) who quoted a world average value of $\sin^2\theta_W = 0{\cdot}21 \pm 0{\cdot}05$.

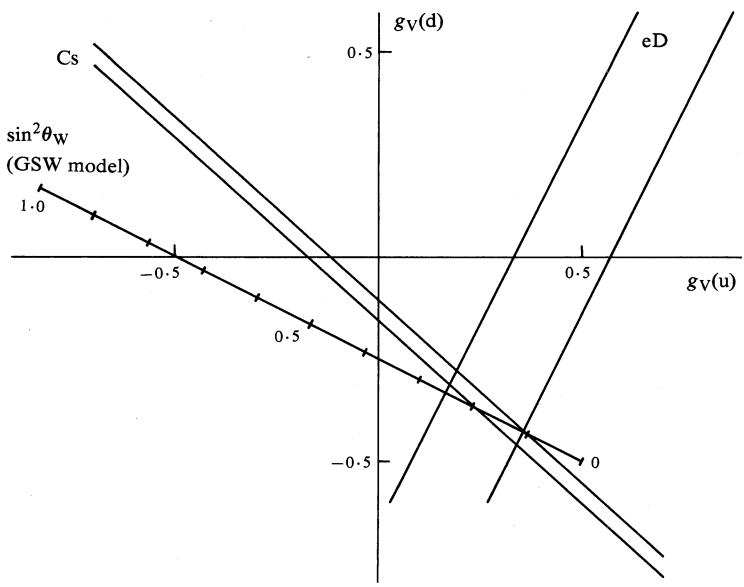

Fig. 50. Limits on the vector couplings $g_V(u)$ and $g_V(d)$ obtained from polarized electron–deuteron scattering (Prescott *et al.* 1979) and from atomic parity violation in cesium (Bouchiat *et al.* 1982). Also shown is the dependence of $\sin^2\theta_W$ on $g_V(u)$ and $g_V(d)$, for the GSW model.

The experiment on polarized electron scattering and those on atomic transitions may be neatly compared in a plot of the $[g_V(u), g_V(d)]$ plane. Taking $g_A(e) = -\frac{1}{2}$, the result of each experiment defines an allowed band in this plane (see Fig. 50). As already stated, these bands are roughly orthogonal. Also shown in Fig. 50 is the GSW prediction as a function of $\sin^2\theta_W$. This line runs approximately parallel to the atomic physics results, causing the lack of sensitivity to $\sin^2\theta_W$ as previously remarked.

Finally, an experiment at CERN (the BCDMS collaboration of Argento *et al.* 1983) has studied μ–carbon inelastic scattering. This experiment is sensitive to the

product $g_A(\mu)\{2g_A(u)-g_A(d)\}$, in the q^2 range $40 < |q^2| < 180\ (\mathrm{GeV}/c)^2$. Using polarized μ^+ and μ^- beams at momenta of 120 and 200 GeV/c, they measured the asymmetry

$$B = \{\sigma^+(-\lambda)-\sigma^-(+\lambda)\}/\{\sigma^+(-\lambda)+\sigma^-(+\lambda)\}$$
$$= (G_F/2\sqrt{2}\,\pi\alpha)\{g_A(\mu)-\lambda g_V(\mu)\}A_0\,F(y)q^2\,, \tag{47}$$

where λ is the μ polarization, y is the momentum fraction carried by the scattered μ, $F(y)$ is as defined above, and the ratio of the weak and electromagnetic structure functions $(xG_3)/F_2$ is $A_0 = \frac{6}{5}\{2g_A(u)-g_A(d)\}$.

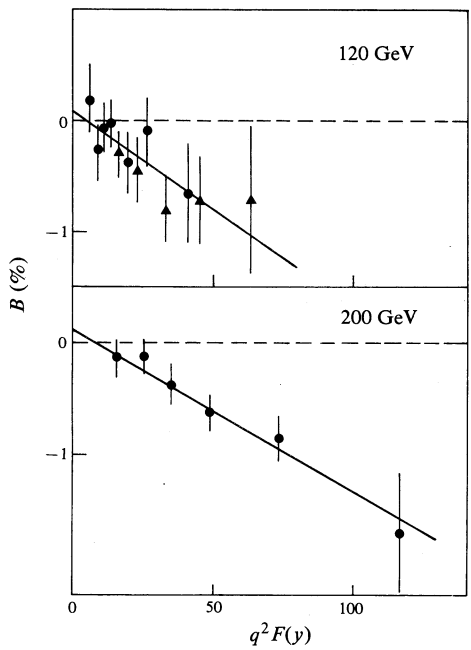

Fig. 51. Asymmetry (47) measured by Argento *et al.* (1983) in μ-carbon inelastic scattering, plotted as a function of $q^2F(y)$, where q^2 is the squared momentum transferred to the IVB and $F(y)$ is a kinematic factor (see Section 4*d*).

Fig. 51 shows the data at both beam momenta. A fit of the asymmetry B is made to the form

$$B = a + bq^2F(y)\,.$$

At both momenta the parameter a is consistent with zero as expected. The fitted parameter b may now be used to determine the combination of couplings specified above. Assuming that all axial couplings take their expected values ($\pm\frac{1}{2}$), this provides a measurement of $g_V(\mu)$ and hence $\sin^2\theta_W$. Argento *et al.* (1983) found

$$\sin^2\theta_W = 0{\cdot}23\pm0{\cdot}07(\mathrm{stat})\pm0{\cdot}04(\mathrm{syst})\,.$$

In conclusion, taken together these experiments on charged-lepton–hadron scattering provide an impressive test of the GSW model. If one assumes that $\rho = 1$ and that all the axial couplings are equal to $\pm\frac{1}{2}$, then experiments at very different values of $|q^2|$ find values of $g_V(u)$, $g_V(d)$ and $g_V(\mu)$ close to those expected.

5. Summary

In Table 12 we summarize measurements of $\sin^2\theta_W$ from the data described in Sections 3 and 4; the data are also shown in Fig. 52. There is no evidence of a systematic deviation $\sin^2\theta_W$ from its average value, for measurements collected in a q^2 range spanning 10^{16} $(\mathrm{GeV}/c)^2$. These measurements apply to both time-like and space-like IVB processes. Furthermore, as expected from the minimal GSW model, or more generally from a model with isospin-zero Higgs particles, there is no evidence of a deviation from $\rho = 1$. The most accurate measurements have been made for the (e, ν_e), (μ, ν_μ) and (u, d') doublets. More precise data are required for other lepton and quark doublets.

Table 12. Compilation of measured $\sin^2\theta_W$ values[A]

Experiment	Typical q^2 (GeV^2)	$\sin^2\theta_W$[B]	Comments
Atomic PV	10^{-12}	$0{\cdot}22\pm0{\cdot}05$	From $g_V(u)$, $g_V(d)$
μN scattering	10^2	$0{\cdot}23\pm0{\cdot}07\pm0{\cdot}04$	From $g_V(\mu)$
e↑D scattering	1	$0{\cdot}218\pm0{\cdot}012\pm0{\cdot}008$	Mainly from $g_V(u)$, $g_V(d)$
$\nu(\bar{\nu})$N scattering	10^2–10^3	$0{\cdot}222\pm0{\cdot}005\pm0{\cdot}006$	Average of three recent results[C]
M_W, M_Z	10^4	$0{\cdot}218\pm0{\cdot}023$	UA1 + UA2; Collider data only
M_W, M_Z, α, G_F	10^4	$0{\cdot}227\pm0{\cdot}006\pm0{\cdot}008$	UA2; Collider and low energy data[D]
M_W, M_Z, α, G_F	10^4	$0{\cdot}216\pm0{\cdot}006\pm0{\cdot}016$	UA1; Collider and low energy data[D]
$\nu_\mu(\bar{\nu}_\mu)$e	10^{-2}–10^{-1}	$0{\cdot}212\pm0{\cdot}023$	Average of CHARM and BNL(E734)
$e^+e^- \to f\bar{f}$	10^3	$0{\cdot}18\pm0{\cdot}02$	Uses observed M_Z

[A] We define $\sin^2\theta_W = 1-(M_W/M_Z)^2$ and assume $\rho = 1$. Radiative corrections are applied following Marciano (1985). Where necessary, the axial couplings $g_A(f)$ are taken to be $\pm\frac{1}{2}$ (see Table 3).
[B] Where one error is quoted it is a combined statistical and systematic uncertainty. Where two errors are quoted, they are usually statistical and systematic, in that order. For $\nu(\bar{\nu})$N, the two quoted errors are the experimental and theoretical uncertainties.
[C] The most precise evaluations from CDHS, CHARM and CCFRR are averaged.
[D] Given the very different systematic errors, which reflect an uncertainty on the absolute energy scale, it is not possible to combine UA1 and UA2 results when the IVB masses are combined with α and G_F.

To compare neutral-current processes over a large q^2 range, radiative corrections must be applied. These corrections are predominantly electromagnetic in origin, and to study weak radiative corrections, $\sin^2\theta_W$ must be measured to better than $\sim\pm0{\cdot}003$. This measurement accuracy should be possible at LEP (Altarelli 1985).

The predicted radiative correction is sensitive to the assumed top-quark mass, and confirmation of the existence of this quark (or indeed the identification of additional quark or lepton doublets) is urgently required.

The mass of the Higgs particle is poorly predicted by the theory, but its coupling strengths to fermions and weak IVBs are precisely specified. The observation of this particle is an important goal. Observations at the $\bar{p}p$ Collider are unlikely because of

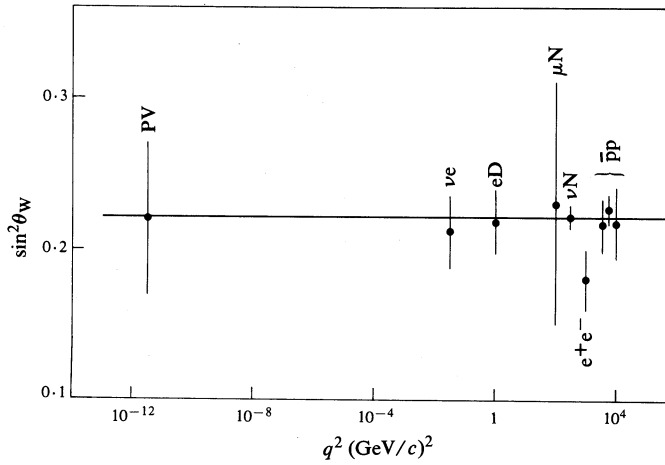

Fig. 52. Dependence of $\sin^2\theta_W$, after radiative corrections, on the squared momentum transferred to the IVB produced.

its small production cross section. However, the cross section increases with $\sqrt{s}$ and its observation is more likely at the proposed supercolliders ($\sqrt{s} \geqslant 10$ TeV).

Another consequence of all reasonable gauge theories incorporating the W and Z^0 is the observation of the self-coupling of the IVBs at a predicted rate (e.g. $Z^0 \rightarrow W^+W^-$). At the second stage of the LEP project, energies required for the direct production of W^+W^- pairs will be available. Observations at the $\bar{p}p$ Collider are difficult, because of the low cross sections involved.

Little has been said here about the charged-current sector of weak interactions; the recent review by Bertin and Vitale (1984) is recommended.

Despite the success of the GSW model, it is surely an incomplete theory. In the context of the $SU(2)_L \times U(1)$ group alone, no *a priori* knowledge of the fermion and Higgs particle masses is provided. Furthermore, $\sin^2\theta_W$ is an experimentally measured quantity, as are the mixing angles of the Kobayashi–Maskawa matrix. Most theories attempting to unify the forces require left–right symmetry in the expanded group structure. This implies the extension of $SU(2)_L \times U(1)$ to $SU(2)_L \times SU(2)_R \times U(1)$ above some energy. A limit for the resultant right-handed W bosons was provided by Carr *et al.* (1983), who searched for ν_R from μ decay and obtained $M_R^W > 380$ GeV. Following plausible theoretical assumptions, measurements of the K_L–K_S mass difference can be used to provide an even stronger limit. To search for the additional gauge bosons which result from the extended group structure provides a powerful motivation for the construction of higher energy colliders.

Acknowledgments

One of us (A.G.C.) would like to thank Professor A. Baxter for the invitation to give these lectures at the Seventh NUPP Summer School, held in Canberra in February 1985. The hospitality and financial support of Professor A. W. Thomas and the Physics Department of the University of Adelaide is gratefully acknowledged. This review was completed at CERN in July 1985. One of us (S.N.T.) thanks the

Australian Research Grants Scheme for a grant that made a visit to CERN possible. Useful discussions with many of our colleagues in the UA1 and UA2 experiments, over an extended time period, have been invaluable, and are much appreciated. A careful reading of the manuscript by G. Goggi was extremely helpful. The contributions of M. Prost in preparing the manuscript, and E. Viale in preparing the figures, are gratefully acknowledged.

References

Abramowicz, H., *et al.* (1982). *Phys. Lett.* B **109**, 115.
Abramowicz, H., *et al.* (1985). *Z. Phys.* C **28**, 51.
Adeva, B., *et al.* (1982). *Phys. Rev. Lett.* **48**, 1701.
Adeva, B., *et al.* (1985). Measurement of $e^+e^- \rightarrow \mu^+\mu^-$: A test of electroweak theories, MIT Technical Rep. No. 144.
Ahrens, L. A., *et al.* (1985). *Phys. Rev. Lett.* **54**, 18.
Aihara, H., *et al.* (1985). *Phys. Rev.* D **31**, 2719.
Aitchison, I. J. R., and Hey, A. J. (1982). 'Gauge Theories in Particle Physics' (Adam Hilger: Bristol).
Alner, C., *et al.* (1984). *Phys. Lett.* B **138**, 304.
Altarelli, G. (1985). Precision test of the electroweak theory at the Z^0. University of Rome Preprint No. 464.
Altarelli, G., Ellis, R. K., Greco, H., and Martinelli, G. (1984). *Nucl. Phys.* B **246**, 576.
Altarelli, G., Ellis, R. K., and Martinelli, G. (1985). *Z. Phys.* C **27**, 617.
Althoff, M., *et al.* (1984). *Z. Phys.* C **22**, 13.
Althoff, M., *et al.* (1985). *Z. Phys.* C **26**, 521.
Argento, A., *et al.* (1983). *Phys. Lett.* B **120**, 245.
Armenise, N., *et al.* (1979). *Phys. Lett.* B **86**, 225.
Arnison, G., *et al.* (1978). A 4π solid-angle detector with the SPS used as a proton–antiproton collider at $\sqrt{s} = 540$ GeV. Preprint CERN/SPSC/78-6.
Arnison, G., *et al.* (1982). *Phys. Lett.* B **118**, 167.
Arnison, G., *et al.* (1983*a*). *Phys. Lett.* B **122**, 103.
Arnison, G., *et al.* (1983*b*). *Phys. Lett.* B **123**, 108.
Arnison, G., *et al.* (1983*c*). *Phys. Lett.* B **126**, 398.
Arnison, G., *et al.* (1984*a*). *Phys. Lett.* B **134**, 469.
Arnison, G., *et al.* (1984*b*). *Phys. Lett.* B **135**, 250.
Arnison, G., *et al.* (1984*c*). *Phys. Lett.* B **147**, 241.
Arnison, G., *et al.* (1984*d*). *Phys. Lett.* B **147**, 493.
Arnison, G., *et al.* (1985). W production properties at the SPS Collider. Preprint CERN-EP/85-108.
Asratyan, A., *et al.* (1984). *Phys. Lett.* B **140**, 127.
Baer, H., Ellis, J., Nanopoulos, D. V., and Tata, X. (1985). *Phys. Lett.* B **153**, 265.
Bagnaia, P., *et al.* (1983). *Phys. Lett.* B **129**, 130.
Bagnaia, P., *et al.* (1984*a*). *Z. Phys.* C **24**, 1.
Bagnaia, P., *et al.* (1984*b*). *Phys. Lett.* B **139**, 105.
Baier, R., Engelis, J., and Peterson, B. (1979). *Z. Phys.* C **2**, 265.
Banner, M., *et al.* (1978). Proposal to study $\bar{p}p$ interactions at 540 GeV centre-of-mass energy. Preprint CERN/SPSC/78-8.
Banner, M., *et al.* (1982). *Phys. Lett.* B **115**, 59.
Banner, M., *et al.* (1983*a*). *Phys. Lett.* B **122**, 322.
Banner, M., *et al.* (1983*b*). *Phys. Lett.* B **122**, 476.
Banner, M., *et al.* (1985). *Z. Phys.* C **27**, 329.
Bartel, W., *et al.* (1984). *Phys. Lett.* B **146**, 437.
Bartel, W., *et al.* (1985). *Z. Phys.* C **26**, 507.
Behrend, M. J., *et al.* (1982). *Z. Phys.* C **14**, 283.
Bender, D., *et al.* (1984). *Phys. Rev.* C **30**, 515.

Berger, Ch., *et al.* (1985*a*). *Z. Phys.* C **27**, 341.
Berger, Ch., *et al.* (1985*b*). *Z. Phys.* C **28**, 1.
Bergsma, F., *et al.* (1985). A precision measurement of the ratio of neutrino induced neutral-current and charged-current total cross sections. Preprint CERN-EP/85-113.
Bertin, A., and Vitale, A. (1984). *In* '50 Years of Weak-interaction Physics' (Eds A. Bertin *et al.*), p. 130 (Italian Physical Society: Bologna).
Billinge, R. (1984). Fourth Topical Workshop on $p\bar{p}$ Collider Physics, Bern (Eds H. Hanni and J. Schacher), p. 357 (CERN: Switzerland).
Billinge, R., *et al.* (1979). CERN $\bar{p}p$ colliding beam facilities. Preprint CERN/PS/AA/79-17.
Bjorken, J. D., and Paschos, E. A. (1969). *Phys. Rev.* **185**, 1975.
Blietschau, J., *et al.* (1976). *Nucl. Phys.* B **114**, 189.
Blondel, A. (1985). Europhysics Int. Conf. on High Energy Physics, Bari, 1985.
Böhm, A. (1985). Rapporteur talk, Workshop on Electroweak Interactions, June 1985, Savonlinna, Finland (unpublished).
Bosetti, P. C., *et al.* (1983). *Nucl. Phys.* B **217**, 1.
Bouchiat, M. A., *et al.* (1982). *Phys. Lett.* B **117**, 358.
Bouchiat, M. A., *et al.* (1984). *Phys. Lett.* B **134**, 463.
Bozzo, M., *et al.* (1984). *Phys. Lett.* B **147**, 392.
Bramham, P., *et al.* (1975). *Nucl. Instrum. Methods* **125**, 683.
Bregman, M., *et al.* (1978). *Phys. Lett.* B **78**, 174 [see also the review Preprint CERN 77-08 (1977)].
Budker, G. I. (1967) *At. Energ.* **22**, 346.
Budker, G. I., *et al.* (1975). Proc. Fourth National Conf. on Particle Accelerators, Moscow, p. 309.
Cabbibo, N. (1963). *Phys. Rev. Lett.* **10**, 531.
Cahn, R. N., and Gilman, F. J. (1978). *Phys. Rev.* D **17**, 1313.
Carr, J., *et al.* (1983). *Phys. Rev. Lett.* **51**, 627.
Carron, G., *et al.* (1978). *Phys. Lett.* B **77**, 353 [see also the review Preprint CERN 77-08 (1977)].
Chau, L. (1983). *Phys. Rep.* **95**, 1.
Cnops, A. M., *et al.* (1978). *Phys. Rev. Lett.* **41**, 357.
Darriulat, P. (1984). The strong interaction: experimental approaches. Lectures at the 1984 Scottish University Summer School, Preprint CERN-EP/84-152.
de Raad, B. (1984). Proc. Fourth Topical Workshop on $p\bar{p}$ Collider Physics, Bern 1984 (Eds H. Hanni and J. Schacher), p. 344 (CERN: Switzerland).
Derrick, M., *et al.* (1985). *Phys. Rev.* D **31**, 2352.
DiLella, L. (1985*a*). *Annu. Rev. Nucl. Part. Sci.* **35**, 107.
DiLella, L. (1985*b*). Rapporteur talk, Europhysics Conf. on High Energy Physics, Bari, 1985 (to be published [see also CERN Preprint EP /85-184).
Dobrzynski, L. (1985). Proc. Fifth Int. Conf. on Physics in Collisions, Autun, France (to be published).
Dowell, J. (1984). Proton–antiproton physics. Lectures at the 1984 CERN-JINR Summer School. Preprint CERN 85-11.
Drell, S. D., and Yan, T. (1970). *Phys. Rev. Lett.* **25**, 316.
Duke, D. W., and Owens, J. F. (1984). *Phys. Rev.* D **30**, 49.
Eichten, E., *et al.* (1985). *Rev. Mod. Phys.* **56**, 579.
Ellis, J. (1984). Proc. Fourth Topical Workshop on $p\bar{p}$ Collider Physics, Bern (Eds H. Hanni and J. Schacher), p. 539 (CERN: Switzerland).
Ellis, S. D., Kleiss, R., and Stirling, W. J. (1985). *Phys. Lett.* B **154**, 435.
Faissner, H., *et al.* (1978). *Phys. Rev. Lett.* **41**, 213.
Fermi, E. (1933). *Ric. Sci.* **4**, 491.
Fernandez, E., *et al.* (1983*a*). *Phys. Rev. Lett.* **50**, 1238.
Fernandez, E., *et al.* (1983*b*). Weak neutral current effects in $e^+e^- \rightarrow \mu^+\mu^-$ at 29 GeV. Preprint SLAC-PUB-3133.
Fernandez, E., *et al.* (1985). *Phys. Rev. Lett.* **54**, 1624.
Feynman, R. P., and Gell-Mann, M. (1958). *Phys. Rev.* **109**, 193.

Fortson, E. N., and Lewis, L. L. (1984). *Phys. Rep.* **113**, 289.
Froidevaux, D. (1985). Proc. Fifth Int. Conf. on Physics in Collisions, Autun, France (to be published).
Gan, K. K., *et al.* (1985). *Phys. Lett.* B **153**, 116.
Glashow, S. L. (1961). *Nucl. Phys.* **22**, 579.
Glashow, S. L., Iliopoulos, J., and Maiani, L. (1971). *Phys. Rev.* D **2**, 1285.
Goggi, G. (1979). *Lett. Nuovo Cimento* **24**, 49.
Goggi, G. (1984). *In* '50 Years of Weak-interaction Physics' (Eds A. Bertin *et al.*), p. 416 (Italian Physical Society: Bologna).
Goldstone, J. (1961). *Nuovo Cimento* **19**, 154.
Haidt, D. (1985). Rapporteur talk, Workshop on Electroweak Interactions, June 1985, Savonlinna, Finland (unpublished).
Harrison, M. (1984). Proc. Fourth Topical Workshop on $\bar{p}p$ Collider Physics, Bern (Eds H. Hanni and J. Schacher), p. 368 (CERN: Switzerland).
Hasert, F. J., *et al.* (1973). *Nucl. Phys.* B **114**, 189.
Heisterberg, R. H., *et al.* (1980). *Phys. Rev. Lett.* **44**, 635.
Higgs, P. W. (1964). *Phys. Lett.* **12**, 132.
Higgs, P. W. (1966). *Phys. Rev.* **145**, 1156.
Humpert, B. (1984). *Phys. Lett.* B **135**, 179.
Hung, P. Q., and Sakurai, J. J. (1978). *Nucl. Phys.* B **143**, 87.
Jarlskog, C. (1982). Proc. 1981 CERN School of Physics, Preprint CERN 82-04, p. 63.
Jonker, M., *et al.* (1981). *Phys. Lett.* B **99**, 265.
Kobayashi, M., and Maskawa, K. (1973). *Prog. Theor. Phys.* **49**, 652.
Kourkoumelis, C., *et al.* (1980). *Z. Phys.* C **5**, 95.
Langacker, P. (1984). Proc. XXII Conf. on High Energy Physics, Leipzig (Eds A. Meyer and E. Wieczorck), p. 215 (Akad. Wissenschaften DDR: Zeuthen).
Levi, M. (1985). UA1 results on W and Z^0 production. Contribution to Europhysics Conf. on High Energy Physics, Bari (to be published).
Levi, M., *et al.* (1984). *Phys. Rev. Lett.* **51**, 1941.
Mansoulié, B. (1983). Proc. Third Moriond Workshop on $\bar{p}p$ Physics, La Plagne (Ed. J. Tran Thanh Van), p. 609 (Editions Frontiéres: Paris).
Mansoulié, B. (1985). Proc. Fifth Workshop on $p\bar{p}$ Collider Physics, St Vincent, Italy (Ed. M. Greco) (World Scientific: Singapore).
Marciano, W. J. (1985). Proc. Winter Physics Conf., Aspen (to be published) [see also Preprint BNL 36147].
Marciano, W. J., and Sirlin, A. (1984). *Phys. Rev.* D **29**, 945.
Mohl, D., *et al.* (1980). *Phys. Rep.* **58**, 73.
Murtagh, M. (1984). Proc. XI Int. Conf. on Neutrino Physics and Astrophysics, Nordkirchen near Dortmund (Eds K. Kleinknecht and E. A. Paschos), p. 290 (World Scientific: Singapore).
Nanopoulos, D., and Savoy-Navarro, A. (1984). *Phys. Rep.* **105**, 1.
Panman, J. (1984). Proc. XI Int. Conf. on Neutrino Physics and Astrophysics, Nordkirchen near Dortmund (Eds K. Kleinknecht and E. A. Paschos), p. 741 (World Scientific: Singapore).
Panman, J. (1985). Proc. Winter Phys. Conf. Aspen, Jan. 1985 (to be published) [see also Preprint CERN-EP/85-35].
Particle Data Group (1984). *Rev. Mod. Phys.* **56**, 1.
Paschos, E. A., and Wolfenstein, L. (1973). *Phys. Rev.* D **7**, 91.
Plothow-Besch, H. (1985). Proc. Fifth Workshop on $p\bar{p}$ Collider Physics, St Vincent, Italy (Ed. M. Greco) (World Scientific: Singapore) [see also Preprint CERN-EP/85-86].
Prepost, R. (1984). Proc. XXII Int. Conf. on High-energy Physics, Leipzig (Eds A. Meyer and E. Wieczorek), p. 227 (Akad. Wissenschaften DDR: Zeuthen).
Prescott, C., *et al.* (1979). *Phys. Lett.* B **84**, 524.
Pullia, A. (1984). *In* '50 Years of Weak-interaction Physics' (Eds A. Bertin *et al.*), p. 333 (Italian Physical Society: Bologna).
Radermacher, E. (1984). *Prog. Nucl. Part. Phys.* **14**, 23.
Reines, F., *et al.* (1976). *Phys. Rev. Lett.* **37**, 315.
Reutens, P. G., *et al.* (1985). *Phys. Lett.* B **152**, 404.

Ross, D., and Veltman, M. (1975). *Nucl. Phys.* B **95**, 135.
Rubbia, C., *et al.* (1977). Prog. Int. Conf. on Neutrinos, Aachen (Eds H. Faissner *et al.*), p. 683 (Vieweg: Braunschweig).
Salam, A. (1968). Proc. VIII Nobel Symposium, p. 367 (Almquist and Wiksells: Stockholm).
Savoy-Navarro, A. (1985). Proc. Fifth Workshop on $p\bar{p}$ Collider Physics, St Vincent, Italy (Ed. M. Greco) (World Scientific: Singapore) [see also Preprint CERN-EP/85-64].
Staff of CERN $\bar{p}p$ Project (1981). *Phys. Lett.* B **107**, 306.
't Hooft, G. (1971 *a*). *Nucl. Phys.* B **33**, 173.
't Hooft, G. (1971 *b*). *Nucl. Phys.* B **35**, 167.
Timmer, J. (1983). Third Moriond Workshop on $\bar{p}p$ Physics, La Plagne (Ed. J. Tran Thanh Van), p. 593 (Editions Frontiéres: Paris).
Van der Meer, S. (1972). Stochastic damping of betatron oscillations in the ISR. Preprint CERN-ISR-PO 72-31 [see also Preprints CERN/SPS/423 (1978) and CERN/PS/AA/78-3 (1978)].
Veltman, M. (1977). *Nucl. Phys.* B **123**, 189.
Veltman, M. (1980). *Phys. Lett.* B **91**, 95.
Wahl, H. (1984). Proc. XV Int. Symp. on Multiparticle Dynamics, Lund (Eds G. Gustafson and C. Peterson), p. 410 (World Scientific: Singapore).
Wang, K. C. (1984). Proc. XI Int. Conf. on Neutrino Physics and Astrophysics, Nordkirchen near Dortmund (Eds K. Kleinknecht and E. A. Paschos), p. 322 (World Scientific: Singapore).
Weidberg, A. R. (1984). Proc. XV Int. Symp. on Multiparticle Dynamics, Lund (Eds G. Gustafson and C. Peterson), p. 349 (World Scientific: Singapore).
Weinberg, S. (1967). *Phys. Rev. Lett.* **19**, 1264.
Yang, C. N., and Mills, R. L. (1954). *Phys. Rev.* **96**, 191.

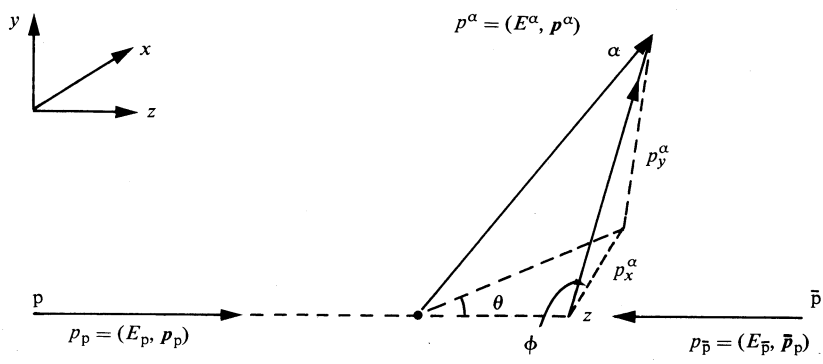

Fig. 53. Coordinate frame (x, y, z) used to define the momentum components (p_x, p_y, p_z) of particle α in terms of the polar and azimuth angles θ and ϕ.

Appendix 1. Kinematic Variables Commonly in Use at the $\bar{p}p$ Collider

(i) The centre-of-mass energy $\sqrt{s}$ is defined by the four-momenta p_p and $p_{\bar{p}}$:

$$s = (p_p + p_{\bar{p}})^2 = m_p^2 + m_{\bar{p}}^2 + 2(E_p E_{\bar{p}} - \boldsymbol{p}_p \cdot \boldsymbol{p}_{\bar{p}}) \approx 4 E_p E_{\bar{p}}.$$

(ii) The polar angle θ and azimuth angle ϕ of an outgoing particle α are defined in Fig. 53, giving

$$p_T^\alpha = \{(p_x^\alpha)^2 + (p_y^\alpha)^2\}^{\frac{1}{2}}, \quad \text{transverse momentum};$$

$$p_L^\alpha = p_z^\alpha, \quad \text{longitudinal momentum}.$$

(iii) The fractional longitudinal momentum x is given by

$$x_{\mathrm{p}} = 2p_{\mathrm{L}}^{\mathrm{p}}/\sqrt{s} \approx 1, \qquad x_{\bar{\mathrm{p}}} = 2p_{\mathrm{L}}^{\bar{\mathrm{p}}}/\sqrt{s} \approx 1, \qquad x_{\alpha} = 2p_{\mathrm{L}}^{\alpha}/\sqrt{s}.$$

(iv) The rapidity y^{α} and pseudo-rapidity η^{α} of a particle α are given as follows. Consider a momentum boost along the z-axis, then

$$\begin{pmatrix} E' \\ p_{\mathrm{L}}' \end{pmatrix} = \begin{pmatrix} \cosh\Delta & -\sinh\Delta \\ -\sinh\Delta & \cosh\Delta \end{pmatrix} \begin{pmatrix} E \\ p_{\mathrm{L}} \end{pmatrix},$$

where $\cosh\Delta = \gamma$ and $\sinh\Delta = \beta\gamma$. It follows that

$$\begin{pmatrix} E'+p_{\mathrm{L}}' \\ E'-p_{\mathrm{L}}' \end{pmatrix} = \exp(-2\Delta) \begin{pmatrix} E+p_{\mathrm{L}} \\ E-p_{\mathrm{L}} \end{pmatrix}$$

and if $y = \frac{1}{2}\ln\{(E+p_{\mathrm{L}})/(E-p_{\mathrm{L}})\}$, then

$$y' = y - \Delta,$$

where $\Delta = \frac{1}{2}\ln\{(1+\beta)/(1-\beta)\}$. In the limit $E \gg m$ we then have

$$y \to \eta = -\ln(\tan\tfrac{1}{2}\theta).$$

(v) The missing transverse momentum $p_{\mathrm{T}}^{\mathrm{miss}}$ is as follows. In a detector which can measure the momentum of every particle α produced in a $\bar{\mathrm{p}}\mathrm{p}$ interaction, we can expect from momentum conservation that

$$\sum_{\alpha} \boldsymbol{p}_{\mathrm{T}}^{\alpha} = 0, \qquad \sum_{\alpha} \boldsymbol{p}_{\mathrm{L}}^{\alpha} = 0.$$

In practice neither relationship is found experimentally. In particular, for hard parton–parton scattering within the nucleon, the two partons will not have the same longitudinal momentum. 'Spectator' partons will continue in approximately the beam direction and in general will not leave the vacuum pipe of the accelerator. On the other hand, 'spectator' partons do not carry significant $\boldsymbol{p}_{\mathrm{T}}$, and if all products α of the parton–parton scattering process are detected, then

$$\left| \sum_{\alpha} \boldsymbol{p}_{\mathrm{T}}^{\alpha} \right| = \beta,$$

where, averaged over many events, $\mathrm{d}n/\mathrm{d}\beta \propto \exp(-K\beta^2)$. The width of the gaussian distribution is determined mainly by the resolution, or accuracy, with which the energy or momenta of the particles α are measured. If a significant number of outgoing particles traverse regions of poor detection capability, non-gaussian tails may result in the distribution of β.

If, as in W decay, a neutrino traverses the apparatus undetected, then

$$\sum_{\alpha} \boldsymbol{p}_{\mathrm{T}}^{\alpha} = -\boldsymbol{p}_{\mathrm{T}}^{\mathrm{miss}} = -\boldsymbol{p}_{\mathrm{T}}^{\nu}.$$

Other effects which degrade the resolution of p_T^{miss} include rest-mass effects when the particle is not identified. Furthermore, in final states involving jet production, a lack of information on the effective jet mass will degrade the resolution.

Appendix 2. Production Cross Sections $p\bar{p} \to W + X$ and $p\bar{p} \to Z^0 + X$

The production of the weak IVBs in $p\bar{p}$ collisions proceeds predominantly via the Drell–Yan (1970) process, illustrated in Fig. 24*a*. The elementary processes, if only valence quarks of the nucleon are considered, are

$$u\bar{d} \to W^+, \quad d\bar{u} \to W^-, \quad u\bar{u}, d\bar{d} \to Z^0. \tag{A1}$$

Given the interacting partons a and b, the kinematics associated with the process of Fig. 24*a* is, neglecting the transverse momentum of the produced IVB,

$$E = \tfrac{1}{2}\sqrt{s}(x_a + x_b), \quad p_L = \tfrac{1}{2}\sqrt{s}(x_a - x_b), \quad p_T \approx 0,$$
$$\hat{s} = M_W^2 = x_a x_b s = \tau s, \quad \tau = M_W^2/s,$$
$$x_{a,b} = \tfrac{1}{2}\{(x_W^2 + 4\tau)^{\frac{1}{2}} \pm x_W\}. \tag{A2}$$

If the fractional longitudinal momenta of the interacting partons a and b in nucleons A and B respectively are x_a and x_b, then for W^+ production

$$\sigma(\bar{p}p \to W^+ X) = \int_0^1 dx_a \int_0^1 dx_b\, \hat{\sigma}(x_a, x_b)\, W^+(x_a, x_b), \tag{A3}$$

where the elementary cross section $\hat{\sigma}$ is

$$\hat{\sigma}(x_a, x_b) = \sqrt{2}\, G_F \pi M_W^2\, \delta(x_a x_b s - M_W^2) \tag{A4}$$

and the left-handed helicity of quarks and right-handed helicity of antiquarks is assumed.

Using (A2) and inserting (A4) in (A3), we get

$$\sigma(\bar{p}p \to W^+ X) = \sqrt{2}\, G_F \pi\tau \int_\tau^1 (dx/x)\, W^+(x, \tau/x). \tag{A5}$$

In evaluating $W^+(x_a, x_b)$, we must sum over all allowed quark flavours. If we consider only u, d and s quarks then

$$W^+(x_a, x_b) = \tfrac{1}{3}[\{u(x_a)\bar{d}(x_b) + \bar{d}(x_a)\, u(x_a)\}\cos^2\theta_C$$
$$+ \{u(x_a)\bar{s}(x_b) + \bar{s}(x_a)\, u(x_b)\}\sin^2\theta_C], \tag{A6}$$

where θ_C is the Cabbibo angle, the factor of $\frac{1}{3}$ takes into account the colour factor, $u(x)$ is the distribution of u quarks within the nucleon, and similarly for $d(x)$ and $s(x)$.

In the case of Z^0 production, the situation is similar:

$$\sigma(\bar{p}p \to Z^0 X) = \sqrt{2}\, G_F \pi\tau \int (dx/x)\, Z^0(x, \tau/x), \tag{A7}$$

where

$$\begin{aligned} Z^0(x_a, x_b) = \tfrac{1}{3}[&\{u(x_a)\,\bar{u}(x_b) + \bar{u}(x_a)\,u(x_b)\}\{g_V^2(u) + g_A^2(u)\} \\ &+ \{d(x_a)\,\bar{d}(x_b) + \bar{d}(x_a)\,d(x_b)\}\{g_V^2(d) + g_A^2(d)\} \\ &+ \{s(x_a)\,\bar{s}(x_b) + \bar{s}(x_a)\,s(x_b)\}\{g_V^2(s) + g_A^2(s)\}], \end{aligned}$$

with

$$g_V^2(u) + g_A^2(u) = \tfrac{1}{2} - \tfrac{4}{3}\sin^2\theta_W + \tfrac{16}{9}\sin^4\theta_W,$$

$$g_V^2(d, s) + g_A^2(d, s) = \tfrac{1}{2} - \tfrac{2}{3}\sin^2\theta_W + \tfrac{4}{9}\sin^4\theta_W.$$

As noted in Section 3, these first-order predictions are modified by higher order QCD corrections, generally involving the emission or absorption of gluons (see Figs 24*b* and 24*c*).

Manuscript received 2 October, accepted 18 November 1985